JOINT TRANSPORTATION
RESEARCH PROGRAM
INDIANA DEPARTMENT OF TRANSPORTATION
AND PURDUE UNIVERSITY

Guardrails for Use on Historic Bridges

Volume 2—Bridge Deck Overhang Design

Robert J. Frosch, Adam J. Morel

SPR-3714 • Report Number: FHWA/IN/JTRP-2016/34 • DOI: 10.5703/1288284316361

RECOMMENDED CITATION

Frosch, R. J., & Morel, A. J. (2016). *Guardrails for use on historic bridges: Volume 2—Bridge deck overhang design* (Joint Transportation Research Program Publication No. FHWA/IN/JTRP-2016/34). West Lafayette, IN: Purdue University. https://doi.org/10.5703/1288284316361

AUTHORS

Robert J. Frosch, PhD, PE
Professor of Civil Engineering
Lyles School of Civil Engineering
Purdue University
(765) 494-5904
frosch@purdue.edu
Corresponding Author

Adam J. Morel
Graduate Research Assistant
Lyles School of Civil Engineering
Purdue University

JOINT TRANSPORTATION RESEARCH PROGRAM

The Joint Transportation Research Program serves as a vehicle for INDOT collaboration with higher education institutions and industry in Indiana to facilitate innovation that results in continuous improvement in the planning, design, construction, operation, management and economic efficiency of the Indiana transportation infrastructure. https://engineering.purdue.edu/JTRP/index_html

Published reports of the Joint Transportation Research Program are available at http://docs.lib.purdue.edu/jtrp/.

NOTICE

The contents of this report reflect the views of the authors, who are responsible for the facts and the accuracy of the data presented herein. The contents do not necessarily reflect the official views and policies of the Indiana Department of Transportation or the Federal Highway Administration. The report does not constitute a standard, specification, or regulation.

COPYRIGHT

Copyright 2016 by Purdue University. All rights reserved.
Print ISBN: 978-1-62260-467-8
ePUB ISBN: 978-1-62260-468-5

TECHNICAL REPORT STANDARD TITLE PAGE

1. Report No.	2. Government Accession No.	3. Recipient's Catalog No.
FHWA/IN/JTRP-2016/34		

4. Title and Subtitle	5. Report Date
Guardrails for Use on Historic Bridges: Volume 2—Bridge Deck Overhang Design	November 2016
	6. Performing Organization Code

7. Author(s)	8. Performing Organization Report No.
Robert J. Frosch, Adam J. Morel	FHWA/IN/JTRP-2016/34

9. Performing Organization Name and Address	10. Work Unit No.
Joint Transportation Research Program Purdue University 550 Stadium Mall Drive West Lafayette, IN 47907-2051	
	11. Contract or Grant No. SPR-3714

12. Sponsoring Agency Name and Address	13. Type of Report and Period Covered
Indiana Department of Transportation State Office Building 100 North Senate Avenue Indianapolis, IN 46204	Final Report
	14. Sponsoring Agency Code

15. Supplementary Notes
Prepared in cooperation with the Indiana Department of Transportation and Federal Highway Administration.

16. Abstract

Bridges that are designated historic present a special challenge to bridge engineers whenever rehabilitation work or improvements are made to the bridges. Federal and state laws protect historically significant bridges, and railings on these bridges can be subject to protection because of the role they play in aesthetics. Unfortunately, original railings on historic bridges do not typically meet current crash-test requirements and typically do not meet current standards for railing height and size of permitted openings. The primary objective of this study is to develop strategies that can be used to address existing railings on historic bridges and to develop solutions that meet current design requirements. In addition to the modification, selection, and design of the bridge railing, the bridge deck is also impacted by changes made to the railing. Due to increased force levels recently required by AASHTO, deck overhangs require significantly more reinforcement than for past practice. These increases are being realized on all bridge decks and may pose particular challenges for the attachment of railing to historic bridges. Therefore, a secondary objective of this project is to investigate the design of the deck overhang and determine whether reduced amounts of reinforcement are possible. For Volume 1 (Replacement Strategies), three phases of research were conducted. First, an overview of current practice for addressing historic bridge railings was performed. Second, an investigation was conducted to document historic bridge railings in Indiana. Finally, rehabilitation solutions were developed to address the specific bridge railings found in Indiana. Based on this research, three retrofit strategies were developed which include an inboard railing, curb railing, and a simulated historic railing. These rehabilitation solutions can be used to address historic bridge railings not only in Indiana, but across the country. For Volume 2 (Bridge Deck Overhang Design), experimental testing of half-scale and full-scale overhang specimens was conducted, and the results were analyzed. Failures of in-service bridge railings were also evaluated. Based on this research, recommendations are provided for the more efficient and economic design of bridge deck overhangs. These recommendations are applicable not only for historic bridges, but for all concrete bridge decks.

17. Key Words	18. Distribution Statement
historic bridge guardrails, historic bridge railings, historic bridges, bridge railing rehabilitation, bridge deck overhang	No restrictions. This document is available to the public through the National Technical Information Service, Springfield, VA 22161.

19. Security Classif. (of this report)	20. Security Classif. (of this page)	21. No. of Pages	22. Price
Unclassified	Unclassified	105	

Form DOT F 1700.7 (8-69)

EXECUTIVE SUMMARY

GUARDRAILS FOR USE ON HISTORIC BRIDGES: VOLUME 2—BRIDGE DECK OVERHANG DESIGN

Introduction

Bridges that are designated historic present a special challenge to bridge engineers whenever rehabilitation work or improvements are made to the bridges. Federal and state laws protect historically significant bridges, and railings on these bridges can be subject to protection because of the role they play in aesthetics. Unfortunately, original railings on historic bridges do not typically meet current crash-test requirements and typically do not meet current standards for railing height and size of permitted openings. The primary objective of this study is to develop strategies that can be used to address existing railings on historic bridges and to develop solutions that meet current design requirements. In addition to the modification, selection, and design of the bridge railing, the bridge deck is also impacted by changes made to the railing. Due to increased force levels recently required by AASHTO, deck overhangs must have significantly more reinforcement than in past practice. These increases are being realized on all bridge decks and may pose particular challenges for the attachment of railing to historic bridges. Therefore, a secondary objective of this project is to investigate the design of the deck overhang and determine whether reduced amounts of reinforcement are possible.

For Volume 1 (Replacement Strategies), three phases of research were conducted. First, an overview of current practice for addressing historic bridge railings was performed. Second, an investigation was conducted to document historic bridge railings in Indiana. Finally, rehabilitation solutions were developed to address the specific bridge railings found in Indiana. Based on this research, three retrofit strategies were developed: inboard railing, curb railing, and simulated historic railing. These rehabilitation solutions can be used to address historic bridge railings not only in Indiana, but also across the country.

For Volume 2 (Bridge Deck Overhang Design), experimental testing of half-scale and full-scale overhang specimens was conducted, and the results were analyzed. Failures of in-service bridge railings were also evaluated. Based on this research, recommendations are provided for the more efficient and economic design of bridge deck overhangs which are applicable not only for historic bridges, but for all concrete bridge decks.

Findings

Volume 1: Replacement Strategies

Indiana's historic bridge inventory was investigated to determine how many historic bridges remain in service as well as to document the types and variety of historic railings in existence. As of January 2014, 658 historic bridges remain in service in Indiana, on which 61 different historic railings were identified. Of these, 7 railing types, along with bridges with no railing, constitute two-thirds of the entire inventory. It is interesting that of the other railings, 25 occur on only one bridge and 11 occur on only two bridges. Therefore, 59% of the different railing types are unique. Based on this analysis, research focused on addressing the most common railings identified. However, an attempt was also made to address as many of the unique railings as possible.

Three different options utilizing modern, previously crash tested railings were identified to upgrade the railings on Indiana's historic bridges. The first option is to install a modern railing inside the original railing. When this option is exercised, the original railing may remain on a bridge. The second option is to install a special inboard railing on the curb. This special railing, which can be used if the bridge has a sidewalk, protects pedestrians on the sidewalk and allows the original railing to be retained. The third option is railing replacement. A collection of approved, crash-tested railings developed by a number of states was used as a baseline to design simulated railings to approximate the appearance of historic railings.

Simulated railings were developed to cover a variety of historic concrete and steel railings. These railings maintained the overall structure and crash-resistant geometry of the base railing while integrating geometric features of the historic railing. In all, it was possible to simulate 42 of the historic railings existing in Indiana. These railings cover 66.3% of all historic bridges in the state. Three timber railing types, which were not considered in the scope of this research, accounted for 8.4% of all historic bridges in the state. Sixteen railing types did not possess a historic look, did not possess acceptable geometry, or did not exemplify historic craftsmanship. These railings accounted for 25% of all historic bridges in the state.

Volume 2: Bridge Deck Overhang Design

Based on the experimental testing program, along with analysis of the results, the following findings were made:

1. A diagonal tension failure in the deck overhang/barrier joint is a potential failure mode. However, this failure mode is only possible for very short bridge lengths (<30 ft) and will not control the capacity of the overhang/barrier system of a typical bridge deck.
2. The strength of the overhang/barrier wall system is controlled by punching shear rather than the yield-line mechanism. This finding is significant in that design of the overhang according to AASHTO requirements is based on the yield line strength. Reviews of in-service barrier impacts support the finding that punching shear controls the capacity of the system, with field failures producing the same failure surfaces as observed in the laboratory.
3. Barrier impact loads are transferred to the bridge system through the deck overhang over a large distribution length. Load was found to be distributed to the overhang at least 10 times the horizontal loading dimension (L_t), significantly larger than considered by current design provisions. Because of this very effective distribution, there are significantly lower demands on the overhang reinforcement from the barrier impact force than considered using current design provisions. Consequently, a significant reduction in transverse reinforcement relative to that currently required by the AASHTO design specification can be achieved.

Implementation

There are two primary targets for implementation of the results of this research: recommendations regarding upgrading historic bridge railings and recommendations regarding design of bridge deck overhangs. The recommendations regarding bridge deck overhang are generally applicable for both new and rehabilitation projects.

Upgrading Railings

Through the use of the strategies developed in this research program, it is possible to retain historic railing appearance for the

majority of historic bridges in Indiana. In many cases, it is also possible to improve aesthetics. Most importantly, however, these strategies allow for improvement in the safety of the traveling public.

Bridge Deck Overhangs

It is recommended that the bridge deck overhang be designed based on vertical forces. Considering the very effective lateral force transfer to the overhang and the maximum applied lateral force as limited through the punching shear capacity of the barrier, design of the overhang to resist the lateral impact force is not required. If the lateral impact force is to be considered, two modifications from current design requirements as specified by AASHTO are recommended:

1. Applied lateral force should be based on the lesser of the punching shear strength of the barrier and the yield line strength.
2. The deck overhang distribution length should be considered as $10L_t$, where L_t is the longitudinal length of distribution of impact force.

By implementing these recommendations, significant cost savings can be realized through the reduction of reinforcement required in the bridge deck overhang.

CONTENTS

LIST OF TABLES

LIST OF FIGURES

1. INTRODUCTION

1.1 Background

An essential component of the rail system is the connection to the bridge deck. Forces resisted by the rail are transferred to the bridge desk typically through the bridge deck overhang. Bridge deck overhangs and structural railing systems function concurrently to withstand collision force effects and contain vehicles on the roadway. Since 1994, the AASHTO Bridge Design Specifications have set requirements for overhang design based upon crashworthiness (AASHTO, 1994). These provisions result from the performance of bridge railings subject to crash testing as conducted by the National Cooperative Highway Research Program (AASHTO, 2014). Based upon the crash test data, AASHTO has rated traffic railings with respect to different collision forces and geometries. These specified design forces have direct implications to the manner in which the overhang is designed. The overhang region is designed to withstand effects from the forces applied to the barrier as well as dead loads and live loads, which are considered in three design cases (AASHTO, 2014).

Due to a recent increase in AASHTO rail forces along with the AASHTO design philosophy, a significant increase in reinforcement relative to past practice is required in the overhang. While this increase is being realized for all bridge decks, increases in both the forces and corresponding reinforcement may pose particular challenges for the attachment of railing to historic bridges.

1.2 Design Force History

Historically bridge railings were designed using a 10 kip transverse force with an elastic analysis (Bligh, Briaud, Kim, & Abu-Odeh, 2010). The increased crash test forces from the NCHRP Report 350 (Ross, Sicking, & Zimmer, 1993) were adopted into the first edition of the AASHTO LRFD specifications with plastic analysis procedures (Bligh et al., 2010). There is an evident recognition in AASHTO that current crash test forces are conservative. According to the 7th edition of the AASHTO LRFD, "The crash testing program is oriented toward survival, not necessarily the identification of the ultimate strength of the railing system" (AASHTO, 2014). Using conservative crash test forces greatly influences the required strength of the overhang. Hence, research is needed to evaluate the overhang system and further optimize bridge deck overhang design.

1.3 Objective and Scope

The objective of this research is to investigate the design of the deck overhang and determine whether reduced amounts of reinforcement in the deck overhangs are possible while maintaining safety requirements. The ability to use a reduced amount of steel within the overhang region can make the bridge more economical and also improve constructability. Experimental testing of half scale and full scale overhang specimens was conducted and the results were analyzed. Failures of in-service bridge railing were also evaluated. Based on the results, recommendations are provided for the more efficient design of bridge deck overhangs and are applicable for both new and rehabilitation projects.

2. BRIDGE RAILING DESIGN

2.1 Yield Line Analysis Background

Yield Line analysis was developed by Ingerslev and further advanced by K.W. Johansen. It provided a tool for computing the ultimate capacity of concrete slabs with any reinforcement configuration (Darwin, Nilson, & Dolan, 2010). When the theory was taken from Sweden to the US through Hognestad, it became the dominant method for calculating slab capacities. This tool is based upon the fundamental principles of virtual work and statics.

When loading a slab, yielding will occur in regions where moment demand is high, and a yield line mechanism will form based upon the geometry and boundary conditions. This mechanism is analyzed based upon the resistance it provides against rotation. Yield line analysis is advantageous because it enables conservative calculation of ultimate resistance without more sophisticated analysis techniques. The capacities calculated through yield line theory are generally 80 to 90 percent of test results due to additional mechanisms that add capacity such as arch action and strain hardening (Hognestad, 1953). While solutions obtained from yield line analysis are not exact, they provide a good measure of ultimate resistance and are utilized in practice for the design of bridge railings.

2.2 AASHTO Yield Line Application

The seventh edition of the AASHTO Bridge Design Specifications adopts yield line analysis for the design of railings with expected failure patterns. Section thirteen of the specification states that yield line analysis and strength design for reinforced concrete and prestressed concrete barriers or parapets may be used (AASHTO, 2014). For this analysis technique to be applicable, the following assumptions must hold: the deck must have adequate strength to force the yield line pattern to occur only in the parapet, the railing must be long enough to develop the proper yield line, and the negative and positive yield moments must be equal for the wall and beam components (AASHTO, 2014).

2.3 Derivation of Yield Line Equations

T. J. Hirsch derived the expression in AASHTO for railing strength through application of the yield line analysis (Hirsch, 1978). The expression can be derived using principles of virtual work and equating external work to internal work. The external work is calculated as the transverse load multiplied by the deformed area under the load. Likewise, the internal work is computed by considering the moment resistance multiplied by the

angle which the element moves through. Equating external and internal work enables for the determination of the ultimate load capacity of the railing.

Concrete parapet bridge rails are analyzed with respect to the height of the rail, length of the distributed loading, and critical wall length of the mechanism. The yield line mechanism for a concrete parapet wall is illustrated in Figure 2.1. Derivation for the yield line equations is provided in Appendix A, and the equations as derived from Hirsch (1978) are presented by Equations 2.1 through 2.4.

Equations from Hirsch (1978) Derivation

$$W_{EXT} = \frac{F_t \Delta L_t \left(L_c - \frac{L_t}{2}\right)}{L_c} \tag{2.1}$$

$$W_{INT} = \frac{8M_b\Delta}{L_c} + \frac{8M_w\Delta}{L_c} + \frac{L_c M_w \Delta}{H} \tag{2.2}$$

$$R_w = \frac{2}{2L_c - L_t}\left[8M_wH + 8M_b + \frac{M_c {L_c}^2}{H}\right]$$

AASHTO A13.3.1−1 (2.3)

$$L_c = \frac{L_c}{2} + \sqrt{\left(\frac{L_t}{2}\right)^2 + \frac{8HM_b}{M_c} + \frac{8HM_w}{M_c}} + \frac{L_t}{2}$$

AASHTO A13.3.1−2 (2.4)

where:

W_{EXT} = total external work applied to the system, kip-ft
W_{INT} = total internal work resisted by the system, kip-ft
F_t = transverse force, kip
L_t = length of transverse force, ft
L_c = critical length of yield line mechanism, ft
M_b = resisting moment of beam component, kip-ft
M_c = resisting moment about longitudinal axis, kip-ft/ft
M_w = resisting moment about vertical axis, kip-ft
H = height of parapet barrier, ft
Δ = virtual deflection of barrier
R_w = nominal railing resistance, kip

Equation 2.1 represents the total external work applied to the system from the transverse force multiplied by the length of the applied load. This external work is set equal to the internal work, provided by the barrier from resisting moment capacities (Equation 2.2). The total railing resistance is represented in Equation 2.3 and designated in AASHTO by Equation A13.3.1-1. Likewise, the critical length of the yield line mechanism was found by differentiating Equation 2.3 with respect to L_c which provides the minimum energy for the developed yield line pattern. Equation 2.4 characterizes the critical length of the yield line mechanism and is presented in AASHTO Equation A13.3.1-2. Through the application of both equations, the overall resistance of any concrete parapet barrier can be determined according to the yield line analysis technique.

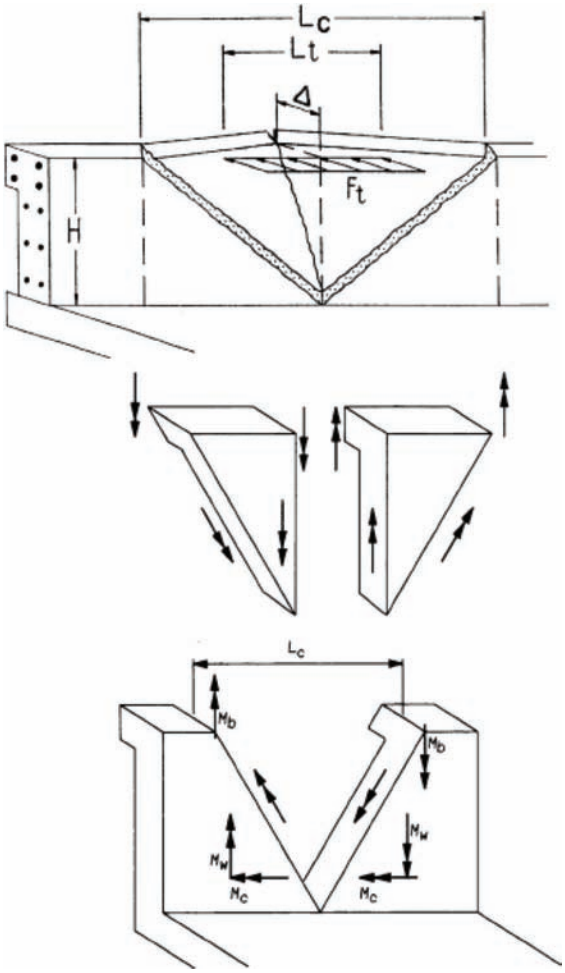

Figure 2.1 Yield line analysis mechanism (AASHTO, 2014).

2.4 Concrete Parapet Railing Calculation

In determining the ultimate resistance of a bridge railing, AASHTO equations A13.3.1-1 (Equation 2.3) and A13.3.1-2 (Equation 2.4) are utilized. The total resistance hinges upon the critical length of the yield line, length of transverse force, height of railing, and corresponding moment resistances about each axis. The geometry and design forces of a railing are specific to the associated test level category which directly affects the total railing resistance as computed through yield line analysis. Railing capacity is crucial to the design of the overhang region as the overhang itself must resist the axial forces and moment developed from loading the parapet. These design forces directly impact the amount of reinforcement provided within the overhang and will be discussed further in Chapter 3. Design forces for TL-1 through TL-6 are shown in Table 2.1, and the railing capacity procedure is illustrated in detail in Appendix B (Example 1).

TABLE 2.1
Railing Design Forces (AASHTO 2014)

Design Forces and Designations	Railing Test Levels					
	TL-1	TL-2	TL-3	TL-4	TL-5	TL-6
F_t Transverse (kips)	13.5	27.0	54.0	54.0	124.0	175.0
F_L Longitudinal (kips)	4.5	9.0	18.0	18.0	41.0	58.0
F_v Vertical (kips) Down	4.5	4.5	4.5	18.0	80.0	80.0
L_t and L_L (ft)	4.0	4.0	4.0	3.5	8.0	8.0
L_v (ft)	18.0	18.0	18.0	18.0	40.0	40.0
H_e (min) (in.)	18.0	20.0	24.0	32.0	42.0	56.0
Minimum H Height of Rail (in.)	27.0	27.0	27.0	32.0	42.0	90.0

Example 1 illustrates the process for computing the ultimate railing capacity given a specified geometry and reinforcement. The moment capacities are computed neglecting compression reinforcement and provide a good estimate of railing strength. In practice, the variability of concrete compressive strengths, variable yield strengths for steel, and fabrication limitations justify this approximate analysis of an exact railing system.

2.5 Effect of Reinforcement on Railing Resistance

M_c and M_w contribute to the overall railing resistance of the parapet as calculated through yield line analysis. The steel positioned along the vertical axis in the barrier contributes to M_c while steel along the longitudinal axis impacts M_w. As a matter of convention, it should be noted that "longitudinal steel" refers to the steel along the longitudinal axis of the parapet and "vertical steel" refers to steel along the vertical axis. Overall railing strength can be quantified by determining the individual contributions of M_c and M_w to calculate railing resistance. This perspective gives engineers insight in regards to optimizing reinforcement and proportioning M_c and M_w to cost effectively achieve the required railing resistance. An analysis was made between the M_c/M_w ratio and the contribution to overall railing capacity as calculated through yield line analysis. Concrete parapet barriers with a TL-4 rating were analyzed from the Oregon Department of Transportation (ODOT), Texas Department of Transportation (TxDOT), and Indiana Department of Transportation (INDOT) to determine typical M_c/M_w ratios in design. Calculations are provided in Appendix B.

The ratio of the cantilever wall moment (M_c) to wall moment (M_w) was determined from the proportioning of vertical and longitudinal steel in the parapet in each DOT detail. For an equal comparison, a typical concrete railing with an identical TL-4 rating was selected from each Department of Transportation. To further quantify the effect from the moment ratio, a study was performed to investigate the effect of different moment ratios to overall railing resistance. As listed in Table 2.2, ODOT uses more vertical reinforcement in the parapet compared with TxDOT or INDOT. Overall, there is a significant variation in this ratio.

The focus within this M_c/M_w analysis is geared toward TL-4 barriers due to their prevalence in practice, although different test levels experience similar results. As previously shown, the Hirsch (1978) equations were developed according to yield line analysis to calculate the railing resistance of a concrete parapet barrier. These equations were used to calculate the clear length of the yield line with varying ratios of M_c/M_w (Figure 2.2). For these calculations, the moment resistance from the beam component (M_b) did not contribute. As shown, with lower M_c/M_w ratios, the length of the yield line mechanism increases while higher ratios result in lower L_c values.

The effect of the railing resistance contribution was determined for an INDOT type FC barrier as shown in Figure 2.3. As previously mentioned, the M_c/M_w ratio is the moment capacity of the vertical steel positioned in the barrier divided by the moment capacity of the longitudinal reinforcement in the barrier. For the INDOT Type FC analysis, the M_c/M_w ratio is 0.40. The contribution of moments was computed with varying clear lengths from 3 to 16 ft. It was determined that with greater L_c values, the effect of M_c has significantly more of an effect on nominal resistance with respect to M_w. This is true despite the 1.24 in^2 of longitudinal reinforcement compared to 0.47 in^2 of vertical steel in the barrier. For this INDOT TL-4 railing, M_c dominates the railing capacity at an L_c value greater than approximately 7 ft. This behavior is due to the fact that

TABLE 2.2
Typical TL-4 Concrete Barrier Reinforcement

State	Rail Designation (TL-4)	A_{sc} ($in.^2$/ft)	A_{sw} ($in.^2$/ft)	H_r (in.)	M_c/M_w	R_w (kip)
INDOT	FC	0.47	1.24	32	0.40	150
TxDOT	T221	0.40	0.80	32	0.52	119
ODOT	32" Concrete Parapet	0.48	0.80	32	0.64	97

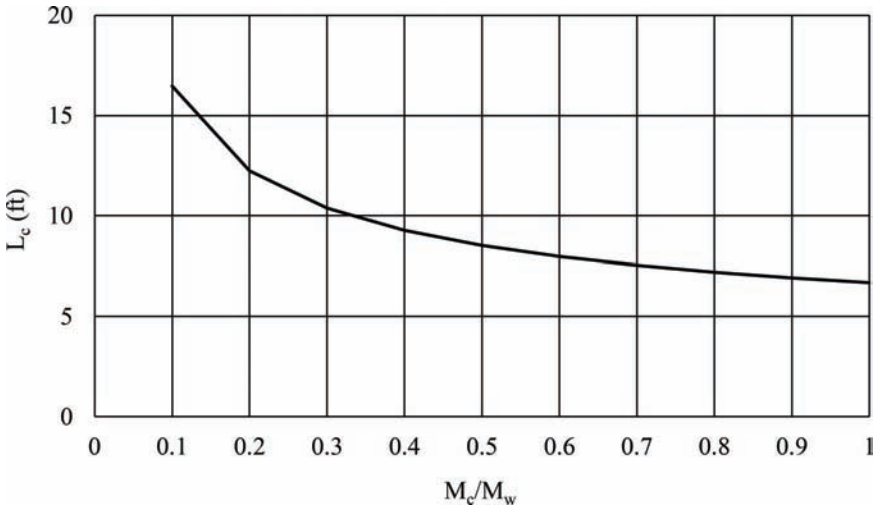

Figure 2.2 Impact of moment ratio on critical length.

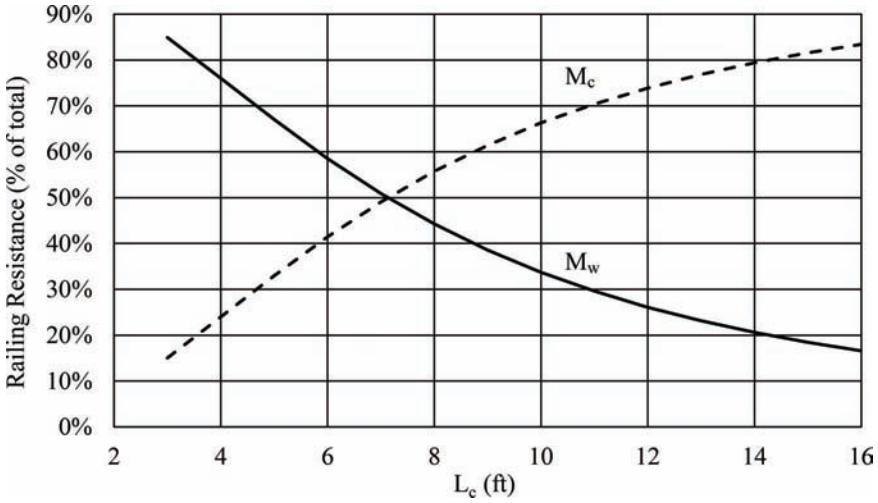

Figure 2.3 Contribution of moment ratio to railing resistance (INDOT Type FC).

the M_c moment is multiplied by the clear length squared in computation of railing resistance while M_w is multiplied by a factor of eight in the Hirsch (1978) equation for R_w. From the derivation of the yield line equations, the angle of rotation for M_c is larger, which explains the greater contribution. Adding more M_c reinforcement relative to M_w has more of an effect on the overall capacity of the railing. The standard INDOT railing actually has an L_c of 9.4 ft as computed in Appendix B. For this L_c, M_c is shown to provide approximately 65% of the overall resistance.

Due to the effect of M_c, placing more vertical reinforcement in the parapet will enable for a large amount of resistance with relatively small amounts of additional reinforcement. On the contrary, much more substantial amounts of reinforcement are needed longitudinally to offer the same effect. Given the influence of vertical and longitudinal reinforcement, railing resistance with less reinforcement can be provided if proportions are optimized. From Table 2.2, ODOT has a M_c/M_w ratio of 0.64 for a typical TL-4 concrete parapet barrier which exceeds INDOT and TxDOT with 0.40 and 0.52, respectively. The greater proportioning of vertical reinforcement allows ODOT and TxDOT to use less longitudinal reinforcement within the barrier while achieving a comparable railing capacity exceeding the minimum resistance specified in Table 2.1.

2.6 Summary

The capacities of bridge railings are calculated using yield line analysis. Through an analysis of the yield line mechanism developed by Hirsch (1978), the effect of vertical and longitudinal reinforcement was investigated to provide tools for optimizing barrier design. It was determined that vertical reinforcement is more effective with respect to total railing resistance. In considering barrier design alone, this reinforcement should be used to more economically resist the barrier loads. Through optimized design of the reinforcement, it is

possible to reduce the total railing resistance. For barriers all meeting TL-4 requirements, the railing resistance can be substantially different as shown in Table 2.2. The railing resistance of the ODOT barrier is reduced by approximately 35% from the INDOT barrier. This has substantial implications for overhang design as will be discussed in the next chapter.

3. BRIDGE OVERHANG DESIGN

3.1 Introduction

The bridge deck overhang is a crucial component of a structural railing system. These overhangs support the bridge railing and must be designed to withstand forces from impact and service load conditions. The AASHTO design strategy pushes the failure mode to occur within the barrier as opposed to the overhang to ease repairs and maintain integrity of the deck. To withstand high transverse forces applied to the parapet, the overhang is typically designed with significantly more reinforcement as compared to adjacent interior bays. Due to changes to the AASHTO provisions in recent editions of the design specifications, greater reinforcement is needed in the overhang region as compared with older designs.

3.2 AASHTO Overhang Design Process

According to AASHTO, deck overhangs are designed with respect to three different design cases and two limit states, extreme event and strength (AASHTO, 2014). The strength limit state refers to the maximum capacity each structural member may experience, and the extreme event limit state considers the effect from natural disasters, extreme weather events, or collisions which may impact the integrity of the bridge. The design cases for the overhang are listed below:

- Design Case 1 consists of transverse and longitudinal forces specified in Article A13.2- Extreme Event Load Combination II limit state.
- Design Case 2 refers to vertical forces specified in Article A13.2- Extreme Event Load Combination II limit state.
- Design Case 3 consists of the loads specified in Article 3.6.1 that occupy the overhang- Load Combination Strength I limit state.

The overhang length is generally taken from the critical girder section to the edge of the slab. There are two critical design sections which must be considered when designing the overhang region for Design Case 1: the face of the barrier and the section over the adjacent beam illustrated in Figure 3.1 According to AASHTO Article A4.6.2.1.6, the design section criterion depends on the type of structural element supporting the overhang (AASHTO, 2014). For instance, the critical design location (Section 2-2) for steel I beams is taken as one quarter of the flange width from the centerline of the beam to the design section. Similarly, concrete beams are computed as one third the flange width from the beam centerline to the critical section, and monolithic elements without top flanges are taken at the face of the

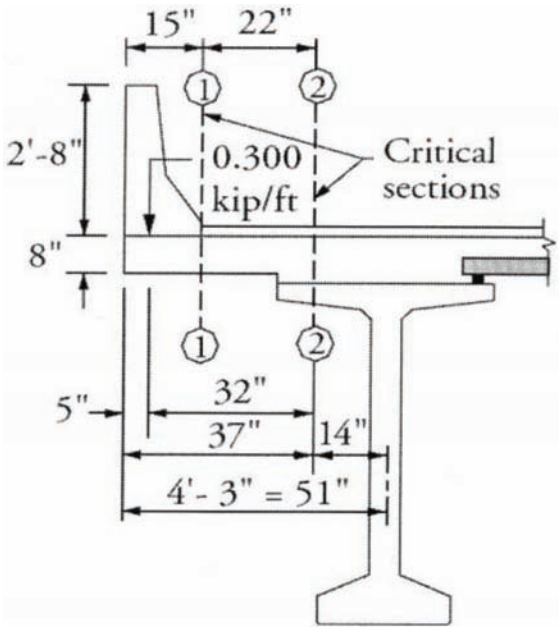

Figure 3.1 Overhang design sections (PCI, 2011).

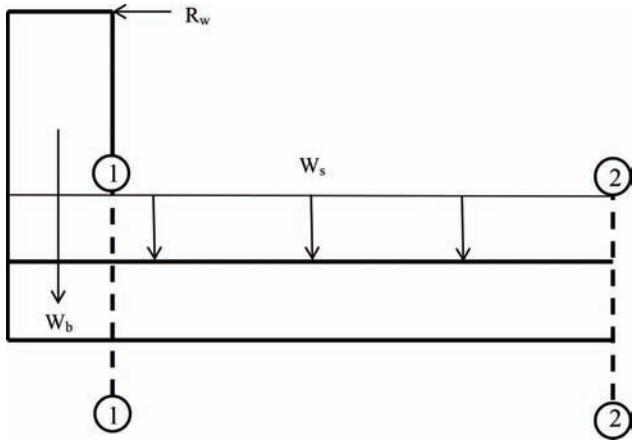

Figure 3.2 Design Case I loading configuration.

supporting element. Critical section 1-1 is always taken at the face of the parapet barrier to account for the possibility of failure at the slab barrier interface. The controlling design section is considered for each design case, and reinforcement is then proportioned to accommodate the greatest moment demand.

3.2.1 Design Case 1

Regarding Design Case 1, the overhang must be designed to resist the moment generated from the self-weight of the slab and barrier in addition to the transverse and longitudinal forces listed in Table 2.1. These loads are designed to simulate moments and forces generated when a vehicle collides with the railing system. The forces are shown in Figure 3.2, and reinforcement is provided based upon the developed tension force and moment within the slab. For critical sections 1-1 and 2-2, the distribution of tension (T) and moment (M_u)

are provided in Equations 3.1 through 3.5 in accordance with AASHTO (2014) and the PCI Bridge Design Manual (2011).

Design Case 1 @ Section 1-1.

$$T = \frac{R_w}{L_c + 2H} \tag{3.1}$$

$$M_u = M_{c1} + \frac{5}{4}(M_s + M_b) \tag{3.2}$$

where:
T = tensile force at slab level, kip/ft
M_u = total factored moment demand in slab, kip-ft/ft
M_b = self-weight moment of barrier, kip-ft/ft
M_s = self-weight moment of deck, kip-ft/ft
M_{c1} = overturning moment of parapet at Design Section 1-1, kip-ft/ft
H = barrier height, ft
L_c = critical length of the yield line mechanism, ft
R_w = nominal railing resistance, kip

For Section 1-1 the tensile force (T) is computed from AASHTO equation A13.4.2-1 (Equation 3.1), and the ultimate moment is determined by considering the overturning moment of the barrier along with factored moments of the slab (M_s) and barrier (M_b). The overturning moment from the parapet wall (M_{c1}) will likely control the design of the overhang as the moment from self-weight is minimal in comparison. M_{c1} is the flexural capacity of the barrier with respect to the vertical reinforcement.

Design Case 1 @ Section 2-2.

$$T = \frac{R_w}{L_c + 2H + 2L_{ds}\tan(30)} \tag{3.3}$$

$$M_{c2} = \frac{M_{c1}L_c}{L_c + 2L_{ds}\tan(30)} \tag{3.4}$$

$$M_u = M_{c2} + \frac{5}{4}(M_s + M_b) + \frac{3}{2}M_{ws} \tag{3.5}$$

where:
L_{ds} = distance Design Section 1-1 and 2-2, ft
M_{c2} = overturning moment of parapet at Design Section 2-2, kip-ft/ft
M_{ws} = self-weight moment of wearing surface, kip-ft/ft

The design moment (M_{c2}) is computed by distributing (M_{c1}) at an angle of 30 degrees within the slab from the face of the barrier to Design Section 2-2 as shown in Figure 3.3 (PCI, 2011). Likewise, the tension force is distributed an additional 30 degrees from the barrier face to Design Section 2-2. This distribution length is determined based upon engineering judgment and some designers use 45 degrees rather than 30 degrees (Wassef, Smith, Clancy, & Smith, 2003). The ultimate moment is then computed considering M_{c2} from force effects along with factored moments of the slab (M_s), barrier (M_b), and the contribution of the wearing surface (M_{ws}).

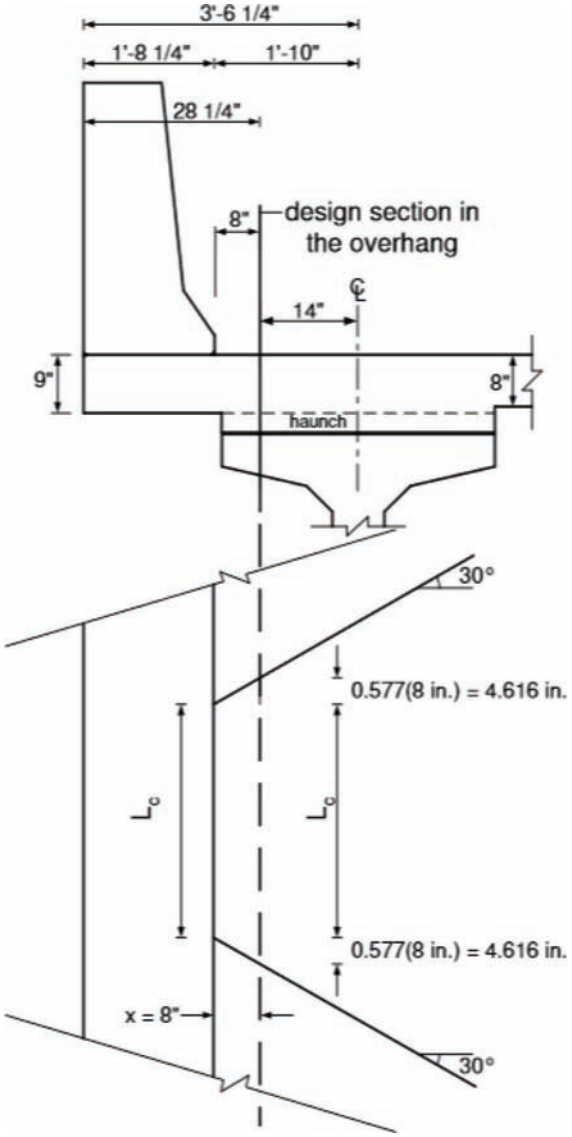

Figure 3.3 Assumed distribution of forces in the overhang (Wassef et al., 2003).

3.2.2 Design Case 2

The next check required is for Design Case 2, which considers vertical force effects. Design Case 2 is representative of a vehicle sitting atop the bridge railing in the case of a rollover incident. When checking this design case, the overhang is designed for applied vertical forces at the edge of the railing as shown in Figure 3.4. The moments produced by this vertical force effect act in conjunction with the moment generated by the self-weight of the slab to produce the ultimate factored demand in the slab. This ultimate value for moment is computed from multiplying the vertical force specified in Table 2.1 by the lever arm to the edge of the overhang. The loading

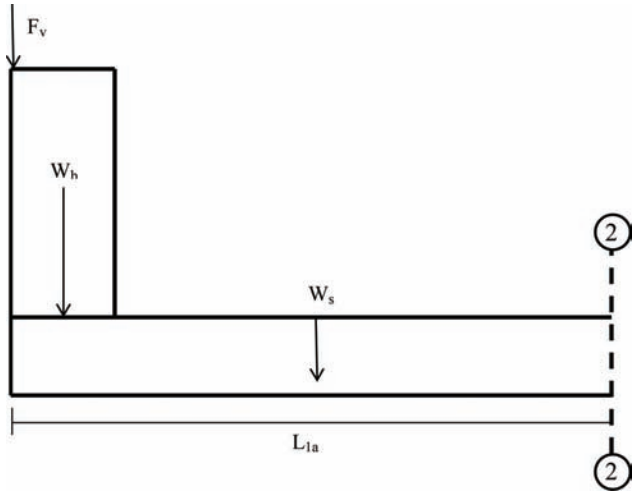

Figure 3.4 Design Case 2 loading configuration.

configuration is shown in Figure 3.4 with respect to Design Section 2-2.

Design Case 2 @ Section 2-2.

$$M_u = \frac{F_v L_{la}}{L_v} + \frac{5}{4}(M_s + M_b) + \frac{3}{2} M_{ws} \qquad (3.6)$$

where:
L_{la} = length of lever arm from applied force, ft
F_v = vertical force applied to barrier, kip
L_v = length of vertical force distribution, ft

3.2.3 Design Case 3

For Design Case 3, the overhang is designed for dead and live loads which occupy the overhang at any given instant of time. The previous design cases consider collision forces and dead loads, but this design case integrates live load effects using the design truck. The HL-93 design truck is considered when calculating the vehicular live load effect. As shown in Figure 3.5, the design truck has two 32 kip axles with a variable spacing between 14 ft and 30 ft to produce the maximum force effect. The transverse spacing of the wheels is specified as 6 ft. In addition, the design tandem needs to be considered which is a pair of 25 kip axle loads spaced 4 ft apart (AASHTO, 2014). This design case attempts to simulate the effect of a truck traveling in the overhang region as a result of swerving from lane of travel.

For design purposes, the live load is based upon the greater of the design truck coupled with a design lane load of 0.64 kips per linear foot in the longitudinal direction or the design tandem in conjunction with the design lane load (AASHTO, 2014). The static effect of either the design tandem or design truck is further scaled by an impact factor and multiple presence factor to account for impulsive loading and the effect of multiple loaded lanes.

On bridges, the number of loaded lanes with variable roadway widths affects the distribution of moments.

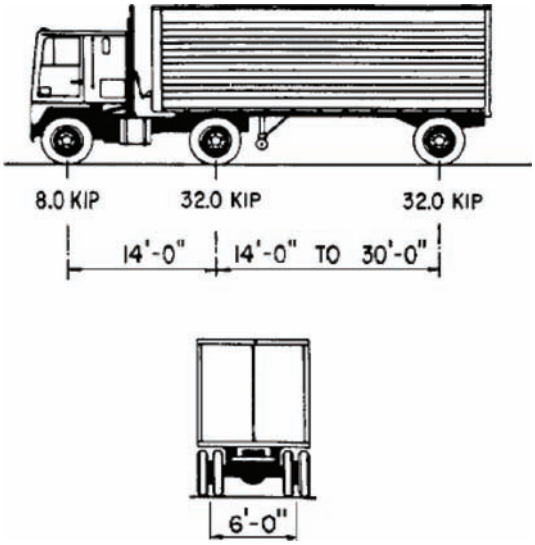

Figure 3.5 HL93 design truck (AASHTO, 2014).

TABLE 3.1
Multiple Presence Factors (AASHTO, 2014)

Number of Loaded Lanes	Multiple Presence Factors, m
1	1.20
2	1.00
3	0.85
>3	0.65

The maximum live load force effect is calculated by considering all combinations of loaded lanes multiplied by a multiple presence factor (AASHTO, 2014). This factor accounts for the probability of simultaneous loading of design lanes with the design truck. The code specifies that the engineer is required to select the worst design case with the corresponding multiple presence factors. The factors in Table 3.1 are considered on the basis of an average daily truck traffic (ADTT) of 5000 trucks in one direction (AASHTO, 2014).

Design Case 3 @ Section 2-2

$$D_l = 45 + 10X \qquad (3.7)$$

$$M_{LL+I} = \frac{W_l}{D_l}(X)(1 + IM)(m) \qquad (3.8)$$

$$M_u = \frac{5}{4}(M_s + M_b) + \frac{3}{2} M_{ws} + \frac{7}{4} M_{LL+I} \qquad (3.9)$$

where:
D_l = distribution length of wheel load, ft
W_l = design truck wheel load, kip
IM = dynamic loading factor
m = multiple presence factor
M_{LL+I} = moment produced by live load and impact, kip-ft/ft
X = distance from wheel load to support, ft

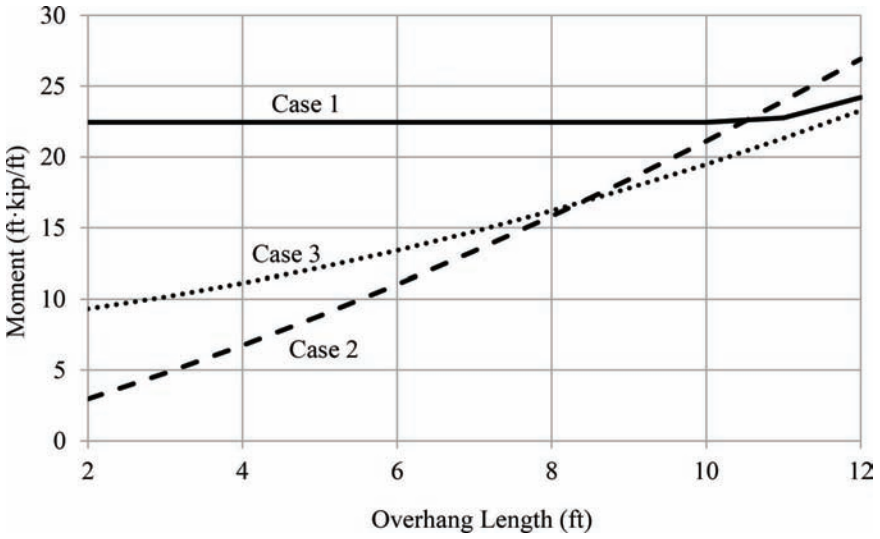

Figure 3.6 INDOT Type FC design moments.

For this case, the dead loads for the railing system are considered along with a 16 kip design truck wheel load (W_l) placed 1 ft from the face of the barrier. In design, the 16 kip wheel load is distributed over an assumed distribution length for calculation of ultimate moment. Subsequently, the axle load is multiplied by a multiple presence factor and further scaled by a dynamic loading factor. The final moment generated from the combination of these is compared with other design cases for the controlling value.

3.3 AASHTO Design Case Comparison

In designing overhangs, careful consideration needs to be given to each design case along with a basic understanding of how the railing system geometry can affect the ultimate moment. The main parameters include overhang length along with the type of railing and test rating of the barrier. Varying these parameters affects the design collision force and moments generated. For this design case comparison, a TL-4 INDOT Type FC railing is analyzed.

As illustrated in Figure 3.6, the overhang length primarily influences the design moments. It is evident that with shorter overhang lengths, Design Case 1 controls due to the fact that the majority of the design moment comes from collision forces at Design Section 1-1. However, when increasing the overhang length, Design Case 2 and 3 become notable contributors as the self-weight moment becomes more significant. In terms of Design Case 2, the design moment is approximately linearly dependent on the overhang length as the vertical force on the barrier remains constant (the self-weight introduces nonlinearity). As shown, the total moment is more prominent and becomes significant at greater overhang lengths. Due to the fact that overhangs are typically designed in the 4 to 5 ft maximum range, Case 2 does not control for TL-4 concrete barriers. Another interesting consideration to note is the impact of Design Case 3. This design case will control under conditions with less transverse force applied to the barrier (weaker rails) as this Case captures an axle force of 16 kip in the overhang.

In Design Case 1 of the AASHTO overhang design procedure, the overhang is designed to withstand the axial tensile force from transverse loading and the full moment capacity of the concrete parapet barrier at its base (M_c). Often in practice, concrete parapet barriers are designed with significantly more railing resistance than specified in the AASHTO code. Many state DOTs have typical concrete parapet designs that are used based on historical factors which have resulted in standardized systems for that locale. Typically, the reinforcement provided in these parapet barriers will contribute to a final railing resistance 150-300% of the transverse force required by code.

The AASHTO overhang design procedure requires the overhang to be designed for the full moment capacity (M_c) of the barrier, thus the amount of reinforcement proportioned in the overhang is controlled by the barrier design. The overhang need only resist the moment and axial forces generated by the minimum test level capacity, but because the parapet is overdesigned, the overhang is governed by the parapet and is also overdesigned. According to AASHTO, "The crash testing program is oriented toward survival, not necessarily the identification of the ultimate strength of the railing system" (AASHTO, 2014). AASHTO further asserts, "This could produce a railing system that is significantly overdesigned, leading to the possibility that the deck overhang is also overdesigned" (AASHTO, 2014). The forces listed in Table 2.1 are generated by crash testing programs, and all tabulated values are based upon safe design. If the conservatism of the crash testing program allows for safe design, designing a barrier which exceeds the design loads results in an overdesigned overhang. Due to the fact that crash testing forces dictate the maximum moment and axial force resisted by the overhang,

there exists a double-penalty resulting from using the overdesigned capacity of the parapet with respect to conservative crash test forces.

3.4 Bridge Deck Reinforcement

Several states are taking measures to reduce the amount of steel used in concrete bridge decks. Many states, such as TxDOT recognize the inherent overdesign and have switched to a more economical deck design scheme. TxDOT in particular has shifted toward empirical bridge deck design as opposed to the traditional method of design. According to TxDOT engineers, the previous top mat in bridge decks designed according to the traditional method used 3 lbs/ft^2 of reinforcement compared to newer empirical deck design with 1.8 lbs/ft^2 (Holt & Smith, 2014). The reduction of steel is nearly 40%, which provides a more efficient, more constructable, and cost effective design.

This shift in reinforcement is based upon research conducted by Beal (1981) in terms of bridge deck capacity. The research indicated that the failure mechanism of bridge decks is typically punching shear rather than flexure as previously suggested. Likewise AASHTO suggests that due to internal arching in the deck, in-plane membrane forces develop from heavily confining structural elements and leads to a punching shear failure before reaching the full flexural capacity (AASHTO, 2014). TxDOT has also indicated that a number of bridges were designed in the early to middle 1980's with an empirical deck design and through observation, these decks are performing comparable to traditional deck designs (Holt & Smith, 2014). The bridge deck has more than sufficient strength when designed with either method as the traditional approach results in a factor of safety of ten and the empirical design method gives a factor of about eight (AASHTO, 2014).

While the empirical design method significantly reduces the amount of steel required in bridge decks, the same is not true for overhangs. According the AASHTO Article 9.7.2.2, the empirical design method does not apply to overhangs (AASHTO, 2014). It is further stated, "Although current tests indicated that arch action may exist in the cantilevered overhang, the available evidence is not sufficient to formulate code provisions for it" (AASHTO, 2014). The effect of arching action would provide more inherent strength to the slab and reduce the amount of reinforcement placed in the overhang region. Physical tests are needed to determine how much excess capacity is contributed to arching action and the relative distribution of forces along the length of the overhang.

3.5 Reduced Overhang Design

3.5.1 INDOT Method

Contrary to the AASHTO method of overhang design, INDOT has taken a different approach in an attempt to minimize overdesign of the overhang. As opposed to designing the overhang for the full resistance of the parapet, INDOT reduces the overturning moment at the base of the parapet. This approach strays from the AASHTO philosophy of designing the overhang for the full capacity of the parapet. The INDOT approach recognizes that the parapet and overhang are not designed for the same capacity, but both can accommodate the minimum transverse force according to AASHTO. As opposed to designing the overhang for the resistance of the overdesigned parapet, the design moment is significantly reduced.

In designing the overhang, INDOT determines the collision design force by taking 125% of the transverse collision force provided by AASHTO. According to the INDOT Design Manual (2008), "Based on observations of impacted bridge railings, an overhang designed according to previous AASHTO bridge-design specifications shows the desired behavior that the overhang does not fail if a railing failure occurs due to a collision." INDOT further states that "the overhang should be designed for a collision force 25% greater than the required capacity, which results in a design approximating present satisfactory practice" (INDOT, 2008).

From this collision force, the axial tension force and overturning moment at the base of the parapet are used to design the overhang. From Hirsch (1978) Equation 2.3 for computing railing resistance, INDOT uses the 125% transverse force (F_t) as R_w and calculates M_c with the conservative assumption that M_w does not contribute to railing resistance ($M_b = 0$ for this rail type). Likewise, the tensile force at the slab level is computed using 125% of the required F_t from Table 2.1, replacing R_w in Equation 3.1. For this method, is important to note that L_c is based on the actual rail geometry. The approach is expressed by Equations 3.10 and 3.11. The results obtained from the INDOT method of overhang design satisfy the design force requirements but deviate from the design philosophy of AASHTO which is based on the capacity of the rail used.

$$R_w = \frac{2}{2L_c - L_t}\left[8M_wH + 8M_b + \frac{M_cL_c^2}{H}\right] \tag{2.3}$$

$$1.25F_t = \frac{2}{2L_c - L_t}\left[0 + 0 + \frac{M_cL_c^2}{H}\right] \tag{3.10}$$

$$T = \frac{R_w}{L_c + 2H} \tag{3.1}$$

$$T = \frac{1.25F_t}{L_c + 2H} \tag{3.11}$$

3.5.2 Alternative Method

Contrary to the INDOT method of overhang design, some engineers take a different approach with further reduces the design moment according to AASHTO. This approach uses 125% of the AASHTO transverse collision force multiplied by the total height of the railing to obtain a moment demand as listed in

TABLE 3.2
Method Specific Overhang Requirements (Sample TL-4)
Overhang Requirements for Sample TL-4 Barrier (L_c = 12.7 ft, R_w = 134 kip, H = 2.75 ft)

Method	M_c (kip-ft/ft)	T (kip/ft)	Primary Reinforcement (in.^{2}/ft)	% Reduction
AASHTO	19.2	7.4	0.89	0%
INDOT	12.6	3.7	0.55	38%
Alternative	10.2	3.7	0.44	51%

TABLE 3.3
Method Specific Overhang Requirements (INDOT Type FC)
Overhang Requirements for an INDOT Type FC TL-4 Barrier (Appendix B, Example 3)

Method	M_c (kip-ft/ft)	T (kip/ft)	Primary Reinforcement (in.^{2}/ft)	% Reduction
AASHTO	22	10.1	1.04	0%
INDOT	16.1	4.5	0.72	31%
Alternative	12.5	4.5	0.55	47%

Equation 3.12. The moment demand is distributed along an assumed distribution length (L_c + 2H). For the calculation of tensile force at the slab level, the approach is identical to the INDOT method as shown in Equation 3.11. For moment, it results in slightly less moment demand.

$$M_c = \frac{1.25F_tH}{L_c + 2H} \tag{3.12}$$

3.5.3 Method Comparison

Both the INDOT and alternative method are conservative methods to designing the overhang region considering design forces are realistic, although engineering judgment is used in assuming the distribution of force and moment along the length of the overhang. Table 3.2 and Table 3.3 present a comparison of results from the three methods (AASHTO, INDOT and Alternative) using two different barriers. As shown, reinforcement required for the alternative method is reduced approximately 50% from requirements provided by AASHTO. There is an important philosophical difference between methods that should be considered. AASHTO is designing the overhang for the maximum capacity that a given rail can resist while other methods are designing for the collision force. Given the wide variety of design methods considering overhang design, research is needed to investigate the appropriate philosophy and the appropriate amount of reinforcement to provide in the overhang.

4. SYSTEM BEHAVIOR: BRIDGE DECK-BARRIER WALL

4.1 Introduction

An experimental program was developed to determine the failure pattern of a bridge deck overhang as loaded by forces applied to the barrier. The experimental program focused on the influence of the amount of transverse reinforcement in the deck overhang to resist forces imparted to the barrier. Scaled 15ft and 27 ft overhang specimens were tested with different amounts of top transverse reinforcement in the slab. The tests enabled observation of the failure mechanism between the slab and the barrier and evaluation of the adequacy of the design procedure.

4.2 Specimen Design

To evaluate the system, two bridge deck overhangs were designed. For this test, it was decided to evaluate a scaled structure based on a typical 8 in. bridge deck so that the entire system could be tested. Therefore, an approximate 50% dimensional scale was selected which resulted in a 4 in. bridge deck. The barrier was appropriately scaled from a typical INDOT Type FC concrete barrier. A rectangular barrier was designed to simplify evaluation of results while introducing similar reinforcement details in the specimen representing the full-scale design. The reinforcement used in the specimens was scaled from #5 bars used in the full scale Type FC barrier to #3 bars in the specimen barrier and slab. This barrier design resulted in the cross section shown in Figure 4.1.

The scaled barrier was analyzed to determine the nominal railing resistance and length of the yield line mechanism, two parameters pertinent to the overhang design. From this analysis, the theoretical length of the yield line mechanism was calculated as 5.5 ft (Figure 4.2). Based on the theoretical yield line, a 15 ft specimen length was originally selected to provide adequate length for yield line development. After testing, the 15ft specimen, it was determined that more length was required. Therefore, the specimen length was approximately doubled to 27 ft.

4.2.1 Specimen 1

The top transverse reinforcement for Specimen 1 was proportioned in the deck using the AASHTO (2014) overhang design procedure. The specimen was designed to have #3 reinforcing bars in both the deck and barrier. The top transverse reinforcement in the slab was placed 4.5 in. on-center and all other reinforcement in the slab was placed on 12 in. centers. The barrier was reinforced with eight longitudinal bars tied to vertical stirrups placed 7 in. on-center. As typical with overhangs in practice, the vertical stirrups in the wall were tied to the bottom longitudinal bars in the slab region. Figure 4.3 provides details of Specimen 1.

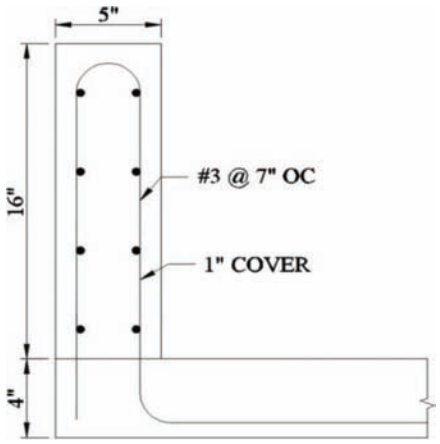

Figure 4.1 Cross section view of scaled barrier.

4.2.2 Specimen 1L

Specimen 1L was designed with the same proportioning of deck reinforcement as in Specimen 1. The top transverse bars in Specimen 1L, however, were detailed with an end hook, and the specimen length was 27 ft, almost twice that of Specimen 1, in attempt to form the yield line mechanism in the barrier. Figure 4.4 provides the details of Specimen 1L.

4.2.3 Specimen 2

Specimen 2 was designed using 50% of the top transverse reinforcement specified in Specimen 1. The design enabled for an equal comparison of overhang behavior with a different amount of primary reinforcement. This amount of reduction is also consistent with that being done in practice (Table 3.2 and Table 3.3). The top transverse reinforcement in the slab was placed 9 in. on-center, and all other reinforcement in the slab was placed at 12 in. centers consistent with Specimen 1. The barrier was reinforced identically with eight longitudinal bars tied to vertical stirrups placed 7 in. on-center. Figure 4.5 provides details of Specimen 2 which had an overall length of 15 ft.

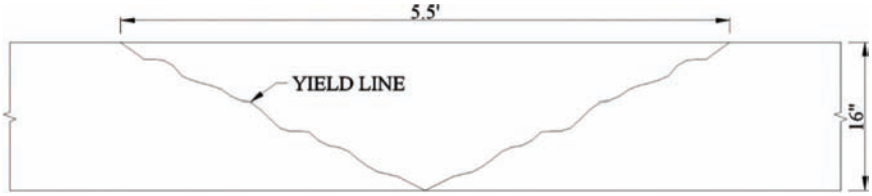

Figure 4.2 Theoretical yield line pattern for overhang specimen design.

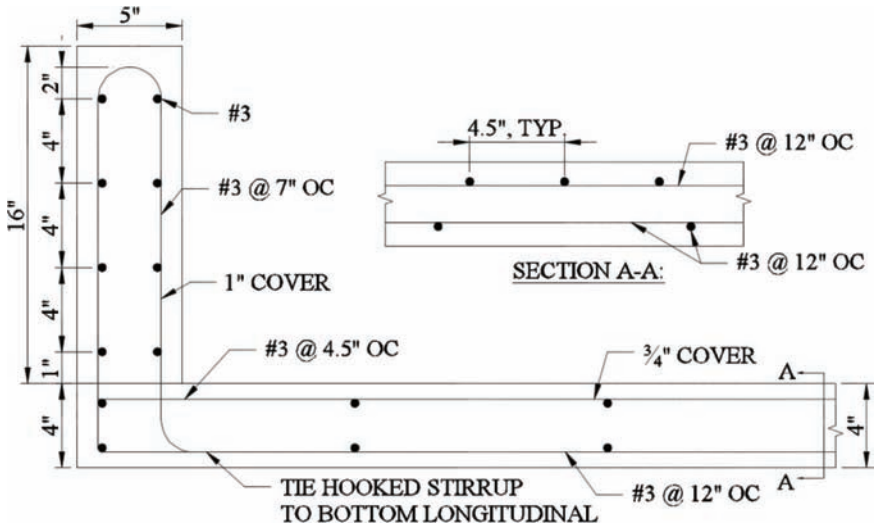

Figure 4.3 Cross section view of Specimen 1.

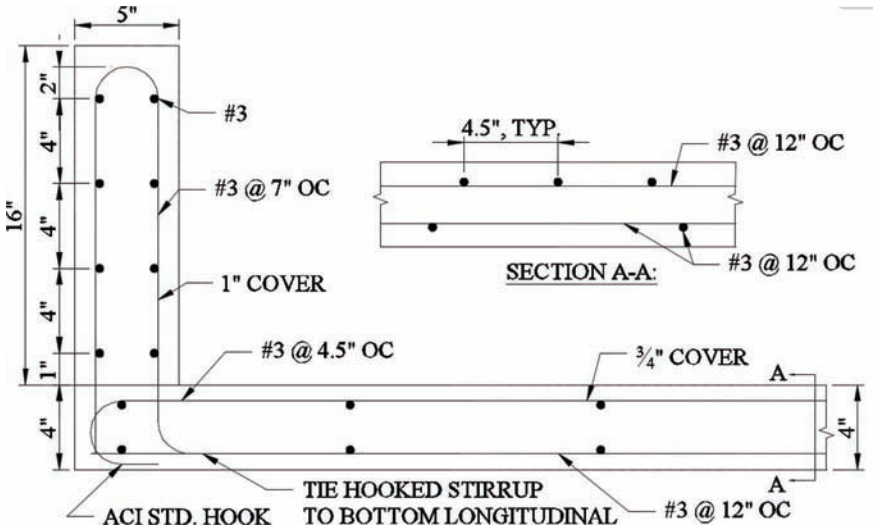

Figure 4.4 Cross section view of Specimen 1L.

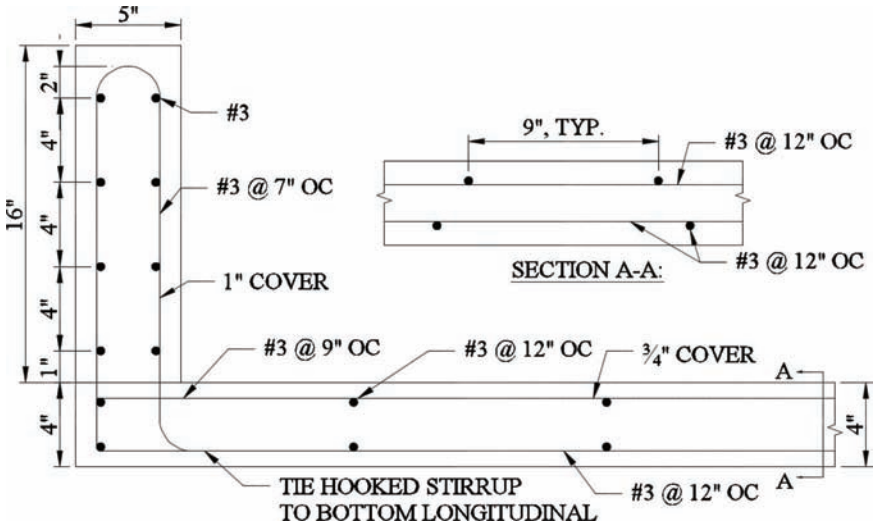

Figure 4.5 Cross section view of Specimen 2.

4.2.4 Specimen 2L

Specimen 2L was designed with the same reinforcement proportioning as in Specimen 2. The top transverse bars in Specimen 2L, however, were detailed with an end hook, and the specimen length was increased to 27 ft from 15 ft in Specimen 2. The increased length and hooked anchorage was designed in attempt to form a barrier mechanism. Figure 4.6 shows Specimen 2L details.

4.3 Construction

The specimens were constructed at the Purdue University Bowen Laboratory by means of a two-phase cast in which the slab and barrier were cast separately. In addition, beams were cast to provide support for the specimens. The formwork was designed to accommodate the lateral pressures experienced during casting, and the construction process for the specimens and support beams is provided in the following sections.

4.3.1 Formwork

The formwork was constructed with SPF construction grade 2x4 lumber and ¾ in. OES plywood. The supporting studs were spaced at 12 in. on-center for both the specimen and support beam formwork, and ¼ in. lag screws were used to attach the side panels to the baseboards. To accommodate post tensioning of the specimen to the strong floor, holes were drilled in the formwork, and 2 in. diameter PVC pipes were installed. Completed formwork is shown in Figure 4.7 for the test specimens and in Figure 4.8 for the support beams.

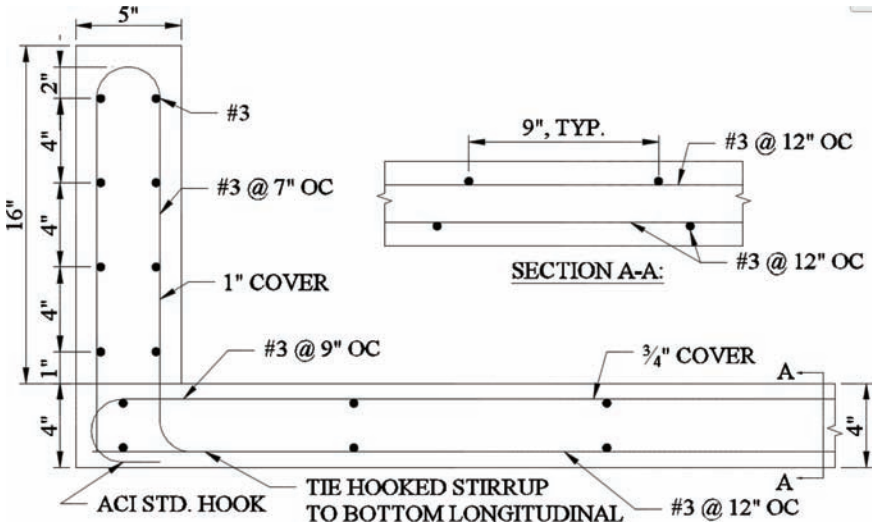

Figure 4.6 Cross section view of Specimen 2L.

Figure 4.7 Completed Specimens 1 and 2 formwork.

4.3.2 Casting

Both test specimens were cast simultaneously with separate casts for the slab and barrier. In preparation for the slab cast, the slab reinforcement and barrier stirrups were placed in the forms. A minimum number of slab bolsters were used to achieve the desired cover while ensuring that the bolsters were oriented longitudinally to eliminate any influence on testing. The as-placed reinforcement layout for Specimens 1 and 2 is provided in Figure 4.9. For Specimens 1L and 2L, the end top transverse bar was placed 4.5 in. from the edge before utilizing the spacing shown in Figure 4.4 and Figure 4.6.

The support beams and specimen slabs were cast from the same batch of concrete. Figure 4.10 through Figure 4.12 illustrate the reinforcement placement and the casting procedure.

Placement of the concrete for the specimens was achieved through chuting directly from the concrete truck and using vibrators to consolidate the concrete. Tape was applied to the PVC pipes in the specimens to indicate the desired height of concrete in the slab. A temporary bridge platform shown in Figure 4.12 was designed to enable finishing the middle portions of the specimens which were difficult to reach from the formwork edge. Support beams were cast using a concrete bucket. The specimens were subsequently finished as shown in Figure 4.13.

As typical in practice, a construction joint was provided between the deck and barrier. A raked joint was created using small garden rakes, and the grooves were approximately located at 1.5 in. centers (Figure 4.14). The joint was made in the transverse direction within the 5 in. width of the barrier interface.

Figure 4.8 Completed support beam formwork.

Immediately following casting of the slab, the longitudinal reinforcement and formwork for the barrier was installed. Side panels were installed using longitudinal walers consisting of 2-2x4's and ¼ in. all-thread rods used for lateral ties with 4x4x1/4 in. steel plates bearing against the walers. The lateral tie system is shown in Figure 4.15, and the complete system is illustrated in Figure 4.16. The concrete for the barrier was placed using a concrete bucket and thoroughly vibrated to ensure consolidation.

The slab and barrier were cast within three days of one another to provide time to install the formwork and lateral tie system. Barrier forms were installed while maintaining wet-curing over the rest of the slab. The overhang specimens, support beams, and testing cylinders were cured by means of wet burlap moistening, followed by an outer layer of plastic sheeting to seal in the moisture as shown in Figure 4.17. Burlap was moistened for 28 days, and the curing conditions were identical for the concrete cylinders, specimens, and support beams.

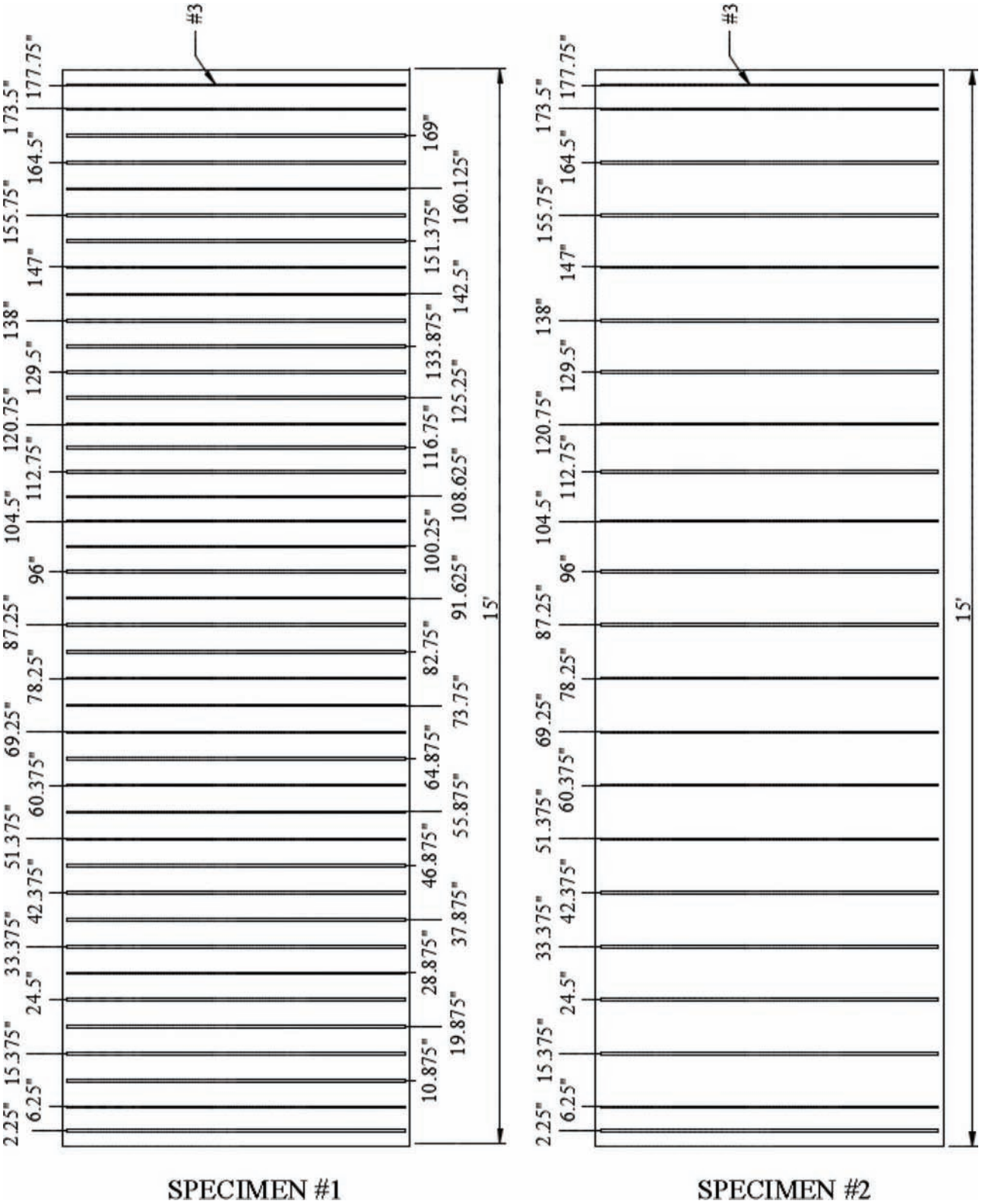

Figure 4.9 Top transverse reinforcement for Specimens 1 and 2 (as-placed).

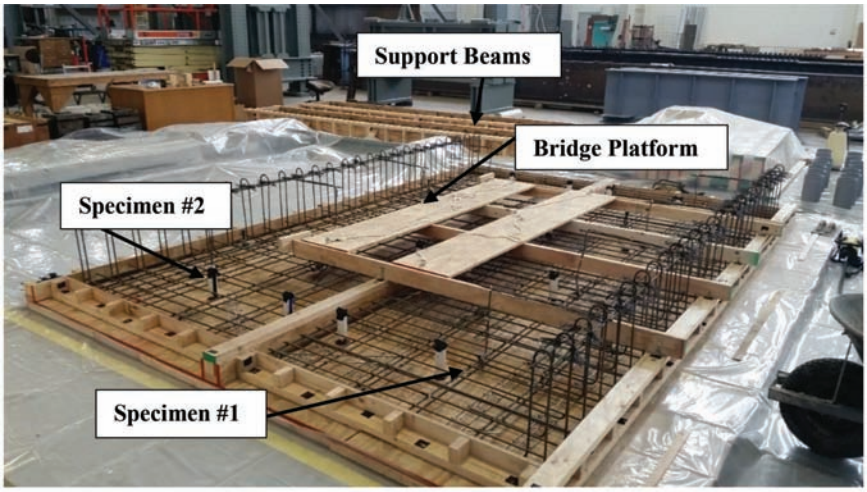

(a) Specimens 1 and 2

(b) Specimens 1L and 2L

Figure 4.10 Slab reinforcement installation.

Figure 4.11 Reinforcement in support beams.

Figure 4.12 Slab cast (Specimens 1 and 2).

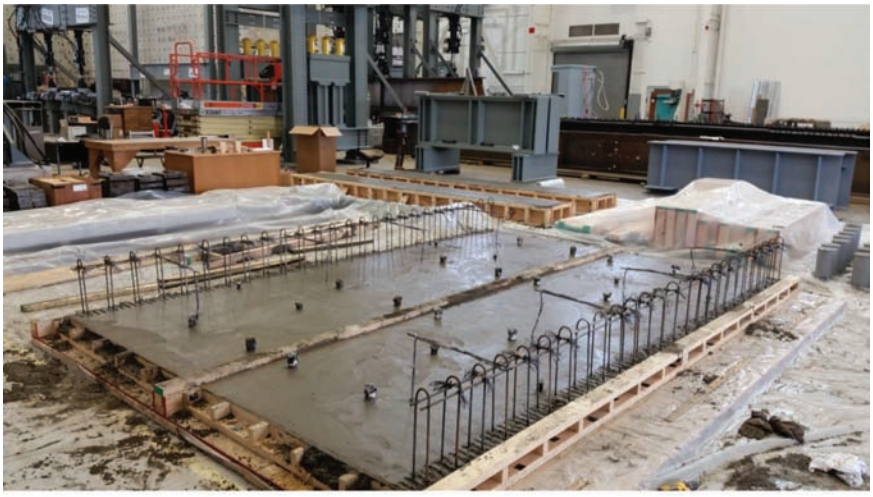

(a) Specimens 1 and 2

(b) Specimens 1L and 2L

Figure 4.13 Completed slab cast.

(a) Specimens 1 and 2

(a) Specimens 1L and 2L

Figure 4.14 Barrier reinforcement.

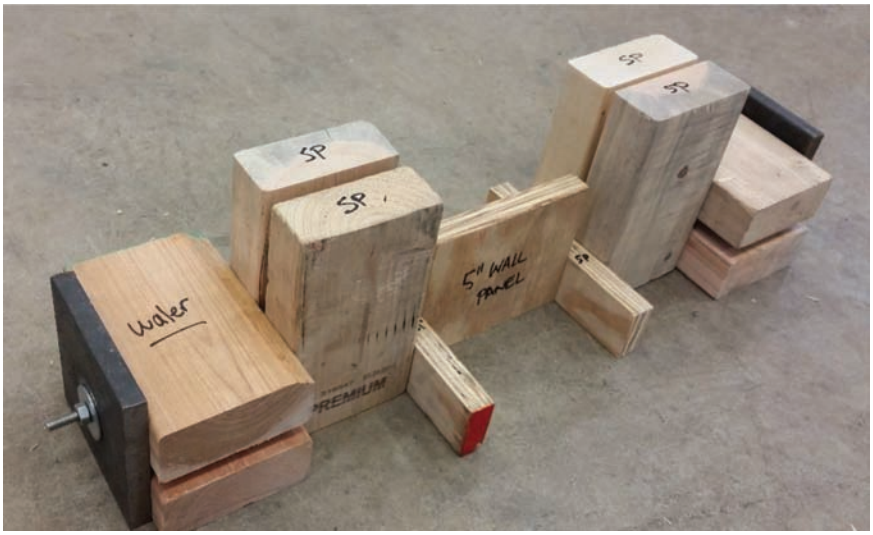

Figure 4.15 Lateral tie design.

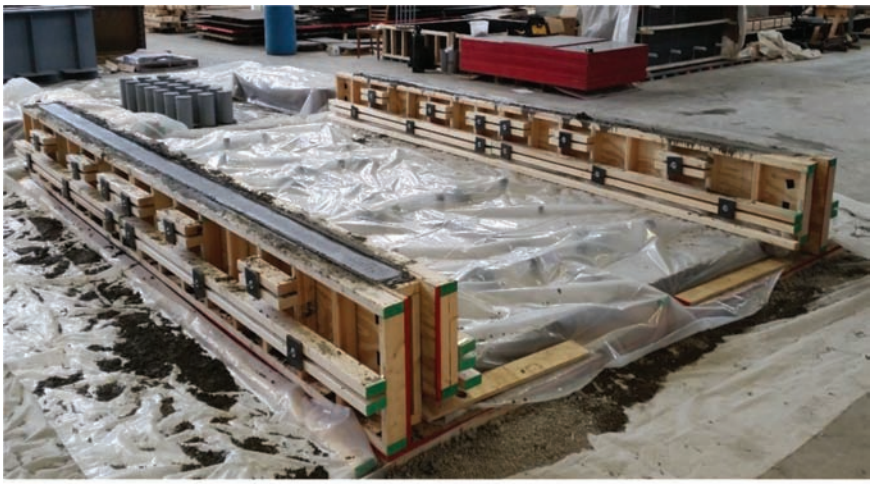

(a) Specimens 1 and 2

(b) Specimens 1L and 2L

Figure 4.16 Completed barrier cast.

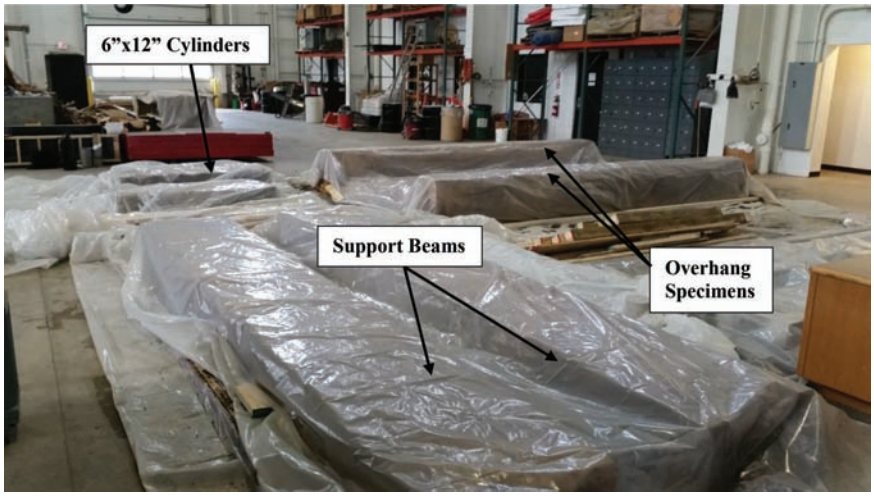

Figure 4.17 Concrete curing area (Specimens 1 and 2).

4.4 Materials

4.4.1 Reinforcing Steel

The rebar used in the support beams and specimens were #3 A615 Grade 60 bars supplied by Harris Rebar and NUCOR Steel. All reinforcement for a given length specimen was taken from the same heat of steel, and the chemical composition is provided in Table 4.1. Three consecutive tensile tests were performed in accordance with ASTM A370 (2014) using an INSTRON universal testing machine, and the test results up to 5% elongation are shown in Figure 4.18. The physical properties of the reinforcement are provided in Table 4.2.

TABLE 4.1
Mill Certification Reinforcement Composition

	% Composition	
Alloying Element	**# 3 Black (15 ft Specimens)**	**#3 Black (27 ft Specimens)**
C/Ni	0.40/0.12	0.41/0.12
Mn/Cr	1.18/0.18	1.16/0.16
P/Mo	0.022/0.03	0.020/0.032
S/V	0.04/0.005	0.044/0.01
Si/Cb	0.23/0.002	0.23/0.003
Cu/Sn	0.32/-	0.40/-

4.4.2 Concrete

Concrete used for the test specimens and support beams was obtained from Irving Materials Inc., a local ready-mix supplier. Two pours were required for casting of each specimen set. In the first pour, the deck and support beams were cast. This was followed by a second pour to cast the barrier in each overhang specimen. The mix design used for both casts was identical. The concrete was a 3500 psi nominal 3/8 in. P-Gravel mix with Type I Portland Cement and a mid-range water reducer. The concrete mix design for each specimen set is provided in Table 4.3 and Table 4.4.

The concrete was tested in accordance with ASTM C39 (2015) to determine the strength gain history (Figure 4.19) as well as the strength on the day of testing. For each test date, the values presented are the average of three cylinders. The 28-day strength for the slab and barrier concrete were measured as 3760 psi and 3780 psi, respectively for Specimens 1 and 2. It should be noted that the concrete testing machine was rehabilitated and recalibrated in the timeframe between Day 28 and Day 55. A jump in compressive strength was observed in the same timeframe. It appears that the early strength may be slightly lower than actual. There is increased confidence in the later strength as the machine had just been calibrated. For Specimens 1L and 2L, the 28-day strength for the slab and barrier were measured as 3650 psi and 3950 psi, respectively. The concrete strength on the day of testing of the specimens is provided in Table 4.5. In addition to compressive strength, split cylinder tensile strengths (average of three cylinders) are also provided.

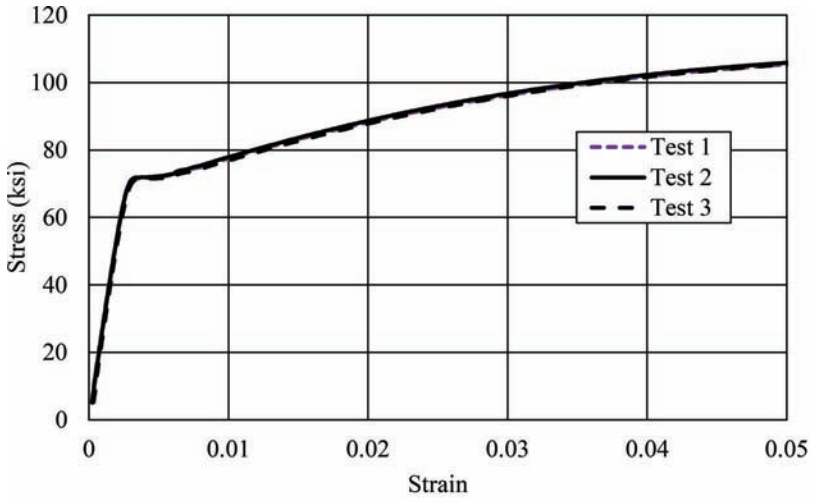

(a) Specimens 1 and 2

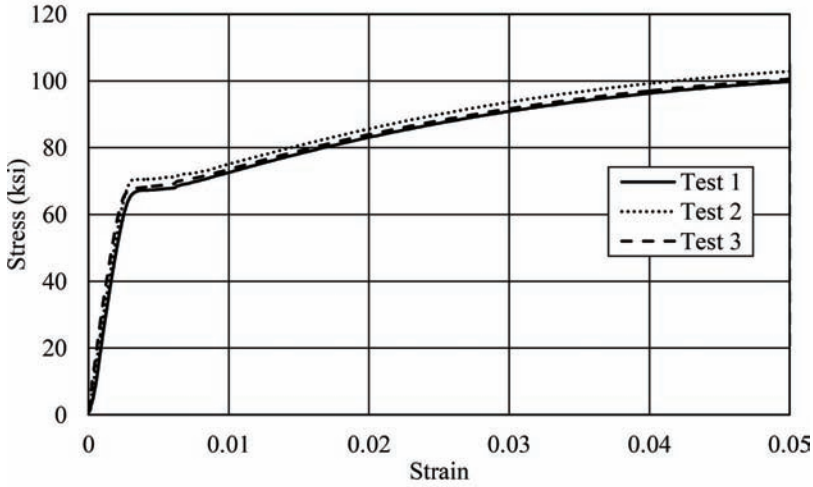

(b) Specimens 1L and 2L

Figure 4.18 Tension test results.

TABLE 4.2
Physical Testing Properties

Bar Designation	f_y (ksi)	f_u (ksi)	% Elongation
Black #3 - 15 ft Sp.	73	110	12.5
Black #3 - 27ft Sp.	69	105	13.0

TABLE 4.3
Concrete Mix Proportions (Specimens 1 and 2)

Material Constituent	Mix Design (lb/cy)	Cast 1 Slab (lb/cy)	Cast 2 Barrier (lb/cy)
Cement (Type 1)	430	429	430
P-Gravel (3/8 MSA)	1800	1792	1808
Sand-23	1540	1596	1592
Water Reducer (Glenium)	4.00/C	17.2 oz	17.6 oz
Water	219.7	238	214
W/C ratio	0.51	0.55	0.50
Slump	6 in.	7.75 in.	4.5 in.

TABLE 4.4
Concrete Mix Proportions (Specimens 1L and 2L)

Material Constituent	Mix Design (lb/cy)	Cast 1 Slab (lb/cy)	Cast 2 Barrier (lb/cy)
Cement (Type 1)	430	422.5	438
P-Gravel (3/8 MSA)	1800	1823	1848
Sand-23	1540	1603	1600
Water Reducer (Glenium)	4.00/C	17.3 oz	16.8 oz
Water	219.7	242	217
W/C ratio	0.51	0.57	0.50
Slump	6 in.	6.5 in.	4 in.

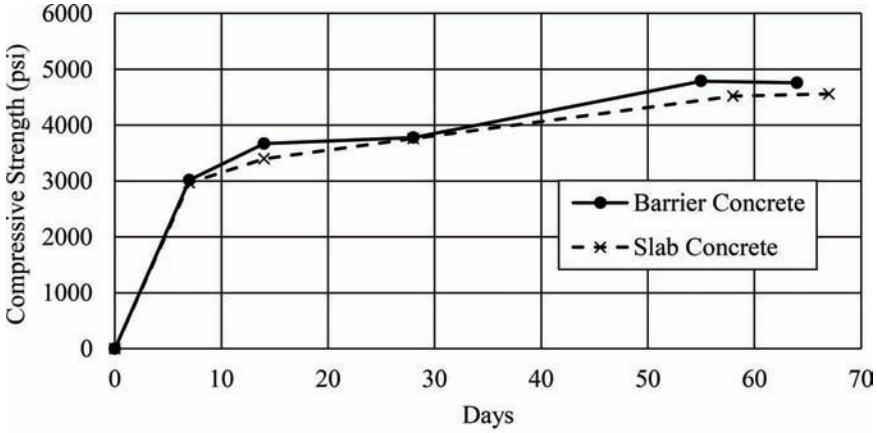

(a) Specimens 1 and 2

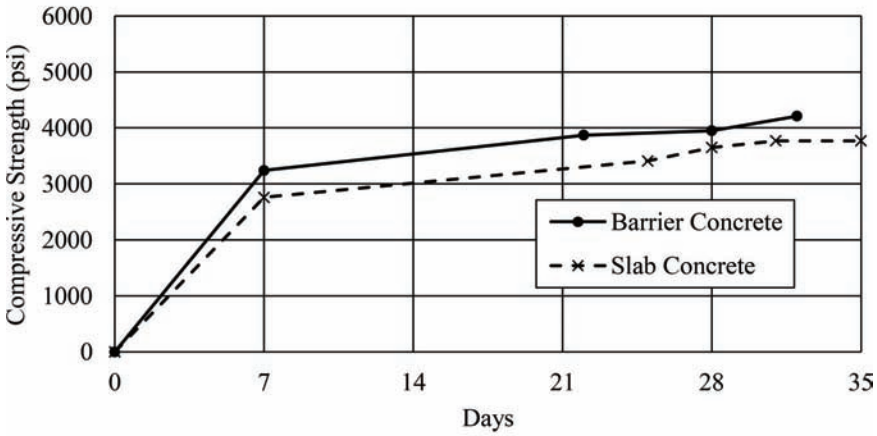

(b) Specimens 1L and 2L

Figure 4.19 Concrete compressive strength.

TABLE 4.5
Testing Day Concrete Strength

Specimen	Concrete	Age (Days)	Compressive Strength (psi)	Tensile Strength (psi)
1	Barrier	55	4790	520
	Slab	58	4520	450
2	Barrier	64	4760	500
	Slab	67	4560	460
1L	Barrier	28	3950	400
	Slab	31	3770	360
2L	Barrier	32	4210	440
	Slab	35	3770	430

4.5 Experimental Setup

The specimens were supported by support beams which were used to simulate girders supporting the deck and provide for the targeted overhang length as illustrated in Figure 4.20. To produce lateral loads on the barrier, a strong-wall was used as a reaction block. A Dywidag rod was anchored to the posterior side of the strong wall and ran through a 2 in. hole in the specimen. A jack, loading beam, and load cell were placed inboard to the barrier with the rod extending through each element. An Enerpac 30 ton hydraulic jack was used to load the HSS 8x4x3/8 in. stub which applied a distributed force at the midspan of the barrier over a 1.5 ft length, 4 in. (centerline) from the top of the wall. This load distribution is scaled from the 3.5 ft distribution specified by AASHTO for a TL4 barrier.

The deck was attached to the support beam through the use of hydrostone and post-tensioning. To accommodate the lateral forces experienced during the experiment, the specimens were post-tensioned to the strong floor using 1¼ in. diameter Dywidag bars and 8x5x1½ in. bearing plates. All bearing plates were hydrostoned to the specimens to reduce stress concentrations from imperfections in the concrete surface and served to provide leveling. The amount of post-tensioning was determined using the measured coefficient of friction between the support beams and strong floor. It was determined that the coefficient of friction between concrete to the strong floor was 0.50. In Specimens 1 and 2, the beam closest to the barrier was post-tensioned with 12.5 kip per rod while the other beam was post-tensioned with 50 kip per rod. The higher force was used for this beam due to the expected tension reaction at this location while the lower force was used for the other as that beam experiences a compressive reaction. The post-tensioning details for Specimens 1 and 2 are provided in Figure 4.21a. Specimens 1L and 2L were post tensioned with 12.5 kip per rod and 25 kip per rod for the compression and tension beam respectively (Figure 4.21). The post tensioning rod spacing and bearing plate dimensions were identical to Specimens 1 and 2 As a result of post tensioning, the specimens experienced minor cracking around the post-tensioned bearing plates. This cracking occurred away from the overhang and did not influence the behavior of the test.

4.5.1 Instrumentation

A Lebow 50 kip load-cell was placed in-line with the jack to measure the force applied at each loading step. Strain gages were installed on the top transverse bars of each specimen to measure the strain distribution, and potentiometers were used to measure horizontal and vertical displacements. Dial gages were also placed on the exterior support beam (opposite the barrier) to ensure that slipping did not occur during testing.

4.5.1.1 Strain Gage Instrumentation. The top transverse bars of each specimen were instrumented with strain gages. For equal comparison between the two test specimens, strain gages were instrumented at identical locations as shown in Figure 4.22 for Specimen 1 and Figure 4.23 for Specimen 2. Similarly, Specimens 1L and 2L were instrumented with strain gages in identical locations relative to one another (Figure 4.24 and Figure 4.25).

The strain gages, obtained from Texas Measurements, were 3-wire foil 1.5x5 mm with a resistance of 120 Ohms and a gage factor of 2. The strain gages were installed on specified top transverse bars which were placed in the slab. The process for installation is illustrated in Figure 4.26 and is as follows:

Step 1: Grinding reinforcement smooth
Step 2: Degreasing the surface
Step 3: Hand-sanding the rebar surface with conditioner
Step 4: Re-applying the surface conditioner with a cotton swab
Step 5: Applying neutralizer with a cotton swab
Step 6: Attaching the gage with installation tape

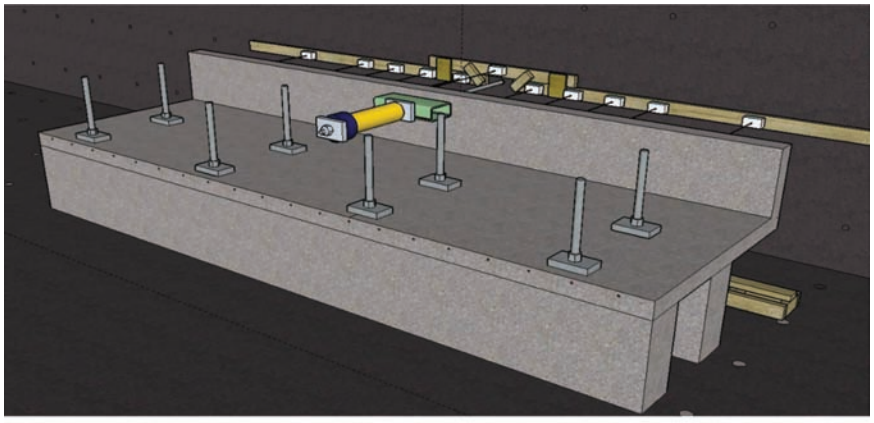

(a) Specimens 1 and 2

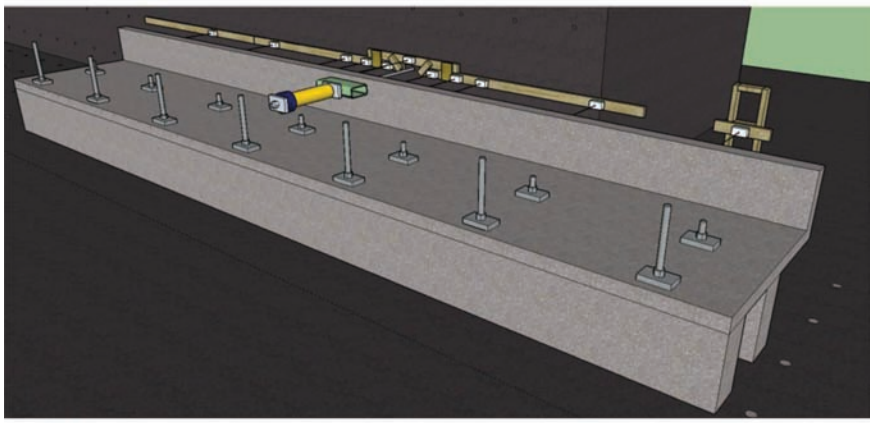

(b) Specimens 1L and 2L

Figure 4.20 Rendering of experimental setup.

Step 7: Applying the M-Bond 200 adhesive and adhering gage
Step 8: Coating the gage and lead wires with M-Coat-D
Step 9: Installing M-Coat-F rubber sealant over the installed gage
Step 10: Applying silicone around the M-Coat-F for additional protection

The rebar was lightly ground with a flap disk grinder on the longitudinal rib to ensure that loss of cross sectional area was minimized. All strain gages were placed at the critical section (edge of overhang) 2 ft from the edge of the parapet, and the bars are illustrated in Figure 4.27.

4.5.1.2 Potentiometer Instrumentation. The barrier of each specimen was instrumented with potentiometers running both longitudinally at the height of force application and under the barrier. The horizontal potentiometers were installed 4" from the top of the barrier with the exception of the middle potentiometer which was located at the top of the barrier due to conflicts with the loading system of the overhang. The vertical potentiometers were placed at the exterior edge of the specimen to measure the maximum vertical displacement. The potentiometers used were the UniMeasure PA Series with a 10 in. displacement range. Details of the locations of the potentiometers are shown in Figure 4.28 while Appendix D provides the sensor identification use for the data acquisition system. The complete experimental setup is shown in Figure 4.29 through Figure 4.31.

All potentiometers were calibrated using an LVDT calibration device. The device attached to the eye-fitting of the potentiometer and adjusted to pull a stainless steel wire to varying displacements. The millivolt reading was recorded at each 1 in. of displacement as indicated by the data acquisition system, and the slope was obtained in mV/V/in. This calibration data was used within the data acquisition system to output the correct displacement in inches.

4.5.2 Testing Procedure

The support beams and test specimen were set up by the strong wall in preparation for testing. The

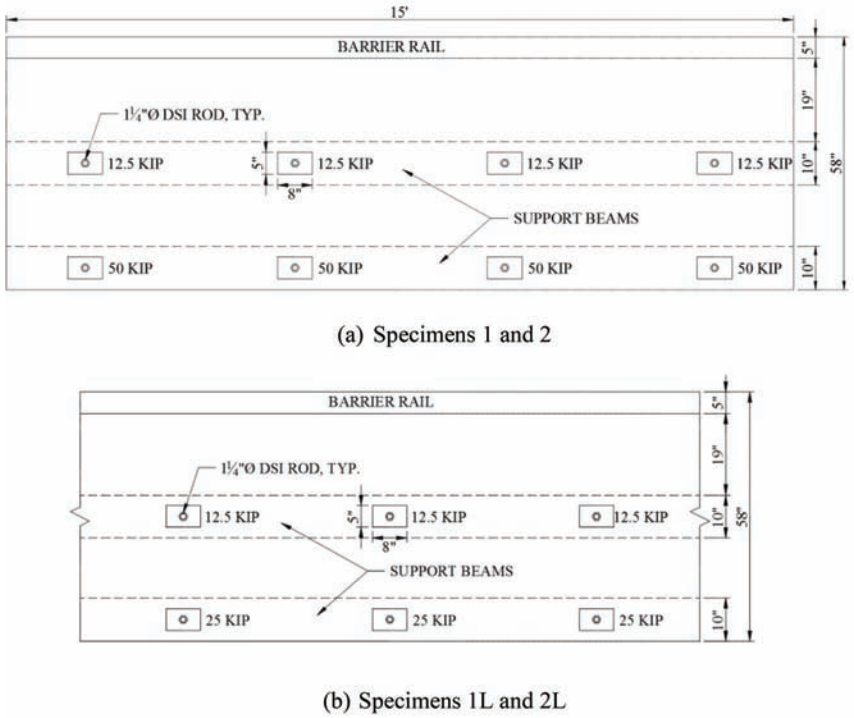

Figure 4.21 Post-tensioning diagram.

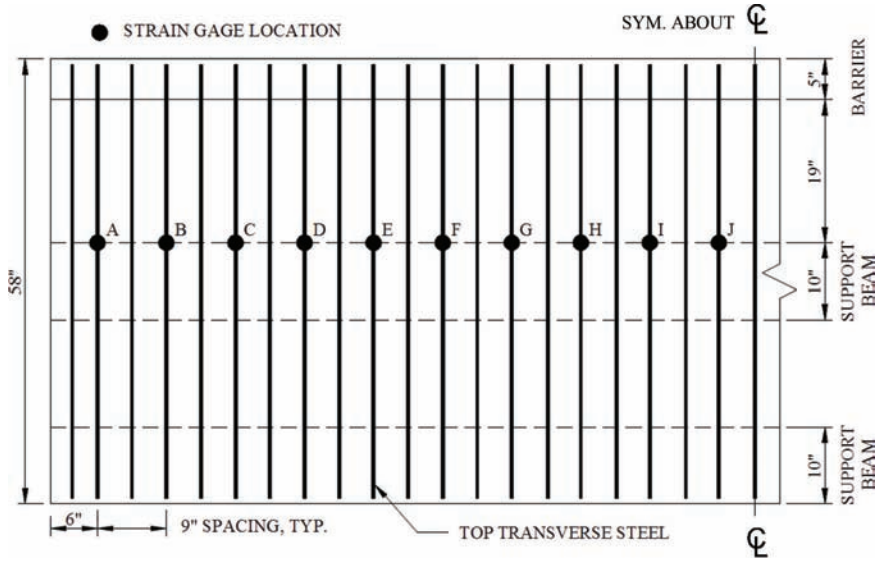

Figure 4.22 Specimen 1 strain gage instrumentation (plan view).

instrumentation was connected to a Micro-Measurements System 7000 for data acquisition. A sampling rate of 0.1 seconds was used for recording the data from the instrumentation. The specimens were loaded in 2 kip intervals with successive monitoring and mapping of cracks at each increment of loading.

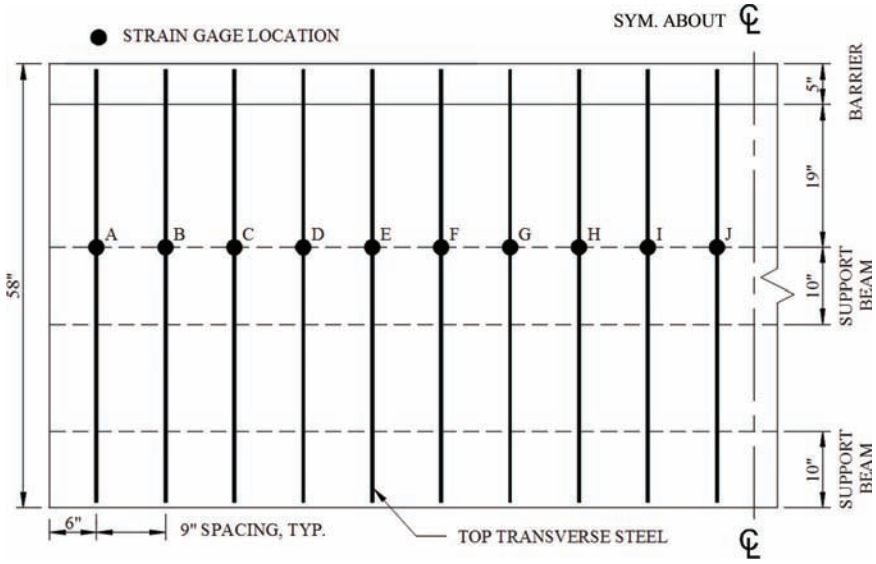

Figure 4.23 Specimen 2 strain gage instrumentation (plan view).

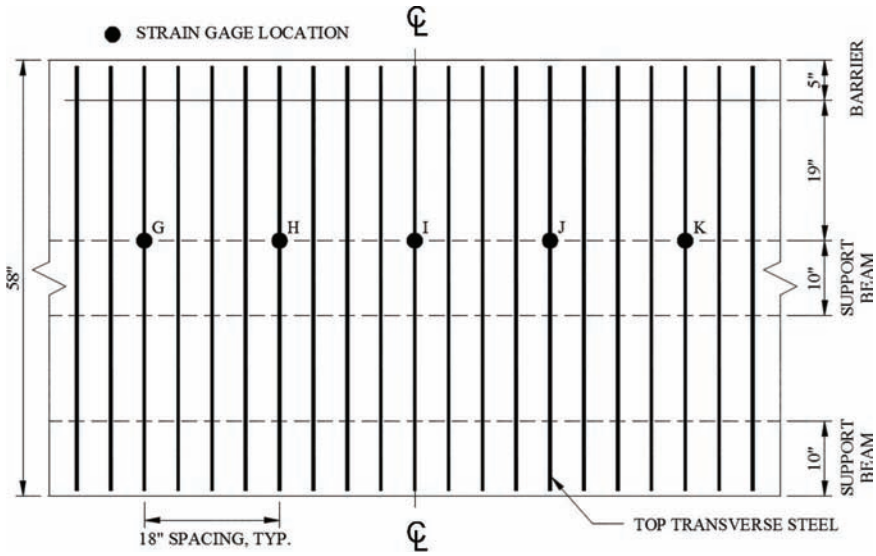

Figure 4.24 Specimen 1L strain gage instrumentation (plan view).

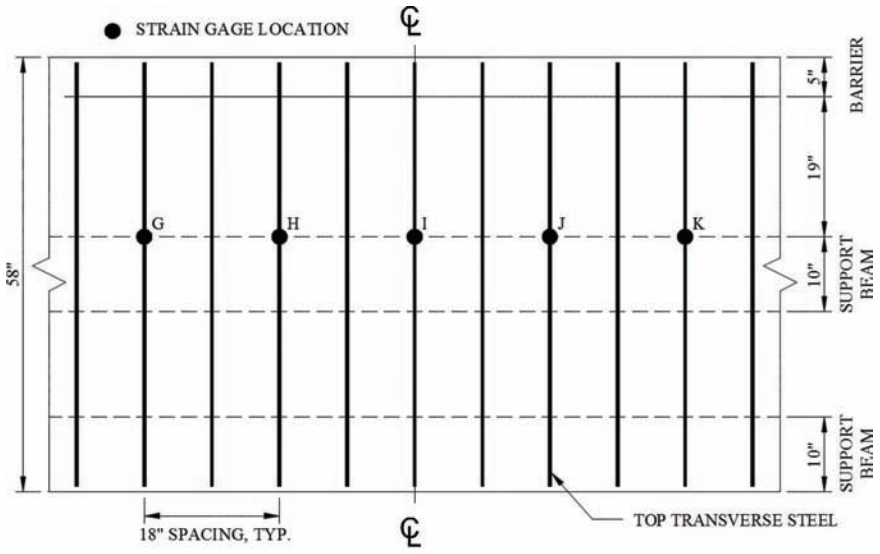

Figure 4.25 Specimen 2L strain gage instrumentation (plan view)

Figure 4.25 Specimen 2L strain gage instrumentation (plan view).

Figure 4.26 Strain gage installation procedure.

Figure 4.27 Completed strain gages on transverse bars.

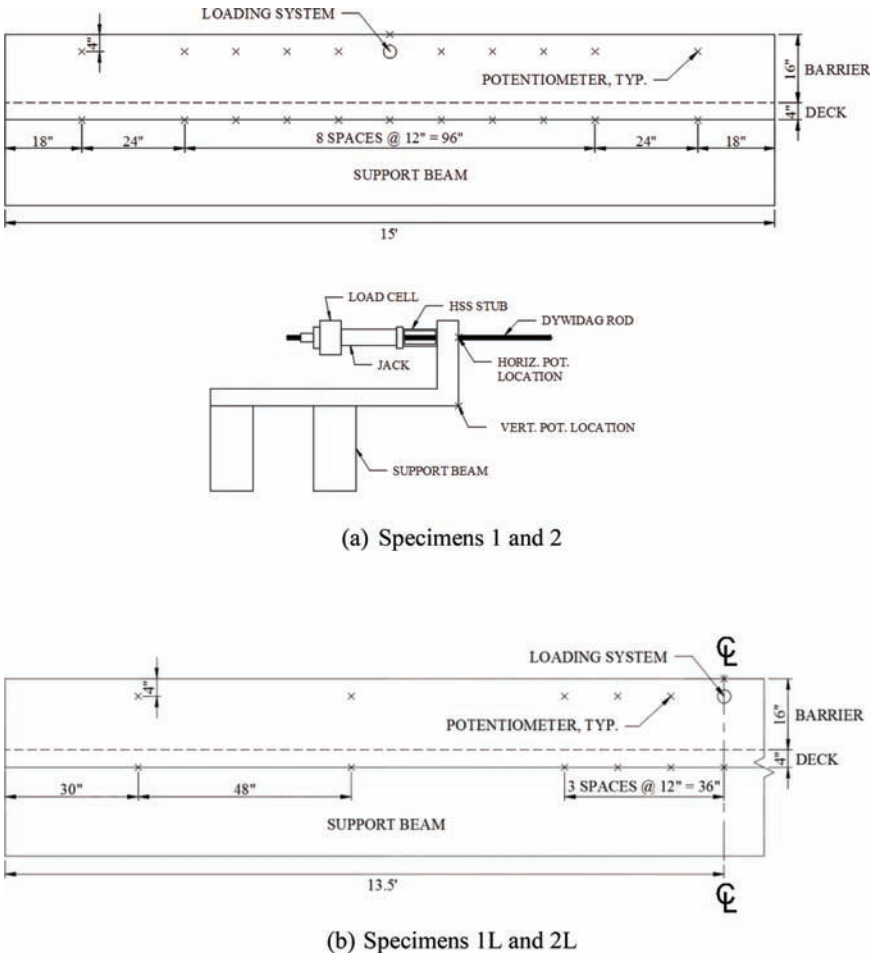

Figure 4.28 Potentiometer locations (elevation view).

Figure 4.29 Complete experimental setup (Specimens 1 and 2).

Figure 4.30 Complete experimental setup (Specimen 1L).

Figure 4.31 Complete experimental setup (Specimen 2L).

4.6 Test Results

The experiments were conducted in the Bowen Laboratory (Table 4.6), and the results for each specimen are provided in the following sections.

TABLE 4.6
Specimen Testing Schedule

Specimen #	Date	Time
1	08/19	9:00 A.M.
2	08/28	12:30 P.M.
1L	1/11	9:00 A.M.
2L	1/15	9:00 A.M.

4.6.1 Overall Behavior

4.6.1.1 Specimen 1. Specimen 1 was loaded in 2 kip intervals, and cracks were first identified in the slab after 18.2 kips. The cracks were located near the critical section of the overhang region and ran longitudinally along the length of the specimen. The highest concentration of moment was located over the edge of the exterior support beam due to the loading condition and self-weight of the overhang. Therefore, the pattern of first

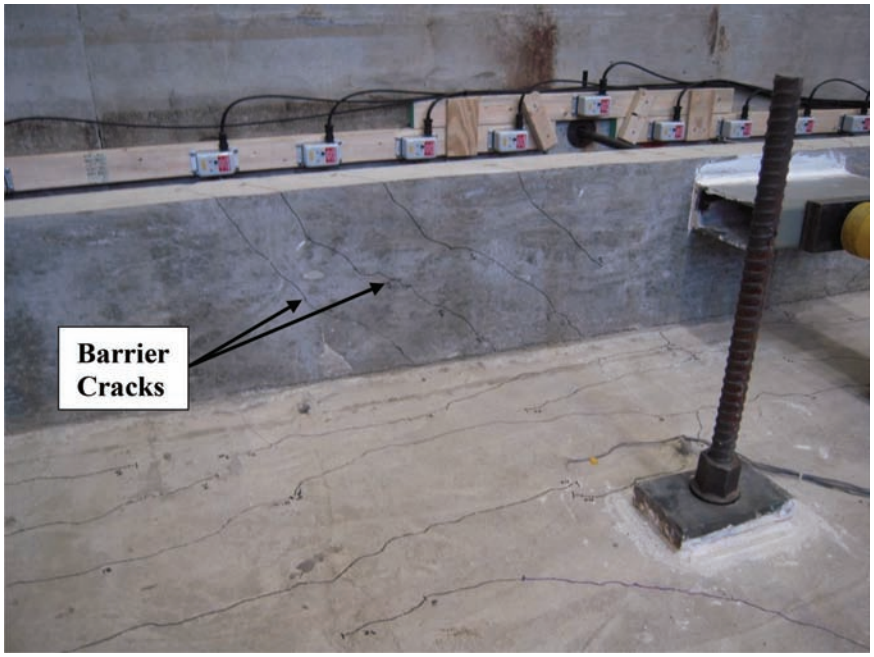

Figure 4.32 Barrier cracking (Specimen 1).

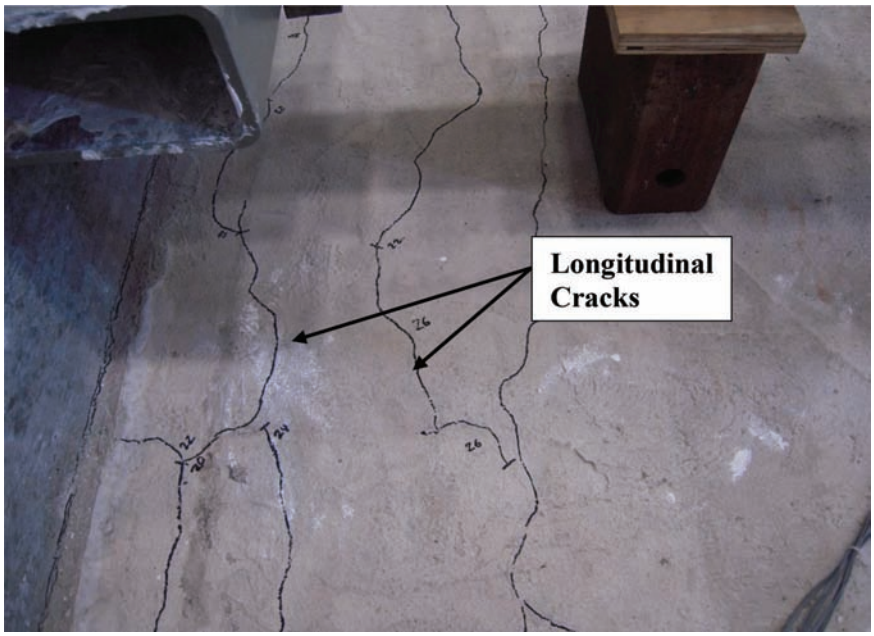

Figure 4.33 Slab cracking at midspan (Specimen 1).

cracking is reasonable with what was expected. In addition, an immediate flattening of the force-displacement curve was also observed on the real-time plot indicating a reduction of stiffness from the cracking in the slab. Another characteristic at this loading step was the development of a crack at the barrier-slab interface at midspan.

The first crack was observed on the barrier at 20.1 kips running diagonally across the barrier. Further barrier cracking resembled the theoretical yield line pattern with diagonal cracks radiating on either side from the applied load. The barrier cracking is shown in Figure 4.32. With subsequent loading, longitudinal cracks ran parallel to the initial crack in the slab and migrated toward the barrier face as shown in Figure 4.33.

At the maximum load of 26.8 kips, Specimen 1 experienced a shear failure and disengagement of the slab region. As the specimen continued to deflect, the barrier was observed to hinge about the slab-barrier interface while the slab maintained a relatively level

Figure 4.34 Deflected shape at 26.8 kip (Specimen 1).

Figure 4.35 Diagonal tension failure (Specimen 1).

profile. Upon close inspection, it was observed that the resultant compression and tension forces led to a diagonal tension failure at the slab to barrier interface. This failure mode dominated across the slab length before the more localized barrier mechanism could be formed. The deflected shape shown in Figure 4.34 shows localized displacement of the barrier near the load point prior to failure. The failure mode is shown in Figure 4.35.

The instrumentation was removed, and the specimen was reloaded until the failure plane was clearly identified. To accommodate a higher rotational capacity with post-peak loading, a rocker bearing was installed in-line with the jack. The rocker moved with the wall while maintaining approximately horizontal alignment of the jack. The increased lateral displacement allowed for further observation of the failure plane (Figure 4.36).

4.6.1.2 Specimen 2. Specimen 2 was loaded in 2 kip intervals, and cracks were first identified in the slab after 13 kips. At this loading increment, there were two observed cracks which ran longitudinally along the

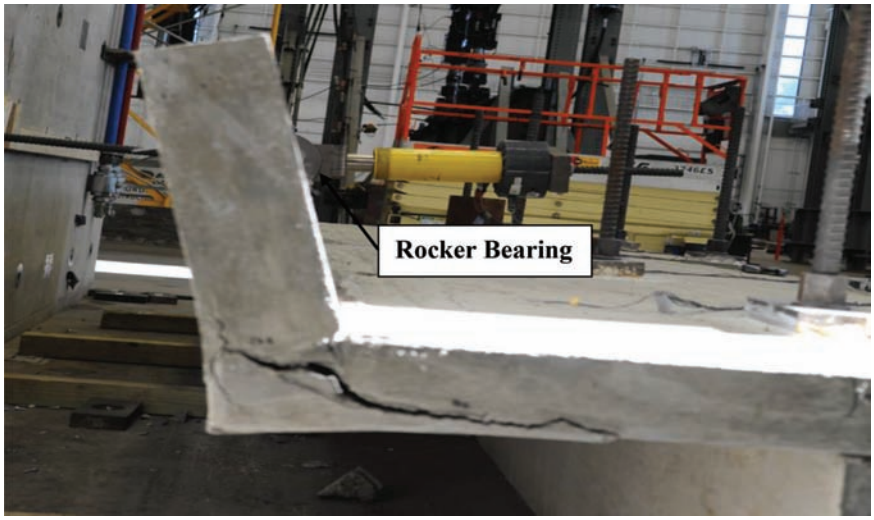

Figure 4.36 Deflected shape after post-peak reloading (Specimen 1).

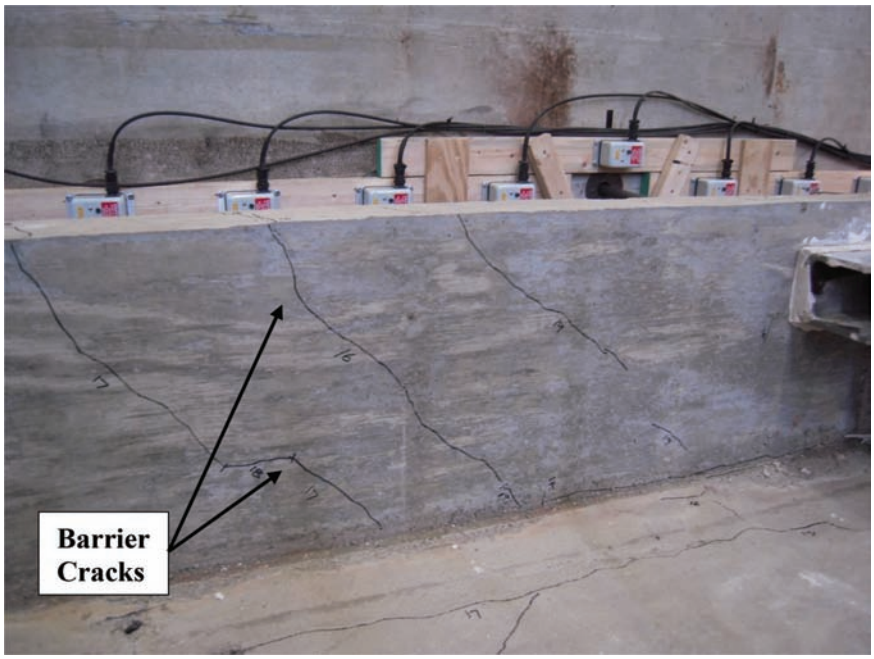

Figure 4.37 Barrier cracking (Specimen 2).

length of the slab. The first was located 1.5 ft from the right edge of the slab and ran 3 ft toward the midspan. At midspan, there was a 1 ft crack directly over the exterior support beam and ran diagonally toward the barrier face. Barrier cracking was first observed at 16 kips as shown in Figure 4.37. Consistent with the first specimen, Specimen 2 experienced symmetrical barrier cracking radiating away from the point of load application.

The slab experienced a full-length longitudinal crack at 17 kips over the edge of the exterior support beam; longitudinal cracking is shown in Figure 4.38. With respect to Specimen 1, the magnitude at which the entire slab cracked was within 1 kip. This similar response was expected due to the fact that each specimen had approximately the same cracking moment. At 21.5 kips, Specimen 2 experienced a diagonal tension failure in the slab. The barrier was observed to hinge about the slab-barrier interface, similar to that observed with the first specimen. Post-peak loading was performed to more clearly observe the failure plane. The deflected shape of Specimen 2 immediately before failure is shown in Figure 4.39 while Figure 4.40 and Figure 4.41 show the specimen post failure.

4.6.1.3 Specimen 1L. Due to the fact that diagonal tension failure dominated the behavior of Specimens 1 and 2, the slab length was increased to 27 ft with hooked

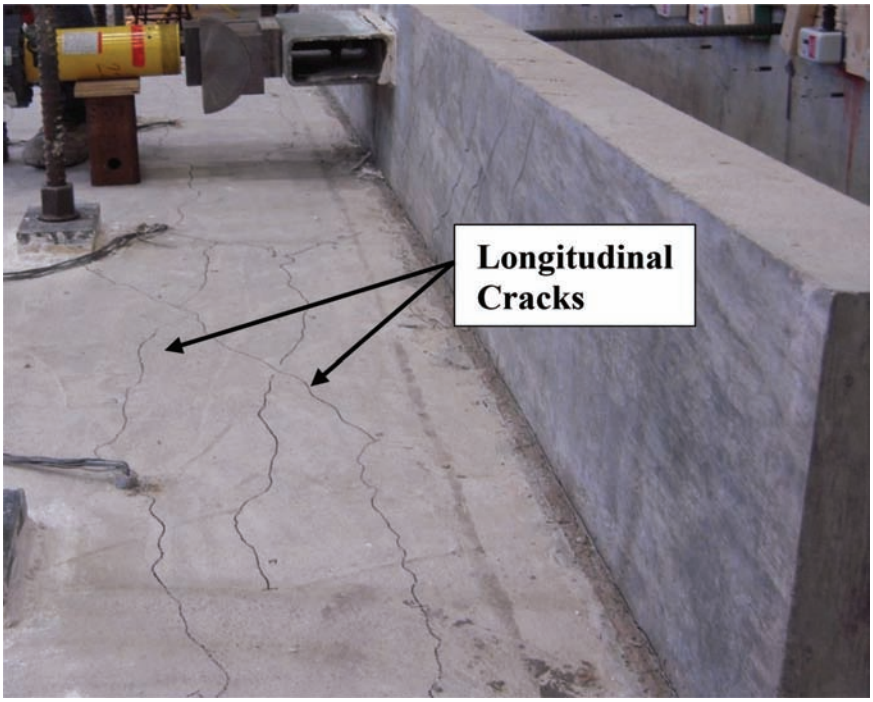

Figure 4.38 Slab cracking (Specimen 2).

Figure 4.39 Deflected shape at 21.5 kip (Specimen 2).

anchorage in Specimen 1L in attempt to form a localized barrier failure. In addition, a hooked anchorage was provided to ensure that anchorage of reinforcement did not contribute to the observed failure mode. Specimen 1L was loaded in 2 kip intervals, and cracks were first identified after 18 kips. At this loading increment, two barrier cracks were observed approximately 3 ft on either side of load application. With further loading, barrier cracks continued to propagate away from the application of load as seen in Figure 4.42. Slab cracks were observed at 26 kips, originating at midspan and extending approximately 5 ft on either side of the applied load. The slab cracks initiated normal to the slab to barrier interface and turned out toward the slab edge (Figure 4.43). With increasing load, two specific barrier cracks started to widen as the

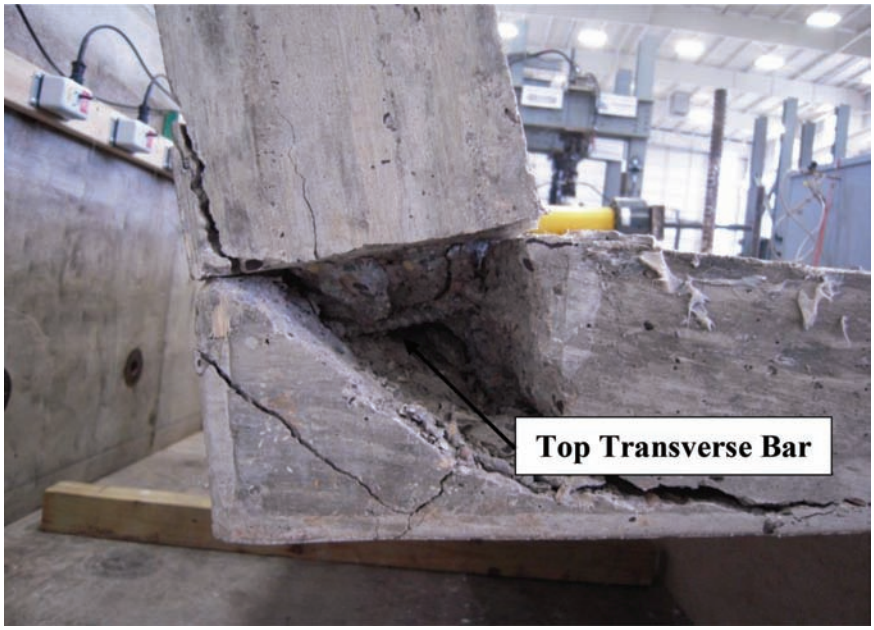

Figure 4.40 Diagonal tension failure (Specimen 2).

Figure 4.41 Deflected shape after post-peak reloading (Specimen 2).

system was defining the location of the barrier mechanism. These cracks were respectively located 51 in. to the left and 47 in. to the right side of the load application. At a load of 29.2 kips, the specimen failed in punching shear as the loading assembly (HSS) punched through the 5 in. barrier. The barrier mechanism was unable to form due to punching shear in Specimen 1L, and the failure is shown in Figure 4.44 through Figure 4.46.

4.6.1.4 Specimen 2L. In attempt to form the barrier mechanism and eliminate the punching shear failure observed in Specimen 1L, an 18 x 12 x ¾ in. plate was used with Specimen 2L to improve the punching shear resistance. This loading configuration was chosen to modify the stress distribution on the barrier while maintaining the same height and length of the load application. Specimen 2L was loaded in 2 kip intervals,

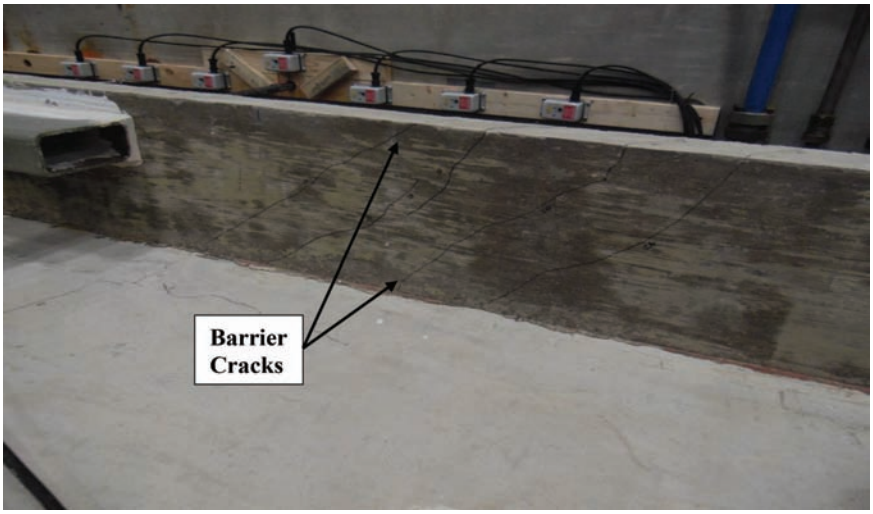

Figure 4.42 Specimen 1L (barrier cracking).

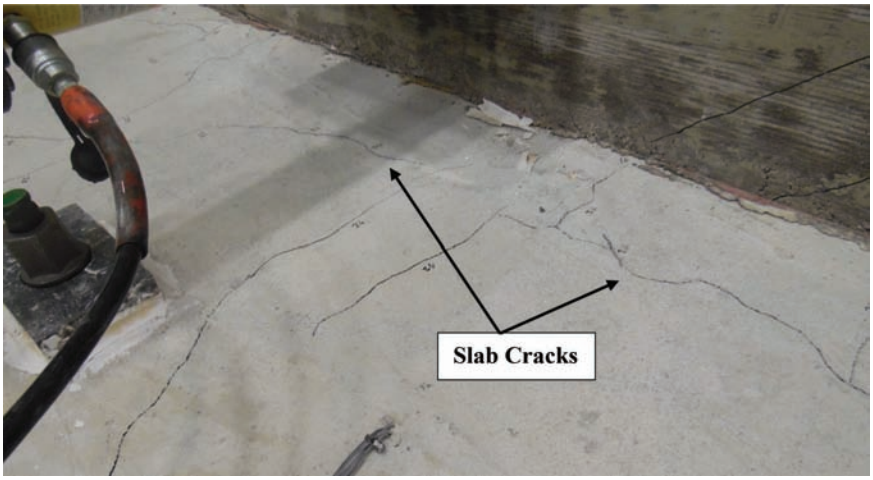

Figure 4.43 Specimen 1L (slab cracking).

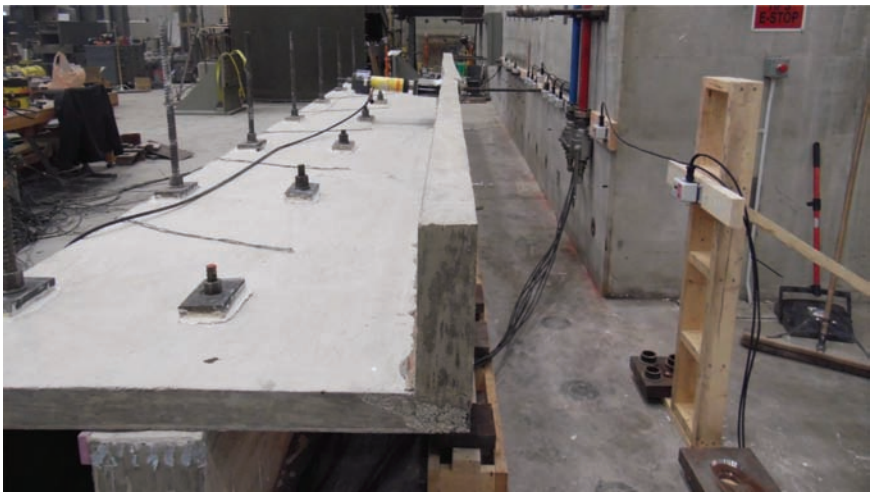

Figure 4.44 Deflected shape at failure (Specimen 1L).

Figure 4.45 Punching shear failure (Specimen 1L).

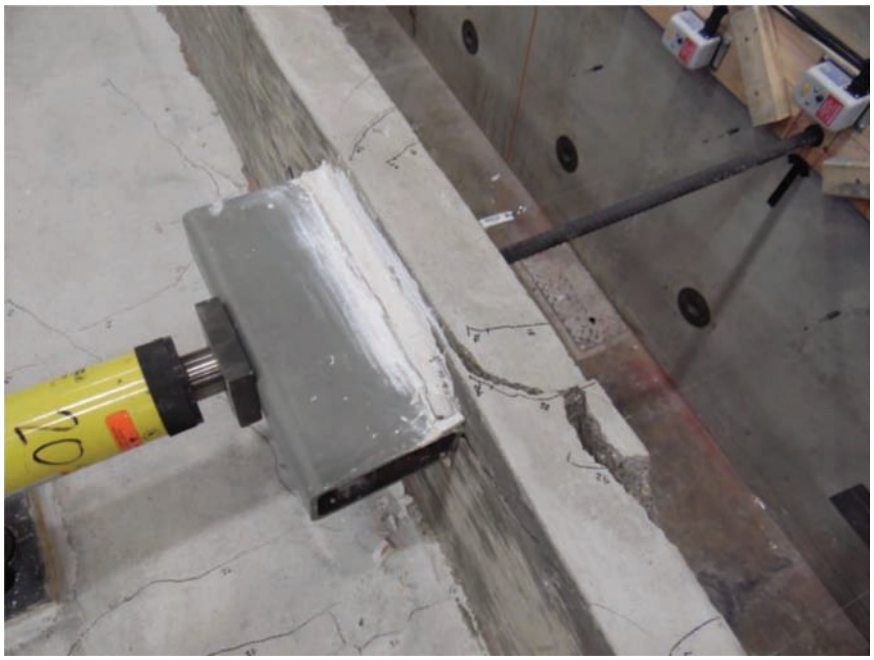

Figure 4.46 Top view of punching shear failure (Specimen 1L).

and a crack was first identified in the slab after 12 kips within the middle 5 ft of the specimen. Barrier cracks were observed at 16 kips approximately 3 ft on either side of load application, consistent with Specimen 1L. With further loading, subsequent barrier cracks symmetrically extended away from the application of load. Figure 4.47 shows the extension of barrier cracks on the left side of loading. In the slab, cracks continued to propagate toward the slab edges with each loading increment. As in Specimen 1L, two specific barrier cracks continued to widen as the system was beginning to use these cracks to form the barrier mechanism. These cracks were respectively located 32 in. and 40 in. to the left and right side of the load application. At a load of 23.7 kips, Specimen 2L failed in punching shear before the barrier mechanism could develop. The failure is shown in Figure 4.48 and Figure 4.49.

4.6.2 Load-Deflection Response

4.6.2.1 Specimens 1 and 2. The load versus midspan deflection for Specimen 1 and Specimen 2 are shown in Figure 4.50. A comparison of both load-deflection curves is shown in Figure 4.51. The slope of both curves in the elastic region prior to cracking were nearly identical. Full length slab cracking was visually observed at 18 kips in Specimen 1 and 13 kips in Specimen 2. Based on the load-deflection response, it appears that cracking

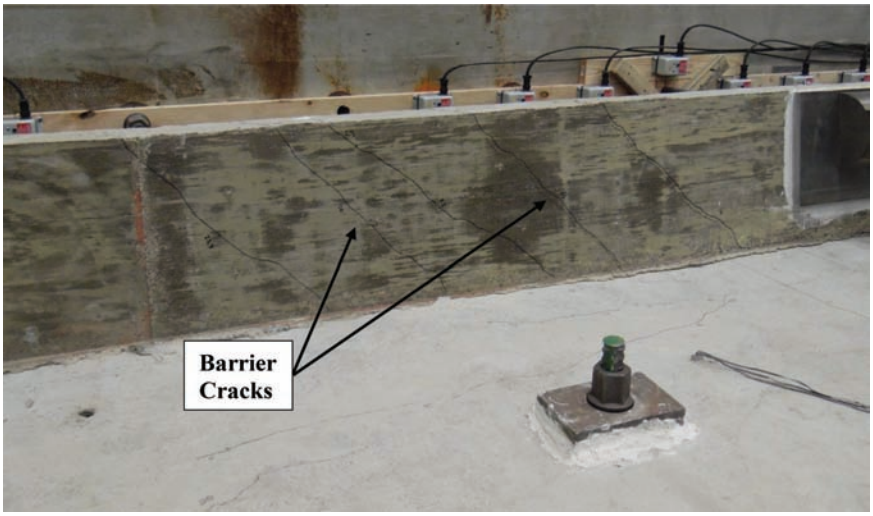

Figure 4.47 Specimen 2L (barrier cracking).

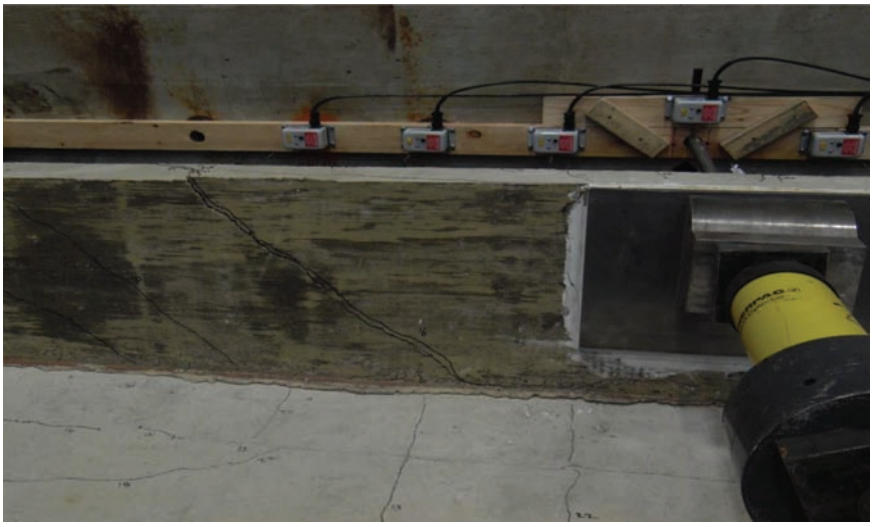

Figure 4.48 Punching shear failure (Specimen 2L).

Figure 4.49 Deflected shape at failure (Specimen 2L).

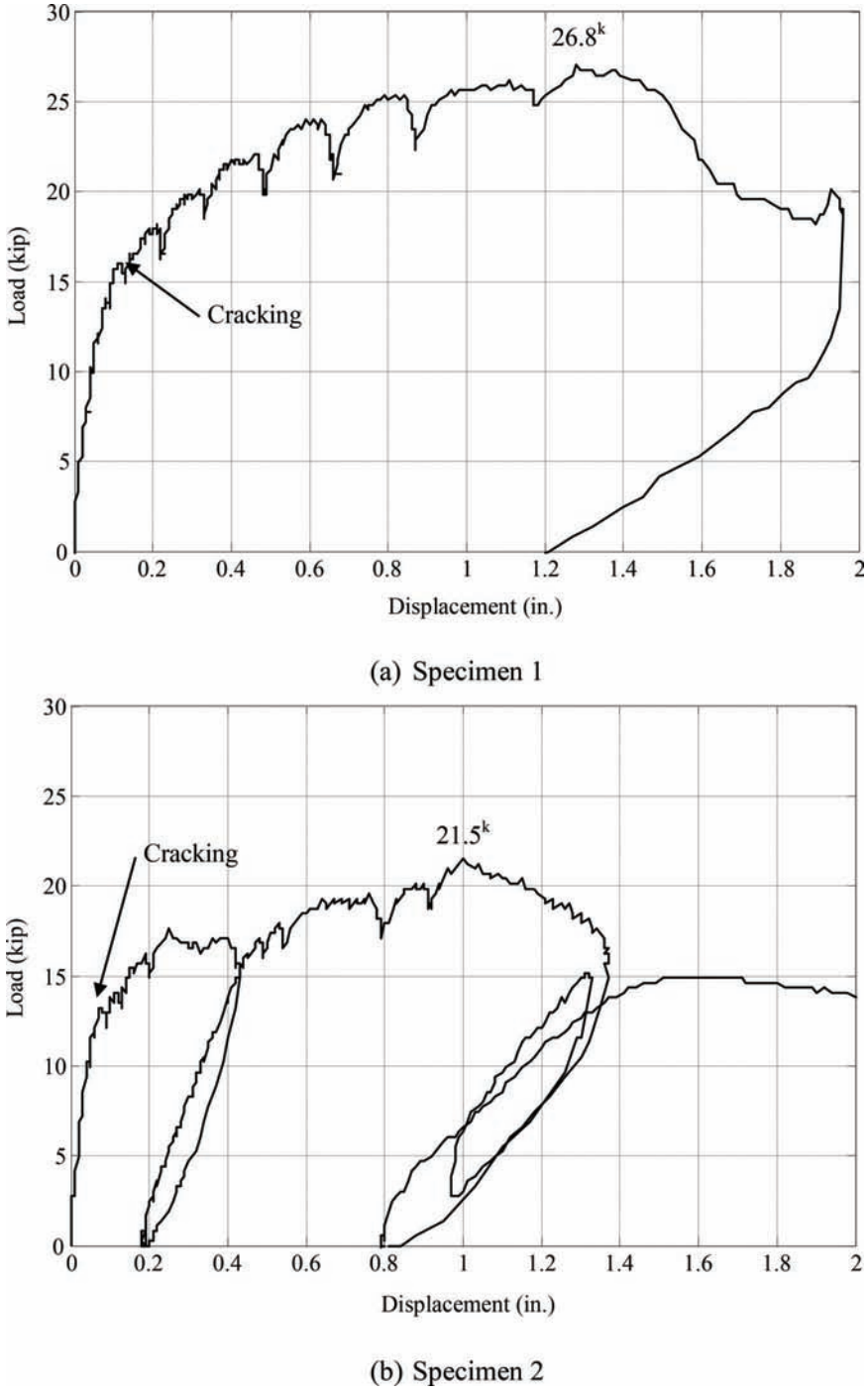

Figure 4.50 Load deflection (Specimens 1 and 2).

originated in Specimen 1 at a slightly lower load (16 kips) while the response for Specimen 2 matches that visually observed. The slightly lower cracking load for Specimen 2 occurs due to the decrease in top transverse reinforcement in the slab for that specimen. Following cracking, a reduction in stiffness was observed. The immediate reduction in load at each loading increment resulted from a combination of increased cracking while maintaining load along with creep.

The maximum loads for Specimens 1 and 2 were 26.8 kips and 21.5 kips, respectively. Due to the fact that each specimen experienced a diagonal tension failure, the maximum load is related to the amount of reinforcement across the shear plane. A higher failure load occurred in Specimen 1 due to the higher amount of primary reinforcement in the slab. Despite the fact that there were approximately half as many top transverse bars in Specimen 2, this did not produce a reduction

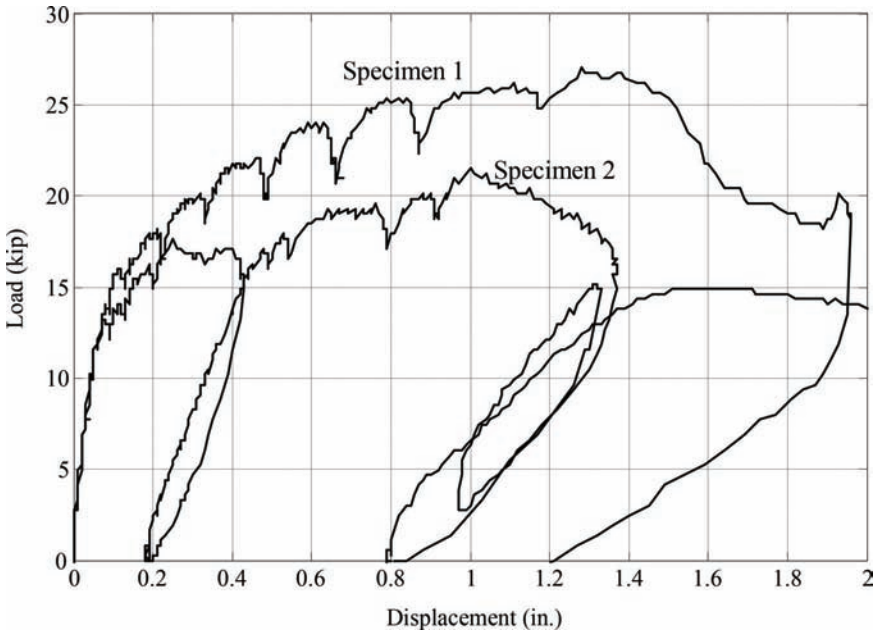

Figure 4.51 Load-deflection comparison (Specimens 1 and 2).

in capacity proportional to the amount of reinforcement. Therefore, the resistance is likely impacted by the stiffness of the reinforcement which is expected when considering diagonal tension failures.

4.6.2.2 Specimens 1L and 2L. The load versus midspan deflection is shown in Figure 4.52 for Specimens 1L and 2L respectively. Both load-deflection curves are plotted together for comparison in Figure 4.53. The reduction of stiffness in the load-deflection curves indicates that cracking occurred at approximately 18 kips in Specimen 1L and 13 kips in Specimen 2L. The slightly lower cracking load for Specimen 2L is due to the decreased amount of top transverse reinforcement in the slab for that specimen. As with Specimens 1 and 2, the immediate reduction in load at each loading increment is attributed to increased cracking under load along with creep.

The maximum loads for Specimens 1L and 2L were 29.2 kips and 23.7 kips, respectively. Each specimen experienced a punching shear failure, and the maximum load is related to application of load and in particular, the different load distribution provided by the loading plate. In both tests, the amount of top transverse reinforcement in the slab did not affect the exhibited failure mechanism.

4.6.3 Global Deflection Response

4.6.3.1 Specimens 1 and 2. The vertical and horizontal displacements were plotted across the 15 ft length of each specimen corresponding to the loading interval to evaluate the global deflection response of both specimens. Figure 4.54 illustrates the vertical displacement behavior of both specimens at different loading increments. It is seen that the specimens maintained relatively uniform deflection across the length of the slab throughout the loading history. Close to failure, there appears to be slightly larger displacements toward the left side of the specimen (left side of graph). In considering a load of 20.1 kips, it is seen that Specimen 2 experienced more than twice the deflection of Specimen 1. At ultimate load (immediately prior to failure), both Specimens deflected vertically approximately 0.4 in. at midspan. This similar displacement is interesting in that both specimens exhibited a shear failure at this point.

The horizontal displacement behavior is shown in Figure 4.55 for the two specimens. The localized deflection of the barrier at midspan as observed in testing is clearly evident. Both Specimens 1 and 2 experienced an increase in deflection closest to the application of load. At the same load of 20.1 kip, Specimen 2 experienced approximately three times the deflection of Specimen 1. At the maximum sustainable load prior to failure, the deflections were approximately 1.3 in. for Specimen 1 and 1 in. for Specimen 2.

4.6.3.2 Specimens 1L and 2L. Vertical and horizontal displacements were plotted across the 27 ft length of each specimen corresponding to the loading interval to evaluate the global deflection response of both specimens. The vertical displacement behavior of both specimens at different loading increments is illustrated in Figure 4.56. Specimen 1L shows higher vertical displacements toward the midspan of the slab length while Specimen 2L had more uniform displacement across the slab length. In considering a load of approximately 24 kips, it is seen that Specimen 2L experienced about twice the deflection of Specimen 1L. At the ultimate load (immediately prior to failure), Specimen 1L deflected 0.22 in. while Specimen 2L deflected 0.28 in. at midspan.

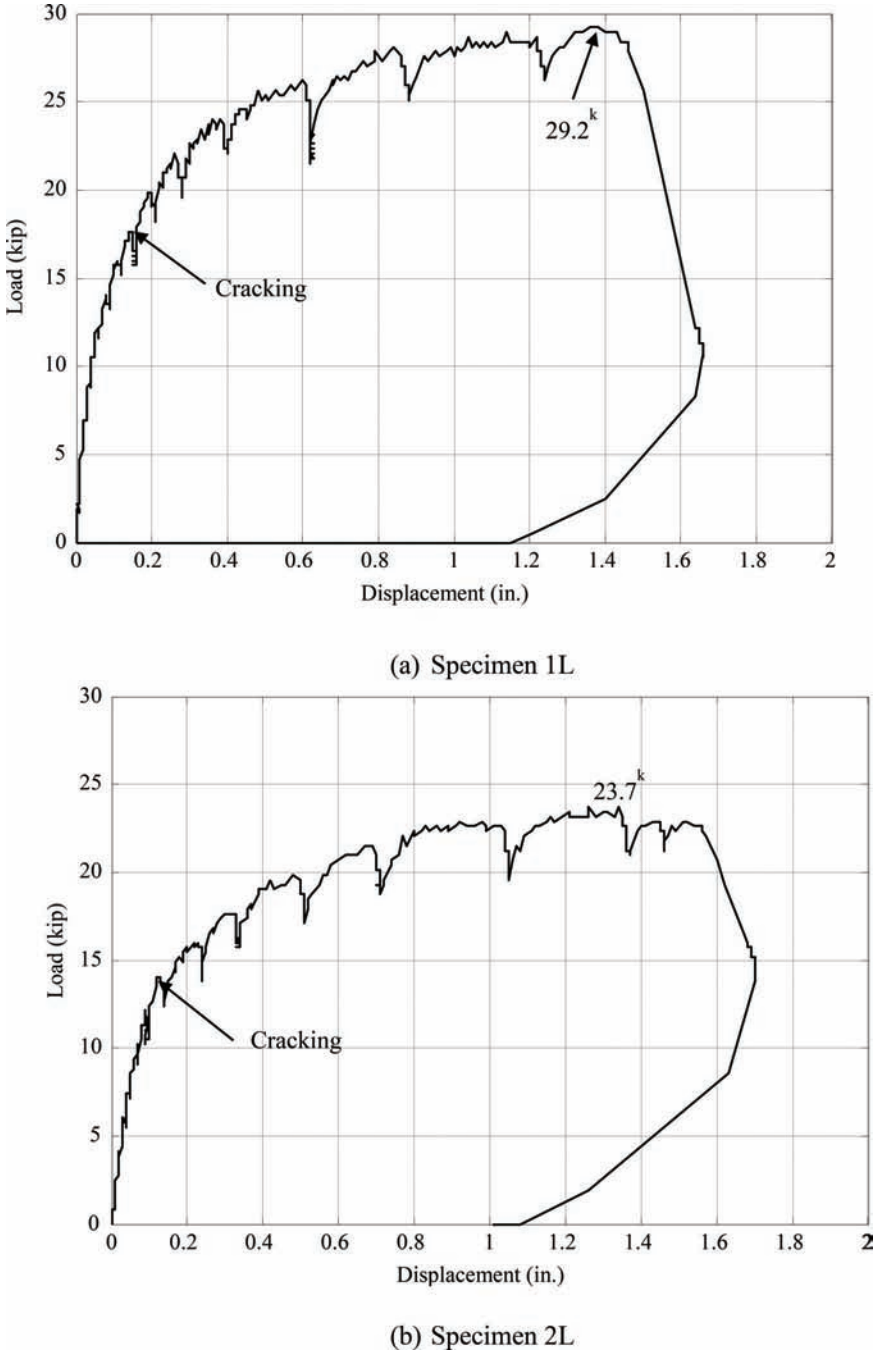

Figure 4.52 Load-deflection (Specimens 1L and 2L).

The horizontal displacement behavior is shown in Figure 4.57 for the two specimens. The localized deflection of the barrier at midspan as observed in testing is again clearly evident. Both Specimens 1L and 2L experienced an increase in deflection closest to the application of load. At the same load of approximately 24 kips, Specimen 2L experienced approximately three times the deflection of Specimen 1. At maximum sustainable load prior to failure, the deflections were approximately 1.3 in. for Specimen 1L and 1.25 in. for Specimen 2L.

4.6.4 Global Strain Response

4.6.4.1 Specimens 1 and 2. The top transverse bars in the slab were instrumented across the 15 ft length of the specimens to observe the strain distribution resulting from the lateral force applied to the barrier. The strain

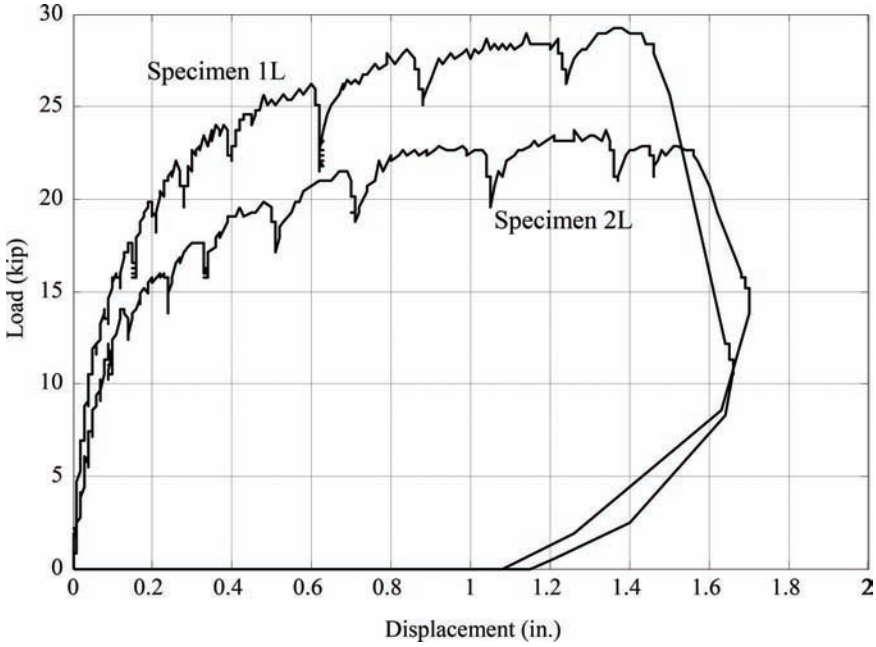

Figure 4.53 Load-deflection comparison (Specimens 1L and 2L).

distribution with respect to the loading increments are shown in Figure 4.58. For both specimens, similar strains are provided across the length of the specimen. In Specimen 1, a non-uniform strain distribution is observed. The strains at the left and right sides are similar, but low strains are noted near the centerline. This drop is unexpected and not consistent with displacement measurements. It is likely that these strains are not realistic and may result from the location of cracking relative to the location of the gage. The strains in Specimen 2 are more consistent across the length of the specimen. In considering the overall behavior, however, the strains measured in both specimens support full-slab engagement, which is consistent with the full-length slab cracking observed in testing. Prior to failure, the average strains across the slab length were approximately 1250 microstrain for Specimen 1 and 1500 microstrain for Specimen 2.

4.6.4.2 Specimens 1L and 2L. The top transverse bars in the slab were instrumented across the 27 ft length of the specimens to observe the strain distribution resulting from the lateral force applied to the barrier. The strain distribution with respect to the loading increments are shown in Figure 4.59 and both specimens demonstrated a non-uniform strain behavior across the deck. It is likely that these strains are not realistic and may result from the location of cracking relative to the location of the gage. Prior to failure, the average strains across the slab length were approximately 280 microstrain for Specimen 1L and 820 microstrain for Specimen 2L.

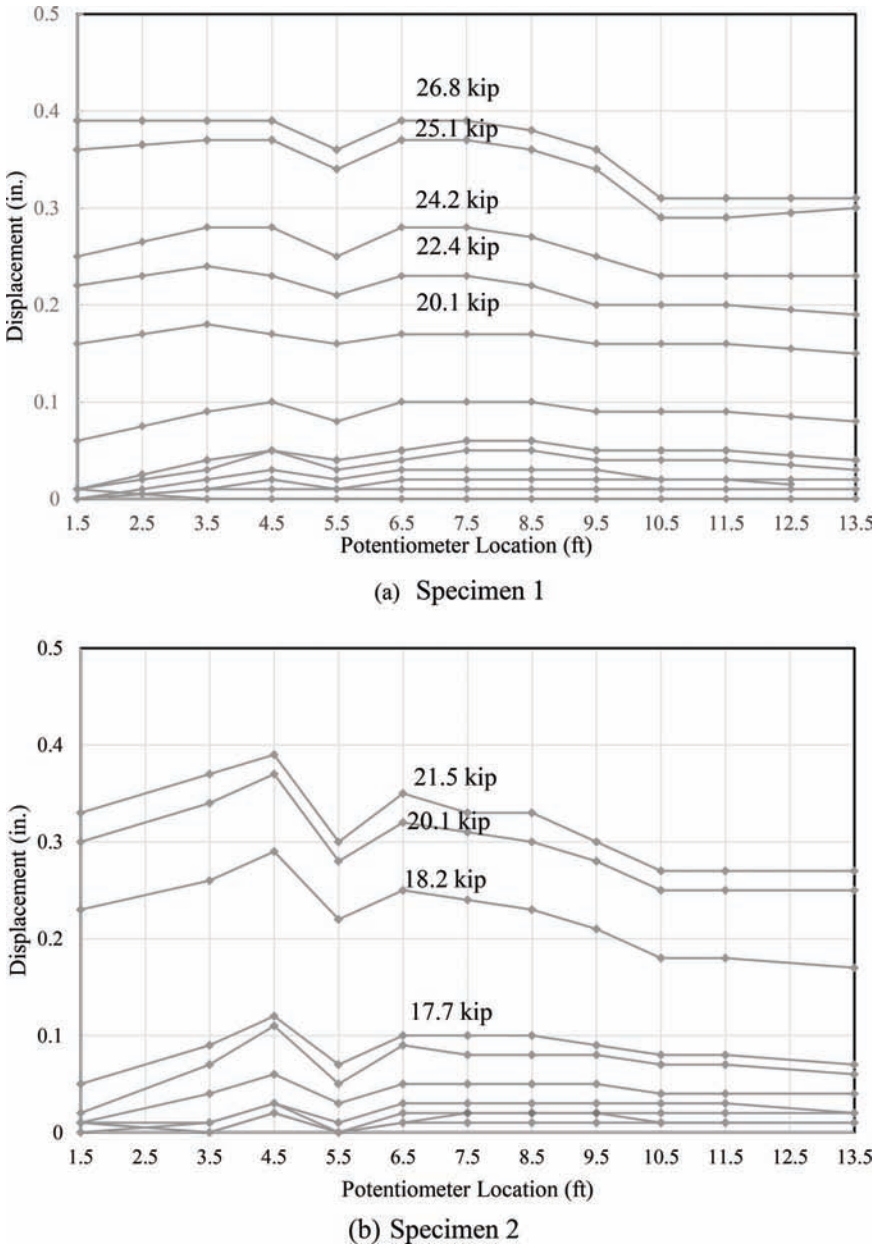

Figure 4.54 Vertical displacement distribution (Specimens 1 and 2).

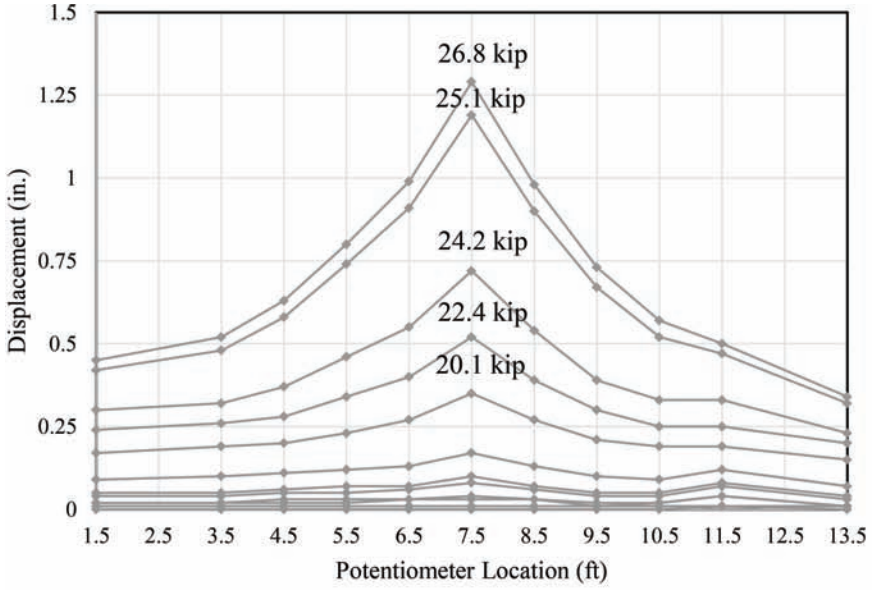

(a) Specimen 1

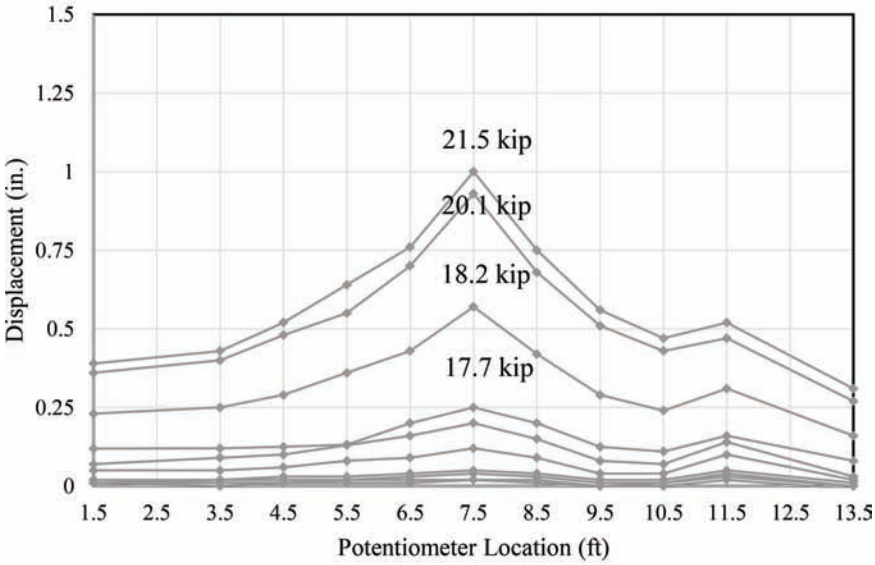

(a) Specimen 2

Figure 4.55 Horizontal displacement distribution (Specimens 1 and 2).

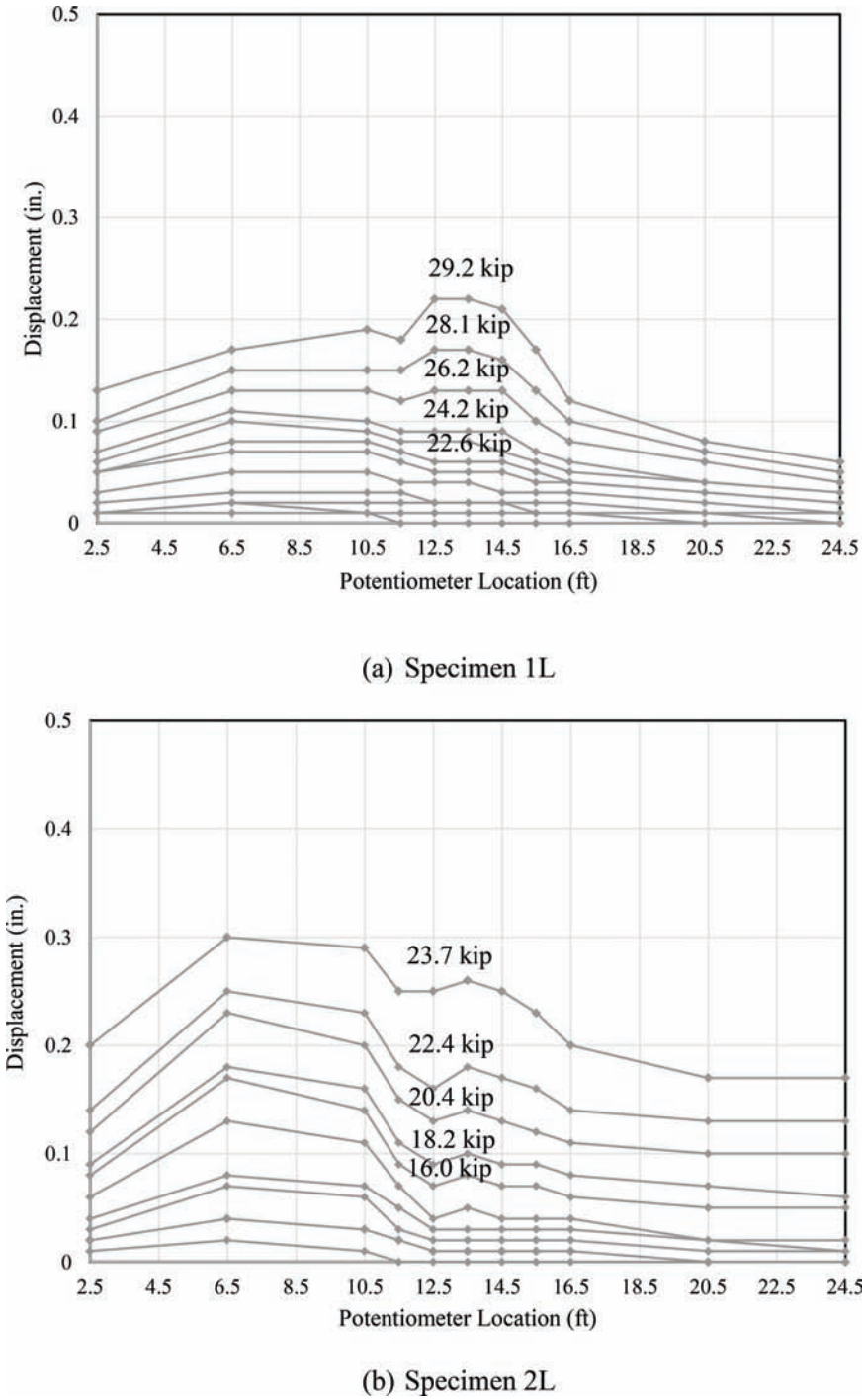

Figure 4.56 Vertical displacement distribution (Specimens 1L and 2L).

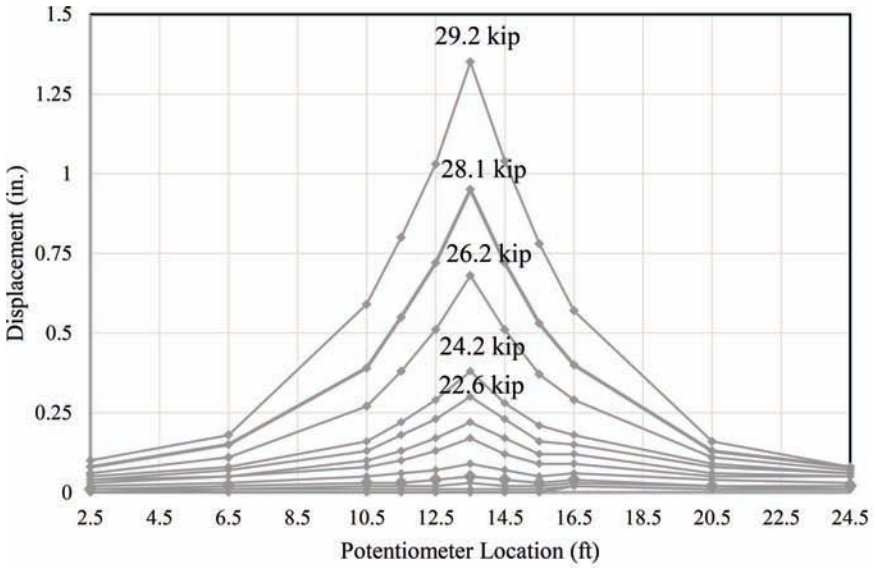

(a) Specimen 1L

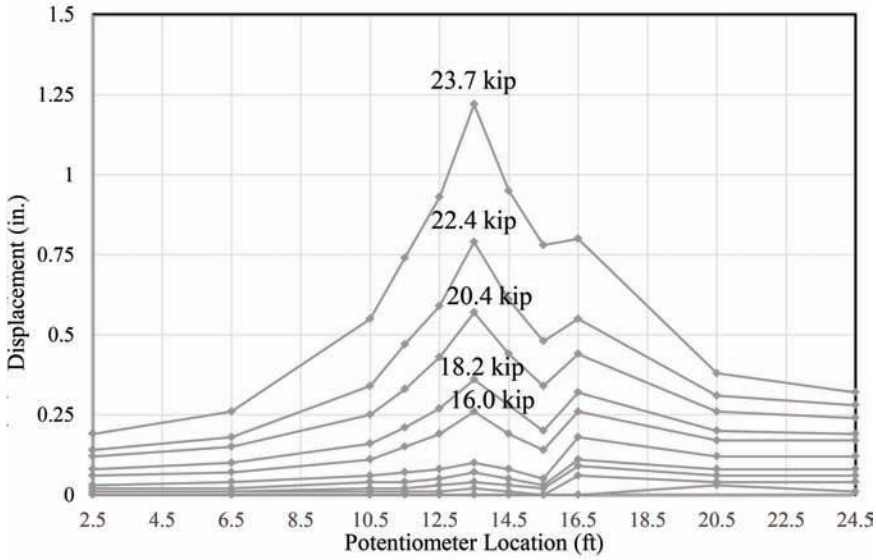

(b) Specimen 2L

Figure 4.57 Horizontal displacement distribution (Specimens 1L and 2L).

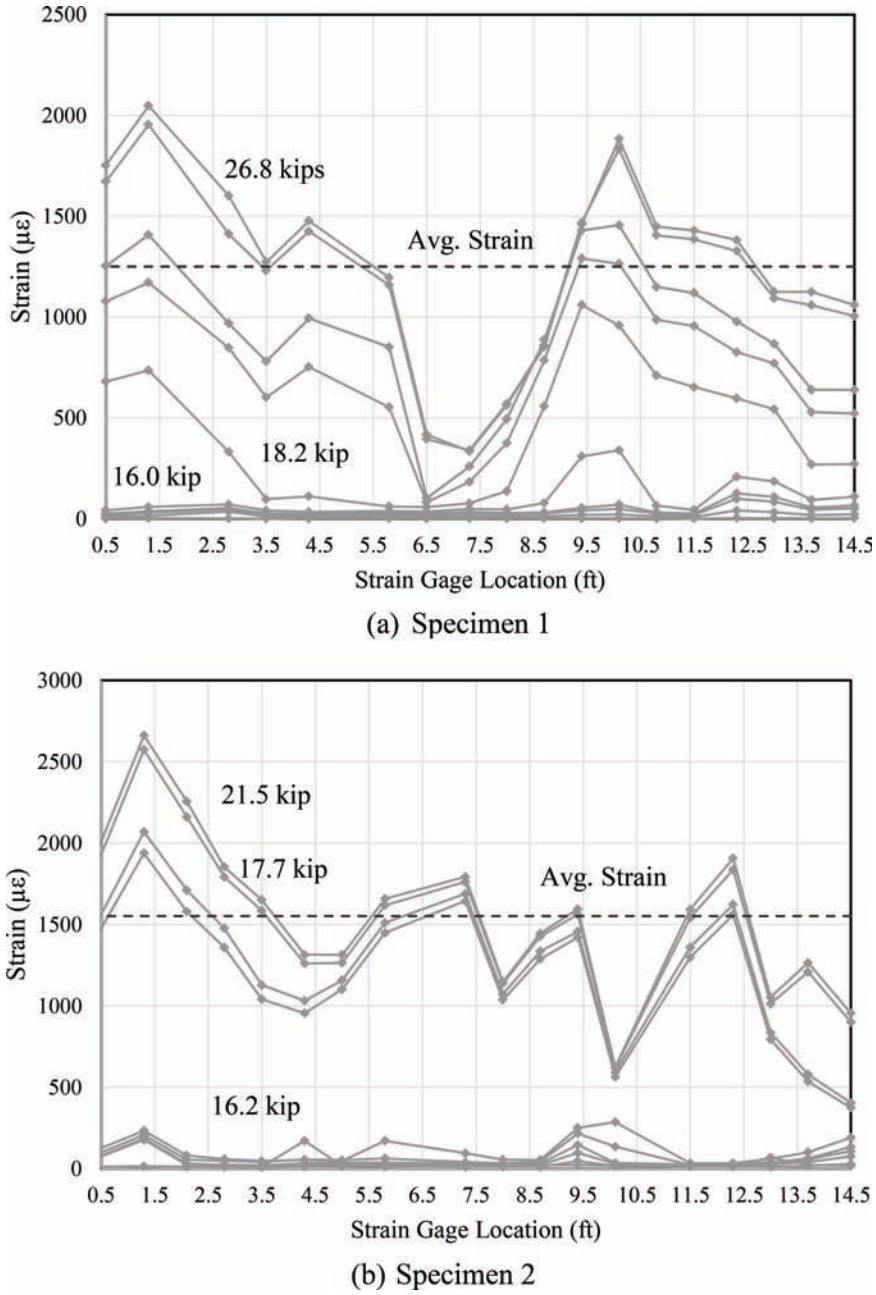

Figure 4.58 Jacking strain distribution (Specimens 1 and 2).

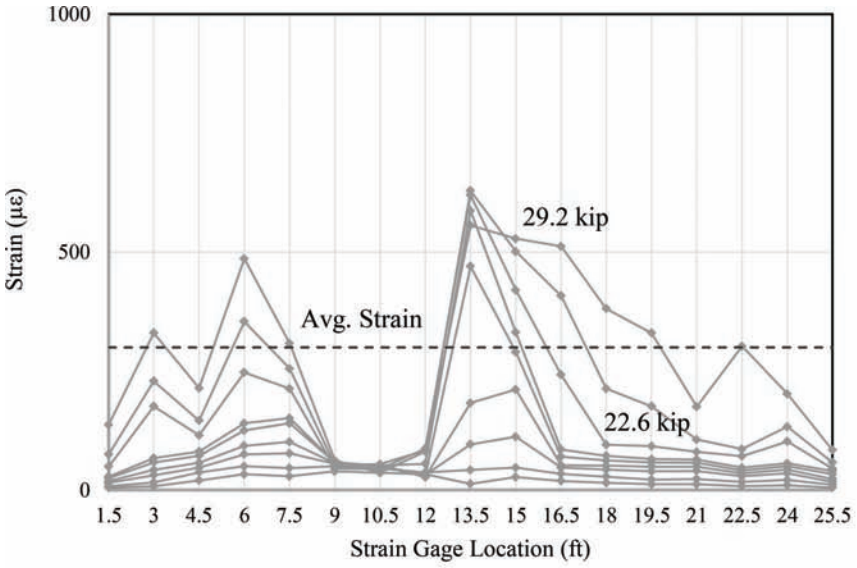

(a) Specimen 1L

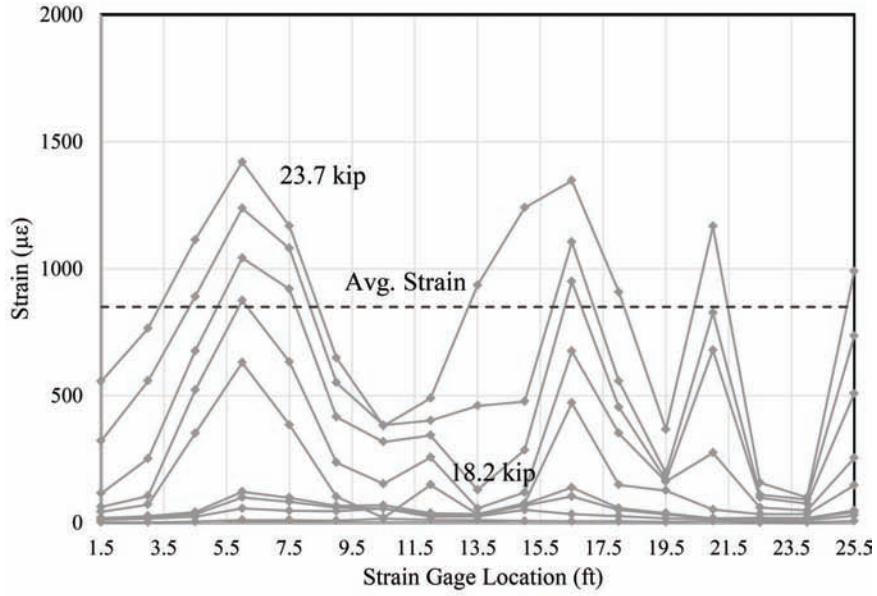

(b) Specimen 2L

Figure 4.59 Jacking strain distribution (Specimens 1L and 2L).

5. SECTIONAL BEHAVIOR: BRIDGE DECK-BARRIER WALL

5.1 Introduction

An experimental program was developed to evaluate the sectional behavior of the bridge deck-barrier wall connection. Of particular interest was the anchorage of the top transverse bars in bridge deck overhangs. The top transverse reinforcement was varied with respect to bar size, bar coating, and anchorage detail. Five full-scale and two half-scale specimens were tested. The different scale specimens allow for connection of the half-scale system behavior presented in Chapter 4 with the full scale system. In addition, behavior at different scales could be compared.

5.2 Specimen Design

Seven 3 ft strip specimens were designed. It was decided to evaluate five full- scale specimens with a typical INDOT Type FC concrete barrier and 8 in. bridge deck to represent field performance. Two half scale specimens were also designed representing an approximate 50% dimensional scale. The half-scale specimens were designed identical to the 15 ft and 27 ft specimens to allow direct comparison of the sectional and overall system behavior. The top transverse reinforcement was designed using the AASHTO (2014) overhang design procedure.

For a given scale, the specimens are geometrically identical with the exception of the deck top transverse reinforcement. A cross section is shown for a full-scale specimen in Figure 5.1 and for a half-scale specimen in Figure 5.2. For the full-scale specimens, the type FC barrier is included while for the half scale specimens, the same rectangular section designed from the overall system test was used. As noted, the top transverse reinforcement was varied. Variable included the size of reinforcement, type of reinforcement (epoxy-coated or black) and the end anchorage of the bar. The primary variables for each specimen are listed in Table 5.1.

5.3 Construction

The specimens were constructed in the Purdue University Bowen Laboratory by means of a two phase cast in which the slab and barrier were cast separately. The construction process for the specimens is provided in the following sections.

5.4 Casting

All seven strip specimens were cast simultaneously with separate pours for the slab and barrier casts. The reinforcement was placed in the slab along with barrier stirrups prior to casting. Bolsters were placed longitudinally in the slab to avoid influencing the overhang behavior in the transverse direction. Figure 5.3 through Figure 5.7 illustrate the reinforcement placement and casting process.

Concrete was placed using a concrete bucket and vibrators were used for consolidation. A construction joint was provided between the slab and barrier in the transverse direction. The joint was created within the 16 in. width of the barrier interface and grooves were placed at approximately 1.5 in. centers (Figure 5.6).

Following the casting of the slab, longitudinal reinforcement was installed along with the formwork for the barrier. The barrier was cast using a concrete bucket as for the slab. A lateral tie system was installed to accommodate the lateral concrete pressure exerted on the formwork and is illustrated in Figure 5.7.

The slab and barrier were cast within three days of one another, and the specimens were cured by means of wet burlap moistening. Burlap was moistened for 14 days, and the same curing procedure was used for the specimens and concrete cylinders.

5.5 Materials

5.5.1 Reinforcing Steel

The rebar used in the Strip Specimens were A615 Grade 60 bars supplied by Harris Rebar and NUCOR Steel. For each bar size and coating, the reinforcement was taken from the same heat of steel. Table 5.2 lists the chemical composition of the bars used in the strip specimens. Three consecutive tension tests were performed in accordance with ASTM A370 (2014) using an INSTRON universal testing machine, and test results up to 5% strain are shown in Figure 5.8 through Figure 5.12. Physical Testing properties are shown in Table 5.3.

5.5.2 Concrete

Concrete used for the strip specimens was obtained from Irving Materials Inc., a local ready mix supplier. Two pours were required for casting the strip specimens. The mix design used for the seven strip specimens was identical and matched the mix design used on the 15 ft and 27 ft system specimens. The concrete was a 3500 psi nominal 3/8 in. P-Gravel mix with Type I Portland Cement and a mid-range water reducer. The concrete mix design is provided in Table 5.4. For the two casts, a 6 in. slump was specified, and the actual slump measured 4 in. for the slab cast and 6 in. for the barrier cast.

The concrete was tested in accordance with ASTM C39 (2015) and the strength gain history is shown in Figure 5.13. The values reported are the average of three test cylinders. The 28-day strength for the slab and barrier was 4330 psi and 4020 psi, respectively (Table 5.4). In addition to compressive strength, split cylinder tensile strengths (average of three cylinders) is provided. Concrete testing was performed to provide a strength range from the beginning of tests (12/14) to the end of testing (12/18) for the strip specimens; and these values are shown.

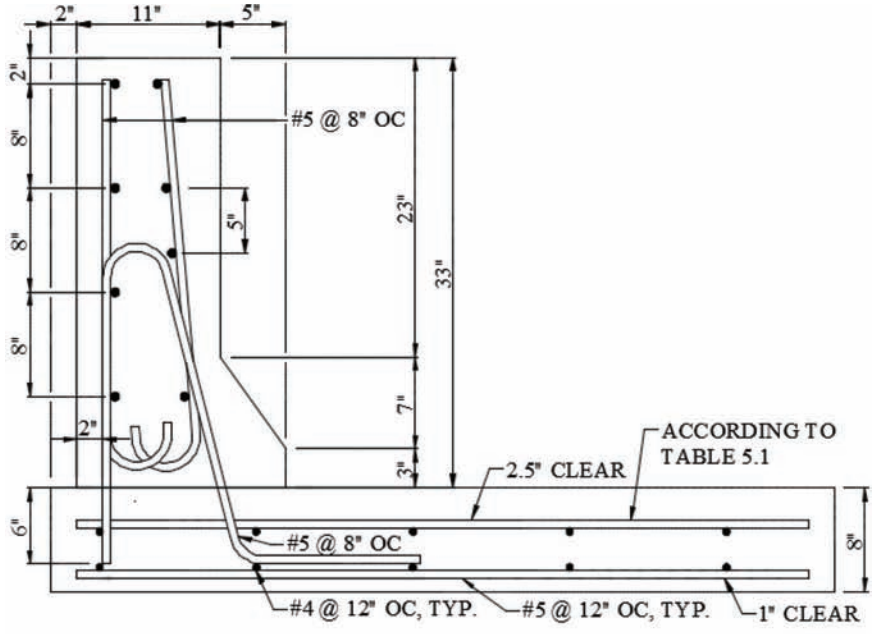

(a) Straight Bars

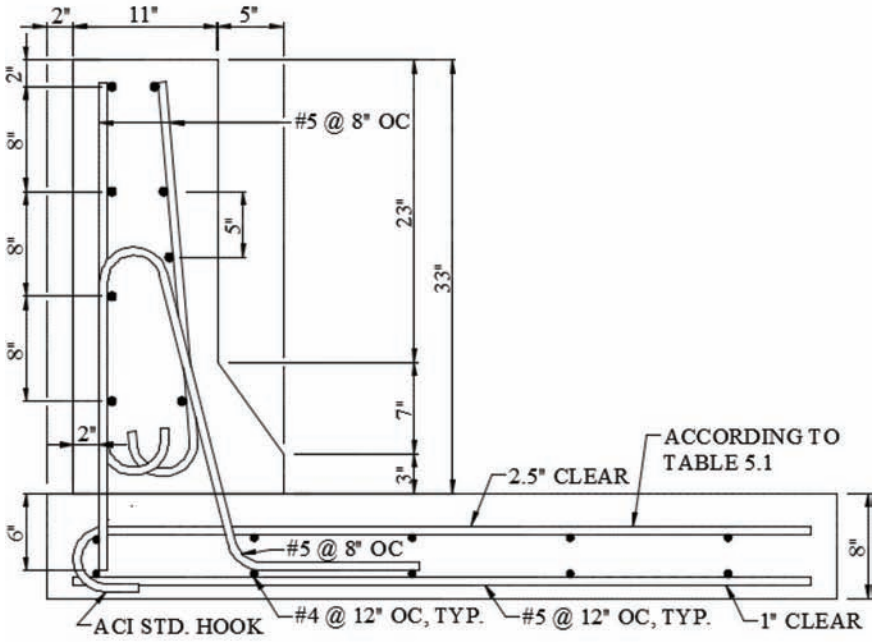

(b) Hooked Bars

Figure 5.1 Cross section view (full-scale strip specimens).

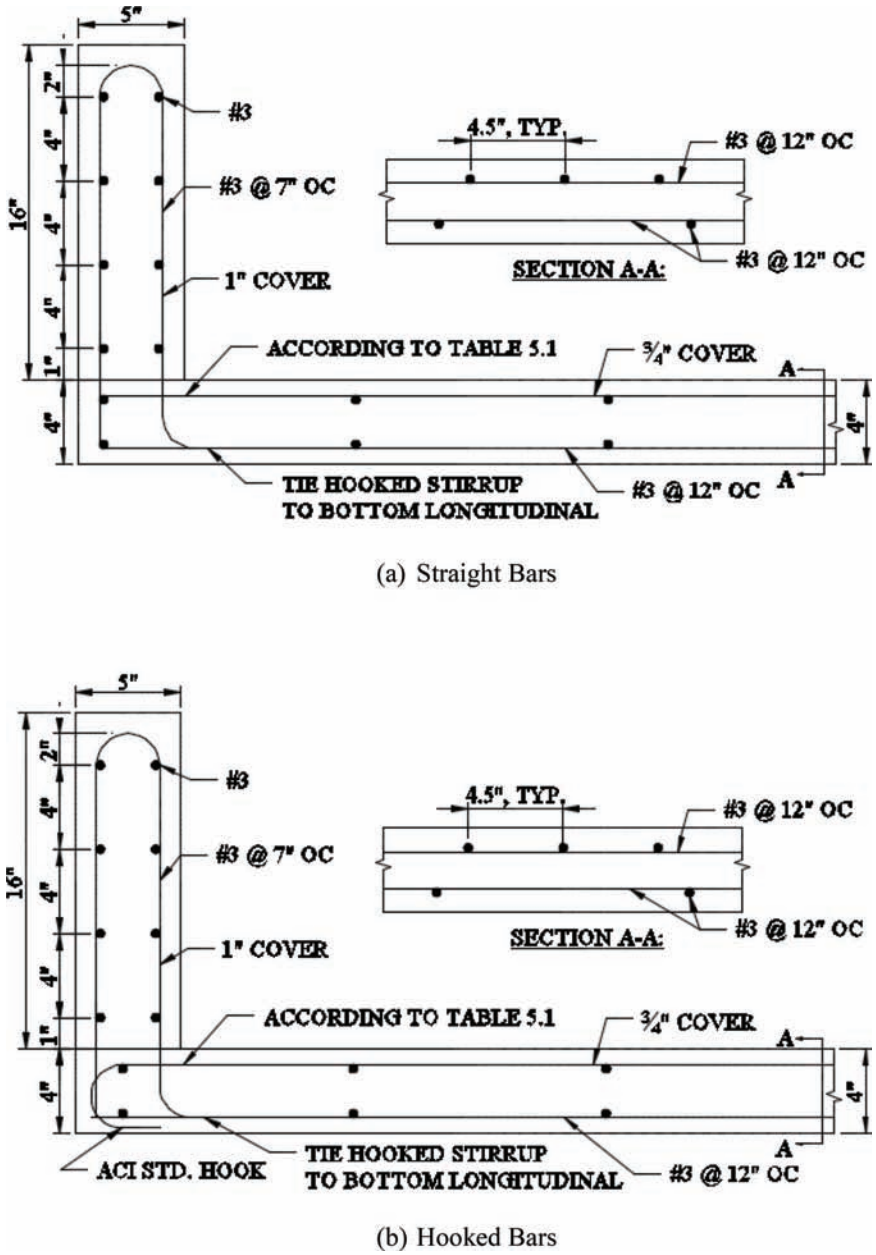

Figure 5.2 Cross section view (half scale strip specimens).

TABLE 5.1
Strip Specimen Test Variables

Specimen	Test Scale	Top Transverse Bar Size	Top Transverse Bar Spacing (in.)	Bar Type	Anchorage
1	Full	#5	3.5	Epoxy	Straight
2	Full	#6	4.75	Epoxy	Straight
3	Full	#5	3.5	Epoxy	Hooked
4	Full	#5	3.5	Black	Straight
5	Full	#6	4.75	Black	Straight
6	Half	#3	4.5	Black	Hooked
7	Half	#3	4.5	Black	Straight

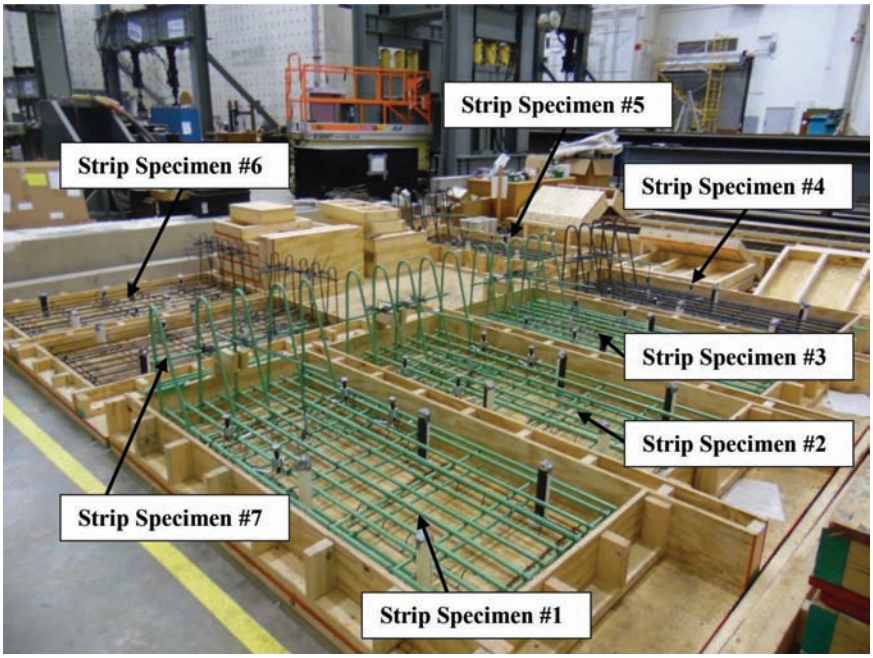

Figure 5.3 Strip specimen slab reinforcement.

Figure 5.4 Strip specimen slab cast.

Figure 5.5 Completed strip specimen slab cast.

Figure 5.6 Barrier reinforcement for strip specimens.

Figure 5.7 Completed barrier cast.

TABLE 5.2
Mill Certification Reinforcement Composition (Strip Specimens)

	% Composition				
Alloying Element	**#6 Epoxy**	**#5 Epoxy**	**#5 Black**	**#6 Black**	**#3 Black**
C/Ni	0.39/0.15	0.40/0.16	0.28/0.15	0.41/0.22	0.41/022
Mn/Cr	1.15/0.12	1.09/0.12	1.21/0.13	1.11/0.12	1.11/0.12
P/Mo	0.018/0.048	0.012/0.054	0.019/0.047	0.011/0.074	0.011/0.074
S/V	0.019/0.0079	0.047/0.0078	0.036/0.044	0.054/0.01	0.054/0.01
Si/Cb	0.23/0.001	0.21/0.001	0.19/0.001	0.16/-	0.16/-
Cu/Sn	0.36/0.019	0.31/-	0.35/0.016	0.36/0.017	0.36/0.017

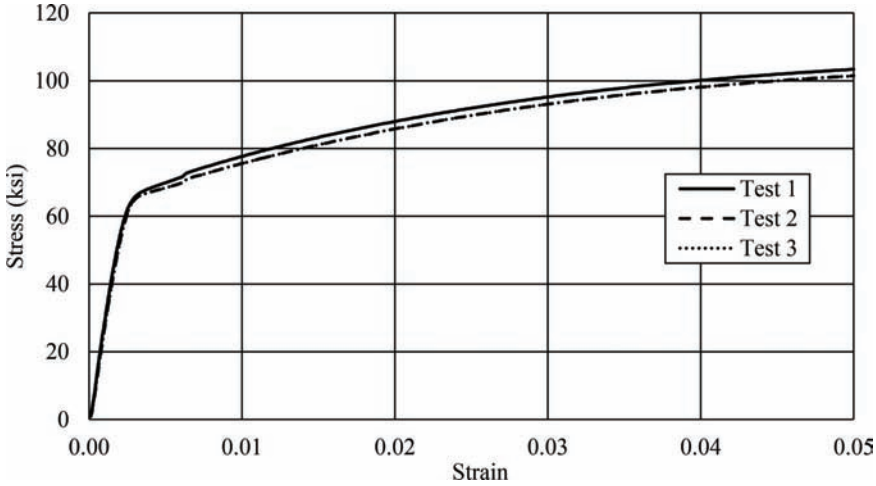

Figure 5.8 Tension test results (Black #3).

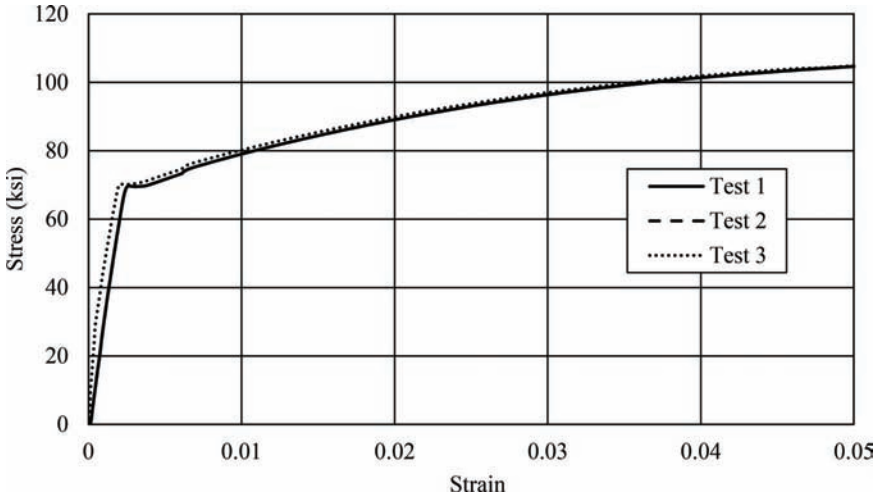

Figure 5.9 Tension test results (Black #6).

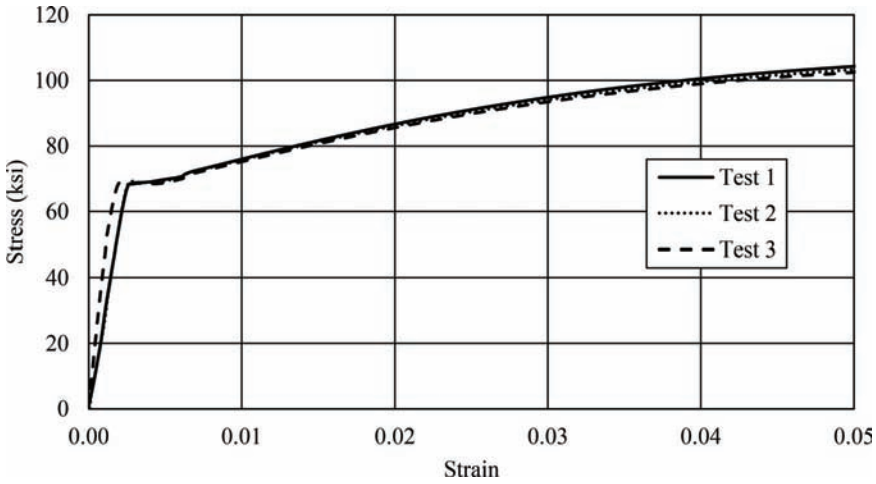

Figure 5.10 Tension test results (Black #5).

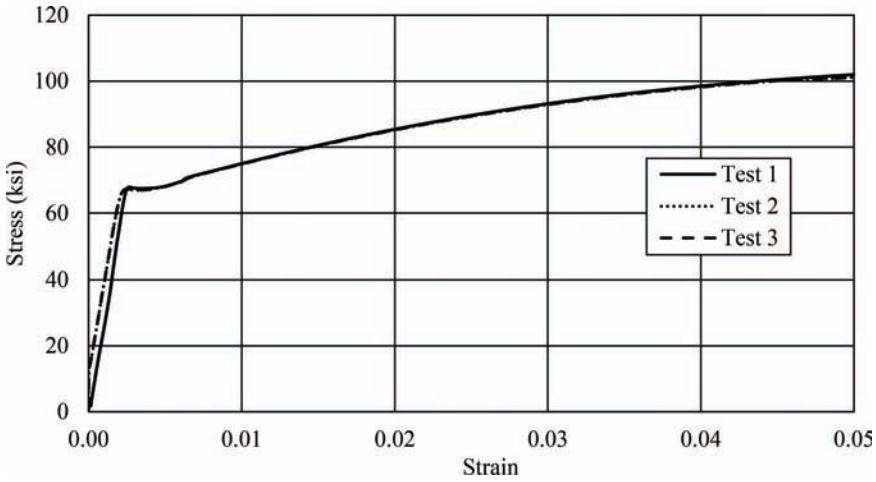

Figure 5.11 Tension test results (Epoxy #5).

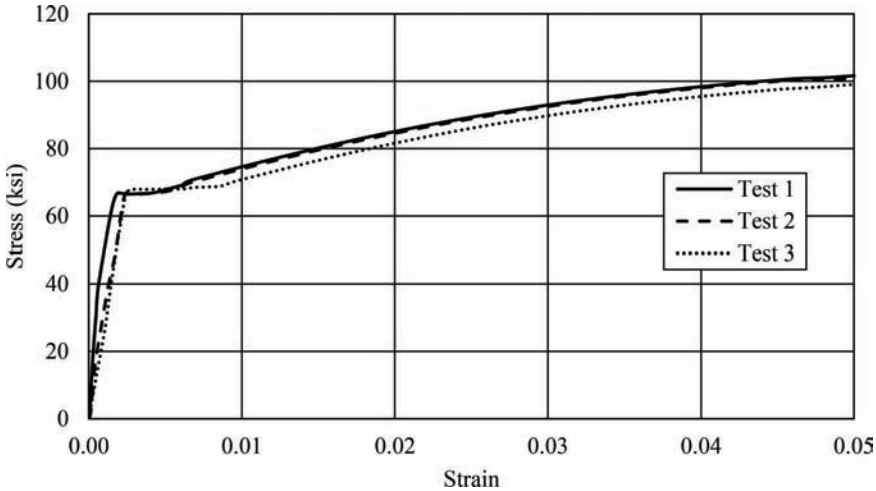

Figure 5.12 Tension test results (Epoxy #6).

TABLE 5.3
Physical Testing Properties (Strip Specimens)

Bar Designation	f_y (psi)	f_u (psi)	% Elongation
Black #5	69	108	14
Epoxy #5	68	107	14
Black #6	70	108	15
Epoxy #6	68	110	14
Black #3	69	108	13

TABLE 5.4
Concrete Mix Proportions (Strip Specimens)

Material Constituent	Mix Design (lb/cy)	Cast 1 (lb/cy)	Cast 2 (lb/cy)
Cement (Type 1)	430	430	426
P-Gravel (3/8 MSA)	1800	1800	1792
Sand-23	1540	1604	1600
Water Reducer (Glenium)	4.00/C	17 oz	17.2 oz
Water	219.7	232	225
W/C Ratio	0.51	0.52	0.55
Slump	6 in.	4 in.	6 in.

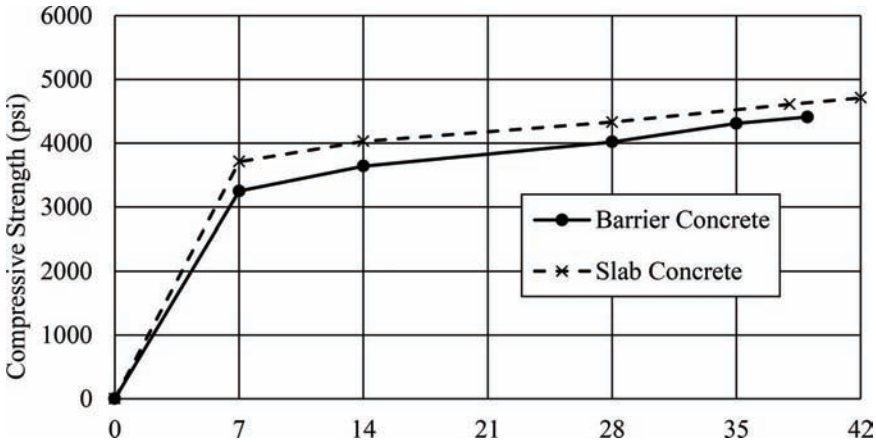

Figure 5.13 Concrete compressive strength (strip specimens).

TABLE 5.5
Concrete Strength Range (Strip Specimens)

Break Date	Concrete	Age (Days)	Compressive Strength (psi)	Tensile Strength (psi)
12/14	Barrier	35	4310	420
	Slab	38	4610	400
12/18	Barrier	39	4410	480
	Slab	42	4710	430

5.6 Experimental Setup

The strip specimens were supported by a 4 ft x 4 ft concrete block which was used to provide fixity and the desired overhang length. It was decided to position the face of the barrier 1 ft from the edge of the support block for the seven strip specimens to avoid introducing a D-region near the deck-barrier interface. Due to the fact that the critical section is at the barrier face, the experiment was designed to focus on the behavior at the joint. A rendering of the experimental setup is shown in Figure 5.14 for both the full scale and half scale strip specimens.

A strong wall was used as a reaction block by which a lateral load was applied to the barrier of the strip specimens. Two 1 in. diameter Dywidag rods were anchored to the strong wall and extended through two holes in the specimen barrier. A loading beam, two jacks, and a load cell were placed inboard the barrier with a Dywidag rod extending through each element. For the full-scale specimens, two Enerpac 30 ton hydraulic jacks were used to load the HSS stub which distributed the force at the midspan of the barrier over a 3 ft length, 5¾ in. (centerline) from the top of the wall. The half-scale specimens were loaded with two

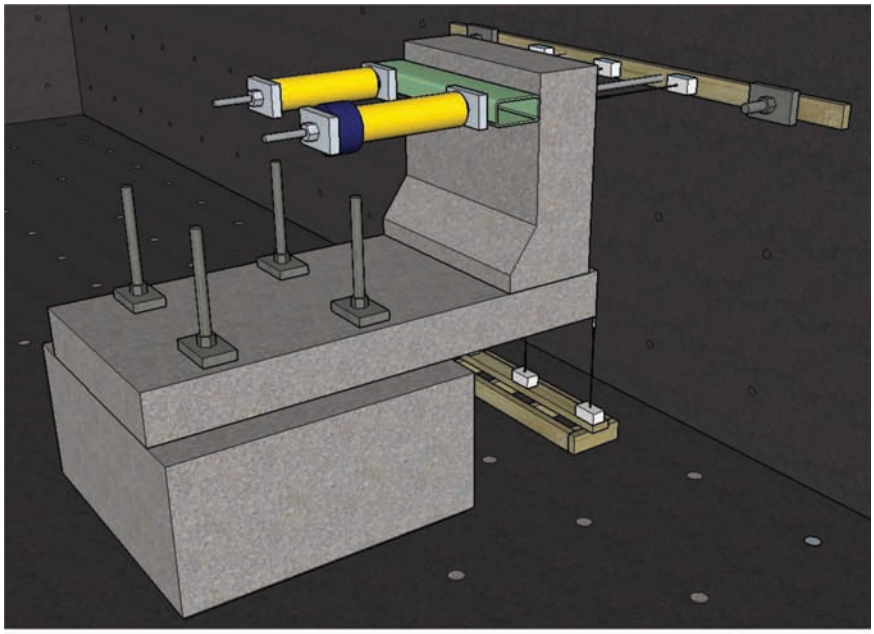

(a) Full-Scale

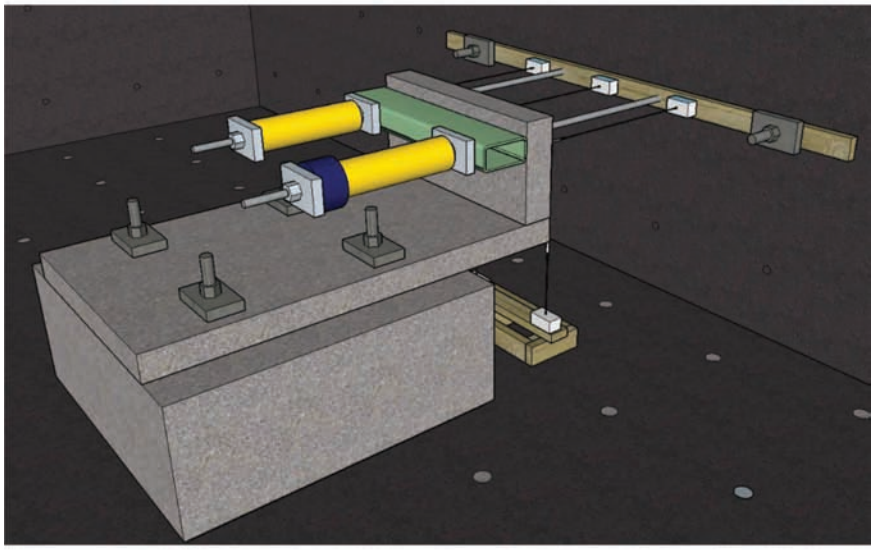

(b) Half-Scale

Figure 5.14 Rendering of experimental setup (strip specimens).

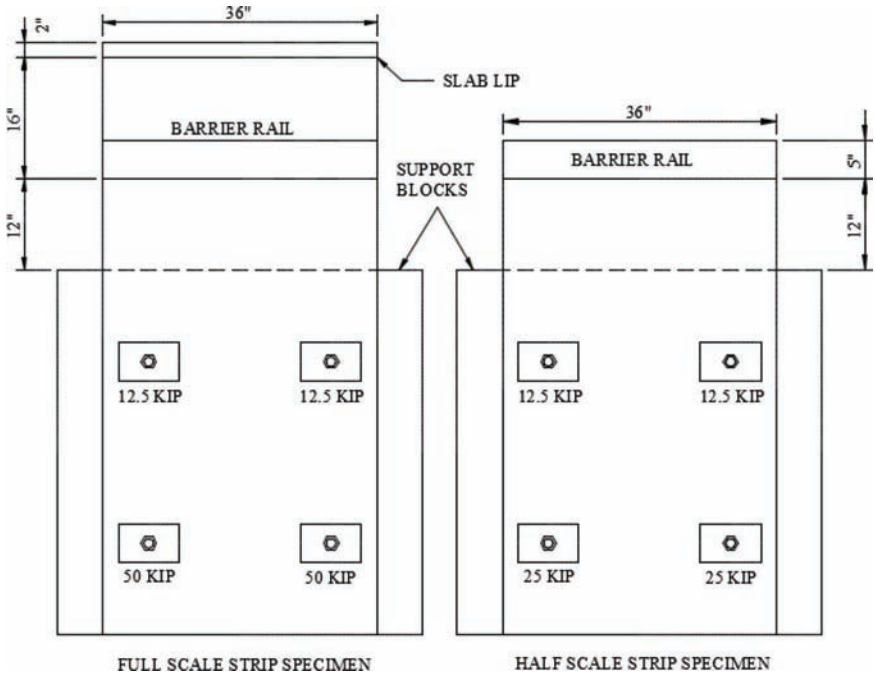

Figure 5.15 Post-tensioning diagram for strip specimens (plan view).

Enerpac 20 ton hydraulic jacks distributing the force across the 3 ft HSS stub, 4½ in. (centerline) from the top of the wall.

The deck was fixed to the support block with hydrostone and post-tensioning. To resist the lateral forces imparted on the barrier, the strip specimens were post tensioned to the strong floor using 1¼ in. diameter Dywidag bars and 8x5x1½ in. bearing plates. The bearing plates were attached to the specimens using hydrostone to reduce stress concentrations and ensure that each plate stayed level during post-tensioning. Post-tensioning details are provided in Figure 5.15.

5.6.1 Instrumentation

Lebow 50 kip and 20 kip load cells were used to measure the force at each loading step for the full-scale and half-scale strip specimens respectively. Strain gages were instrumented on transverse bars in the slab at the face of the barrier and edge of support block. The gages were used to measure strain at each location and quantify the stress in the bars during testing. Potentiometers were used to measure horizontal displacement of the barrier and vertical displacement of the slab. The complete experimental setup for the strip specimens is shown in Figure 5.19.

5.6.1.1 Strain Gage Instrumentation. Two top transverse bars at slab midspan were instrumented in each of the seven strip specimens. The strain gages were 3-wire 1.5x5 mm with a resistance of 120 Ohms and a gage factor of 2. The gages were placed at the barrier face and edge of support in each of the strip specimens. The exact location of each gage in the slabs are shown in Figure 5.16 and Figure 5.17.

5.6.1.2 Potentiometer Instrumentation. The strip specimens were instrumented with potentiometers on the barrier and slab. Potentiometers were positioned at the height of loading on the barrier and at the slab edge to measure horizontal displacement near the application of load and maximum vertical displacement. The potentiometers used were the UniMeasure PA Series with a 10 in. displacement range. Details of the potentiometer locations are shown in Figure 5.18 and provides sensor identification information.

5.6.2 Testing Procedure

The support blocks and strip specimens were set up by the strong wall in preparation for testing. The instrumentation was wired to a Micro-Measurements System 7000 for data acquisition, and a sampling rate of 0.1 seconds was used for data recording. The full and half scale strip specimens were loaded in 2 kip and 1 kip increments, respectively. At each load stage, the specimen was inspected and cracks were mapped.

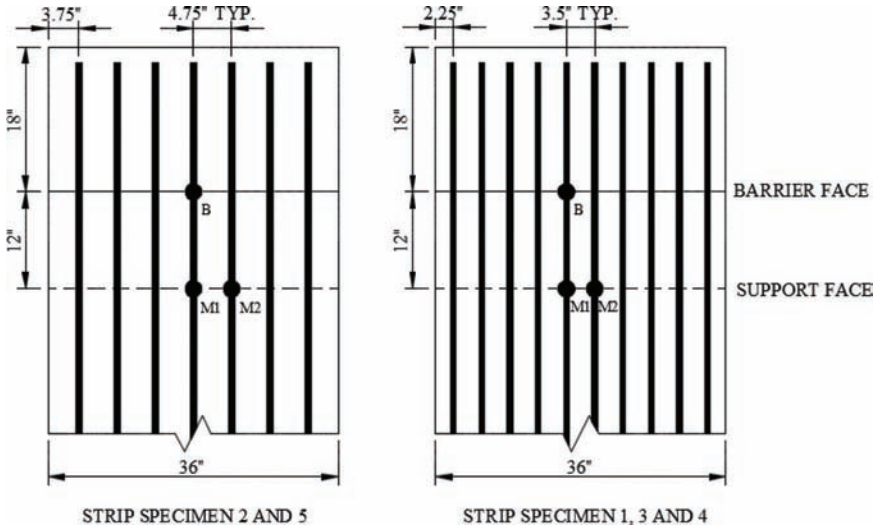

Figure 5.16 Full-scale strain gage instrumentation (plan view).

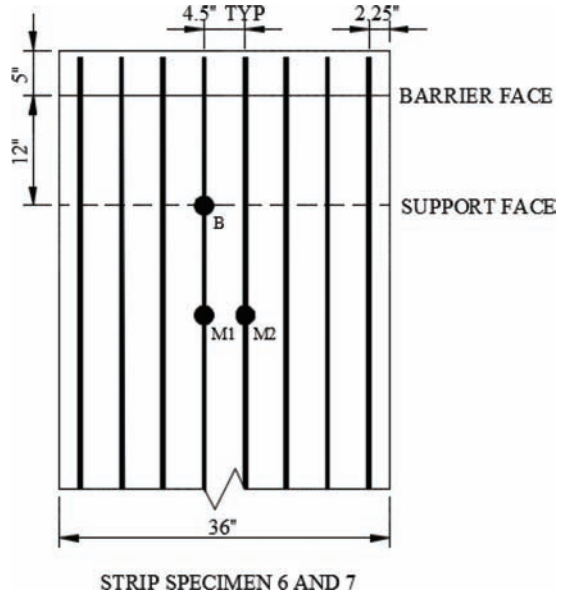

Figure 5.17 Half-scale strain gage instrumentation (plan view).

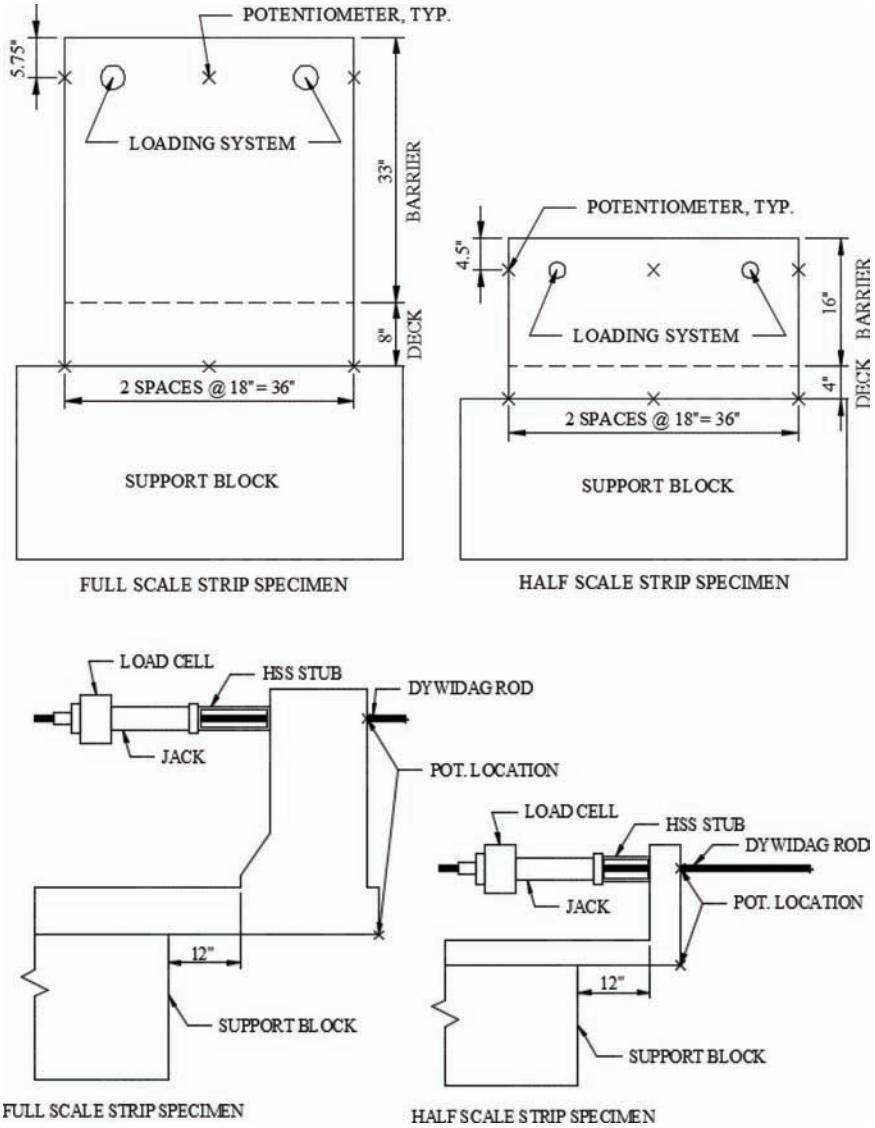

Figure 5.18 Strip specimen potentiometer locations (elevation view).

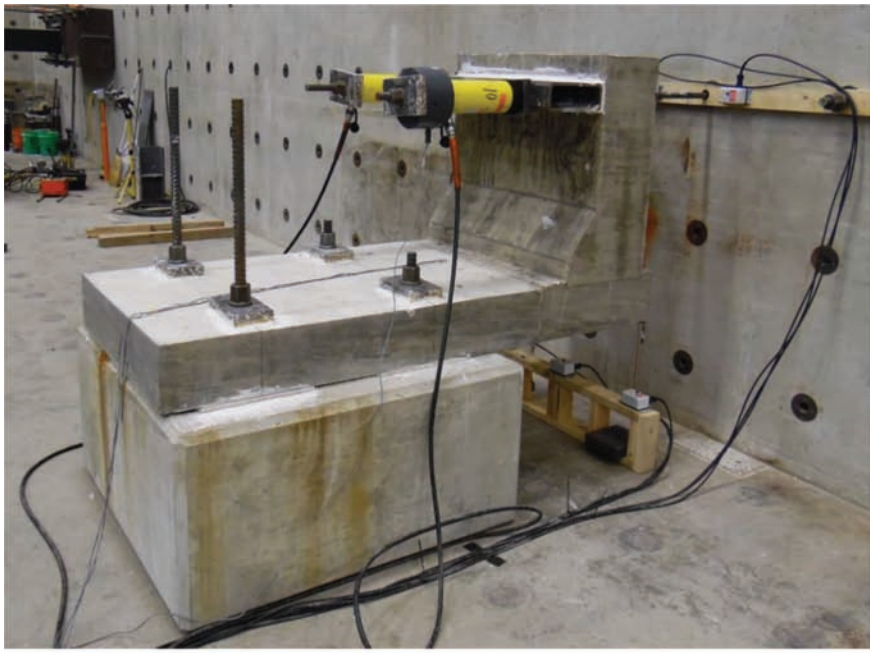

(a) Full-Scale

(b) Half-Scale

Figure 5.19 Strip specimen experimental setup.

5.7 Test Results

Testing was conducted from December 14th through December 21st (Table 5.6). The results are provided in the following sections.

5.7.1 Overall Behavior

5.7.1.1 Strip Specimen 1. Strip Specimen 1 was loaded in 2 kip intervals, and cracks were first identified in the slab after 10 kips. The cracks extended longitudinally the full slab length and were located near the barrier interface and over the edge of the support block. At 10 kips, the load deflection curve showed a flattening indicating a reduction in stiffness followed by a sharp decrease in load to approximately 5 kips. This sharp reduction in load is attributed to excess hydrostone between the loading rod and specimen in the loading hole which prevented movement until disengagement. This initial hydrostone binding was remedied in latter testing of other strip specimens.

TABLE 5.6
Strip Specimen Testing Schedule

Strip Specimen #	Date	Time	Ultimate Capacity (kip)
1	12/14	9:00 A.M.	14.3
2	12/15	12:30 P.M.	14.3
3	12/16	12:30 P.M.	15.5
4	12/17	9:00 A.M.	14.9
5	12/18	1:00 P.M.	14.3
6	12/18	4:00 P.M.	8.2
7	12/21	9:00 A.M.	6.2

At the interface, a horizontal crack extended approximately 3 in. back across the open corner of the barrier and down 1.5 in. into the slab at a load of 14 kips (Figure 5.20). Also, a crack at the barrier-slab interface was observed starting 2 in. from the back edge of the barrier extending down diagonally toward the bottom of the slab (Figure 5.20). With the greater displacements observed at 14 kips, rocker bearings were installed in the loading system to accommodate larger rotations and evaluate the failure plane. Figure 5.21 illustrates the opening of the horizontal interface crack along with an extension of diagonal cracks in the slab both toward the support and back face of the barrier. Upon close inspection, it was observed that a diagonal tension failure was experienced in the slab.

5.7.1.2 Strip Specimen 2. Strip Specimen 2 was loaded in 2 kip intervals, and a crack was first identified in the slab after 6 kips. The crack extended longitudinally, partially across the length of the slab, located at the edge of the support block. At 8 kips, cracks formed extending the original crack the entire slab length. In addition, an interface crack was observed across the length of the specimen. With further loading, a 3 in. horizontal crack formed at the open corner of the barrier interface at a load of 10 kips. The interface crack continued to extend another 1 in. horizontally before shooting down into the slab at 12 kips. A reduction in stiffness was observed on the load deflection plot until a diagonal crack formed in the slab at 14 kips (Figure 5.22).

Rocker bearings were again installed to accommodate larger rotation and evaluate the failure plane as in Strip Specimen 1. Figure 5.23 depicts the opening of the

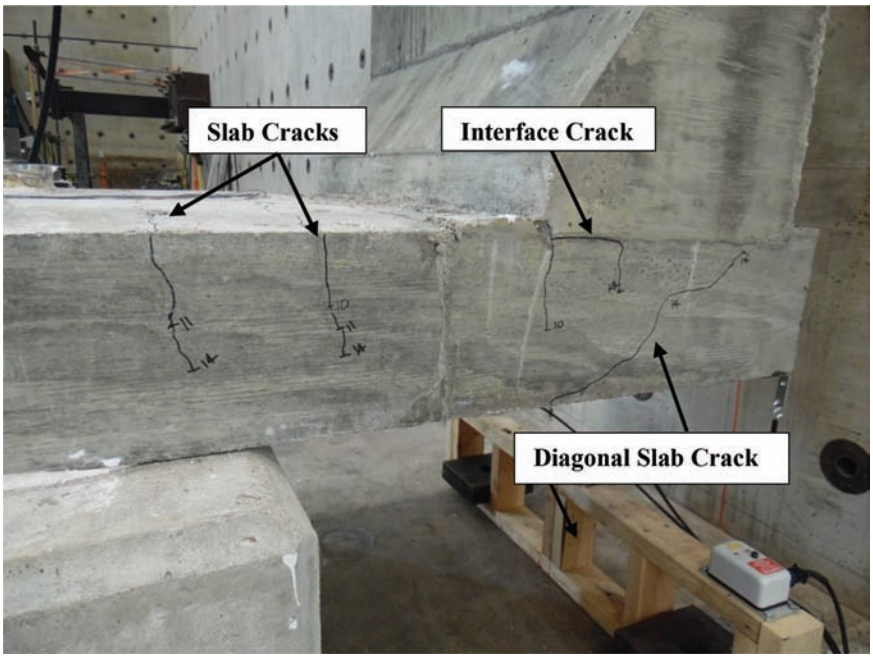

Figure 5.20 Strip Specimen 1 cracking at 14 kip.

Figure 5.21 Strip Specimen 1 failure plane at 14 kip.

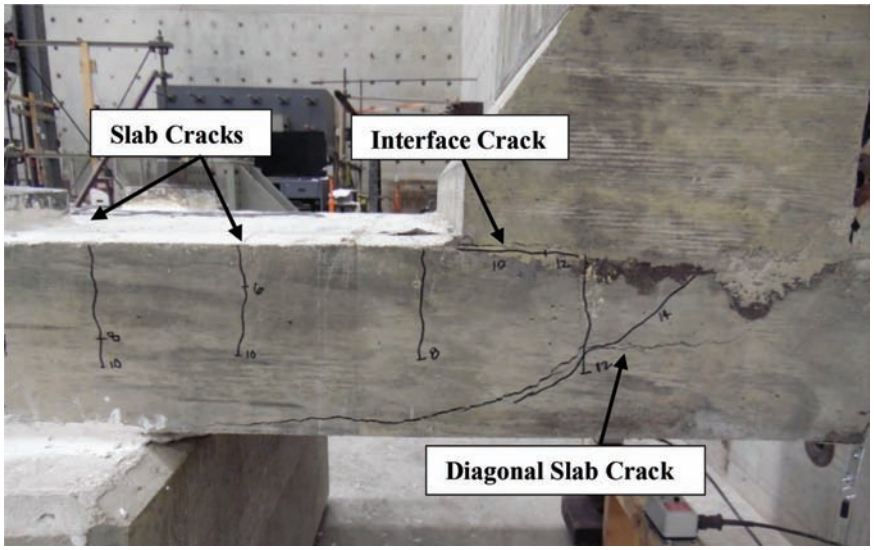

Figure 5.22 Strip Specimen 2 cracking at 14 kip.

Figure 5.23 Strip Specimen 2 failure plane at 14 kip.

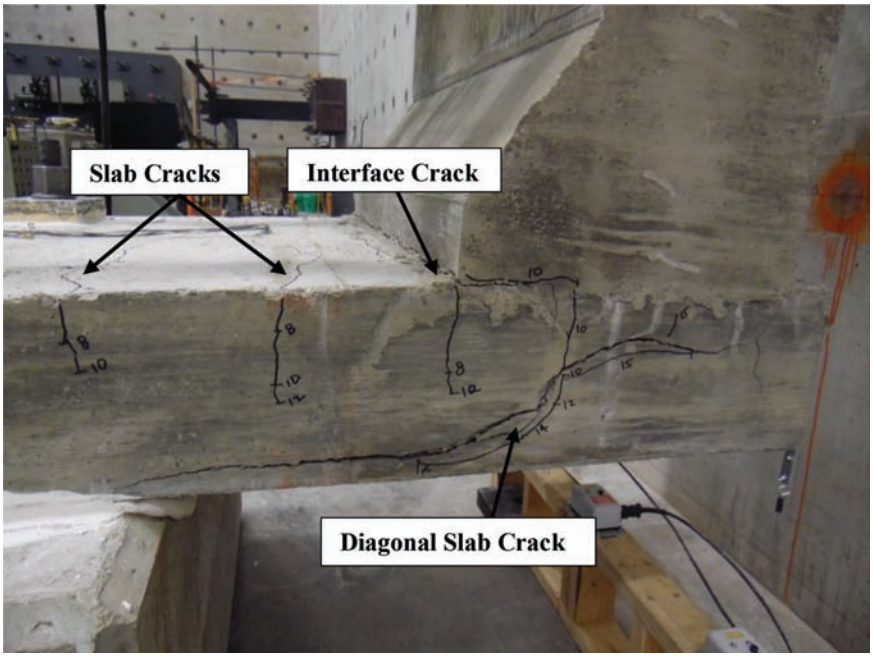

Figure 5.24 Strip Specimen 3 cracking at 15 kip.

horizontal interface crack and extension of diagonal cracks in the slab both toward the support and back face of the barrier. Failure of the specimen was caused by diagonal tension.

5.7.1.3 Strip Specimen 3. Strip Specimen 3 was loaded in 2 kip intervals and a partial slab crack over the support block was first identified in the slab after 5 kips. At 8 kips, cracks extended across the entire slab length and a full length interface crack was observed. After applying a load of 10 kips, a horizontal crack extended 3 in. at the open corner of the barrier interface, and a vertical crack shot down into the slab. This vertical crack extended another 1 in. into the slab at 12 kips while beginning to turn diagonally toward the support block. At 14 kips, the crack reached the edge of the support, and at a maximum load of 15 kips, the diagonal crack extended horizontally toward the slab edge (Figure 5.24). Despite having hooked anchorage, it was determined that Strip Specimen 3 experienced a diagonal tension failure in the joint region of the slab.

5.7.1.4 Strip Specimen 4. Strip Specimen 4 was loaded in 2 kip intervals, and a slab crack located over the support block was first identified in the slab after 7 kips. When loading to 8 kips, the cracks extended across the entire slab length and a full length interface crack was observed. At 10 kips, the horizontal crack extended approximately 1 in. at the open corner of the barrier interface, and a vertical crack shot down into the slab. It was difficult to determine the exact length of the crack at the open corner due to an accumulation of cement paste on the slab from casting. The vertical crack extended 1 in. at 12 kips while beginning to turn diagonally left toward the support block. At 13 kips, the crack continued to shoot toward the support and moved horizontally in the direction of the slab edge. Shortly after reaching 14 kips, the diagonal slab crack propagated further toward the support and slab edge. The maximum sustainable load was 15 kips in which the diagonal crack extended to the edge of the support and further toward the slab edge (Figure 5.25). Strip Specimen 4 experienced a diagonal tension failure in the slab consistent with the previous three strip specimens.

5.7.1.5 Strip Specimen 5. Strip Specimen 5 was loaded in 2 kip intervals and a slab crack located over the support block was first identified in the slab after 6 kips. After reaching a load of 8 kips, the initial cracks extended across the entire slab length and a full length interface crack was observed. Also at 8 kips, a horizontal crack extended approximately 2 in. at the open corner of the barrier interface, and a vertical crack moved down into the slab. The specimen was loaded further, and at 13 kips, the vertical crack began to slightly turn toward the support and move horizontally to the slab edge. Figure 5.26 shows the propagation of the vertical crack at 14 kips. The specimen continued to deflect until the diagonal crack moved suddenly toward the support and slab edge simultaneously (Figure 5.27). A diagonal tension failure in the slab was also experienced in this specimen.

5.7.1.6 Strip Specimen 6. Strip Specimen 6 was loaded in 1 kip intervals, and a full length slab and interface crack was identified in the slab after 5 kips. At the same load, a horizontal interface crack extended approximately 1.5 in. at the open corner of the barrier interface

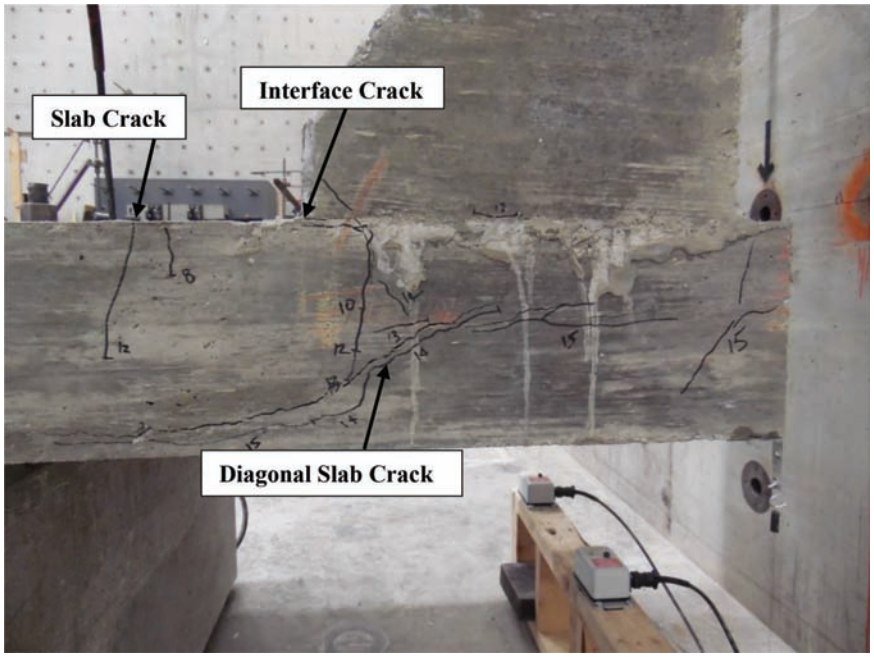

Figure 5.25 Strip Specimen 4 cracking at 15 kip.

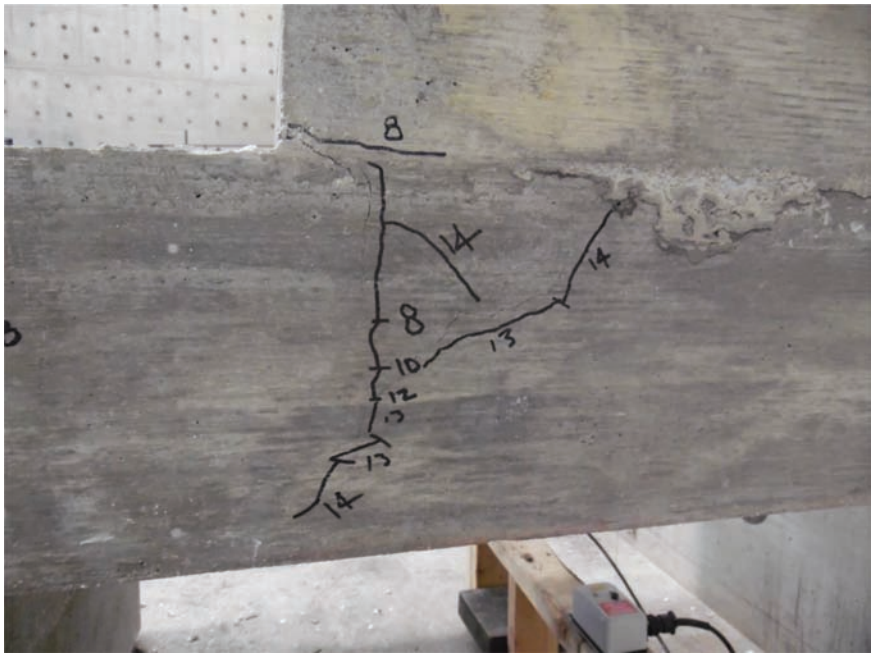

Figure 5.26 Strip Specimen 5 diagonal crack formation.

and a vertical crack moved down into the slab. After loading to 7.5 kips, the vertical crack started turning toward the support. Figure 5.28 shows the extension of the vertical slab crack at a maximum sustainable load of 8 kips. Strip Specimen 6 experienced a diagonal tension failure in the slab.

5.7.1.7 Strip Specimen 7. Strip Specimen 7 was loaded in 1 kip intervals, and a partial slab crack and an interface crack were identified after 4 kips. At the same load, a horizontal interface crack extended approximately 1.5 in. at the open corner of the barrier interface. A vertical crack was observed to extend down into the slab at 5 kips, and cracks propagated in the slab across the entire slab length. After loading to approximately 6.4 kips, the vertical crack started turning toward the support and simultaneously extended back in the direction of the slab edge. Figure 5.29 shows the extension of the

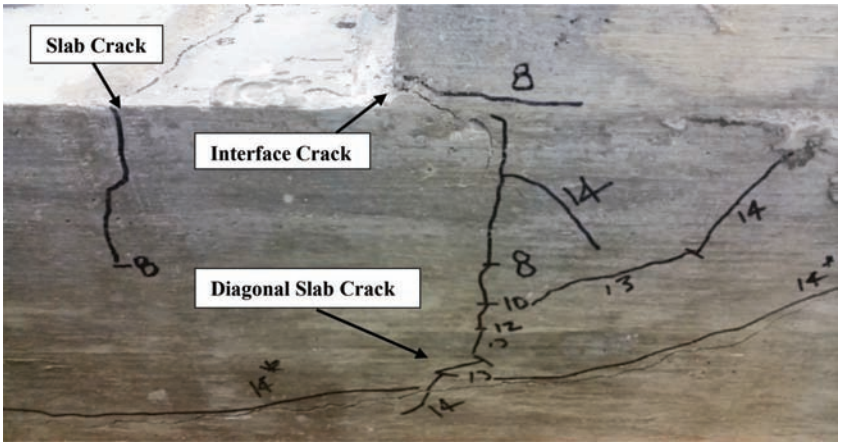

Figure 5.27 Strip Specimen 5 cracking at 14 kip.

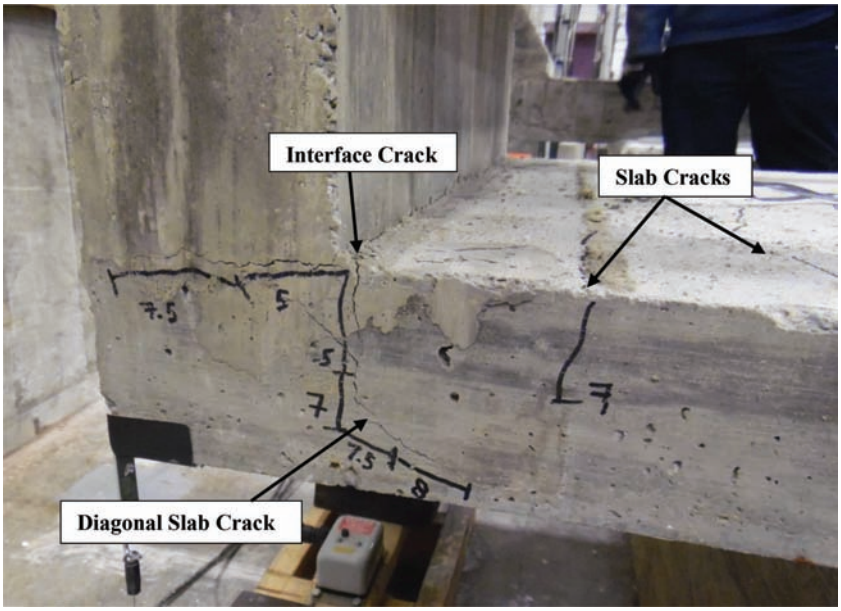

Figure 5.28 Strip Specimen 6 cracking at 8 kip.

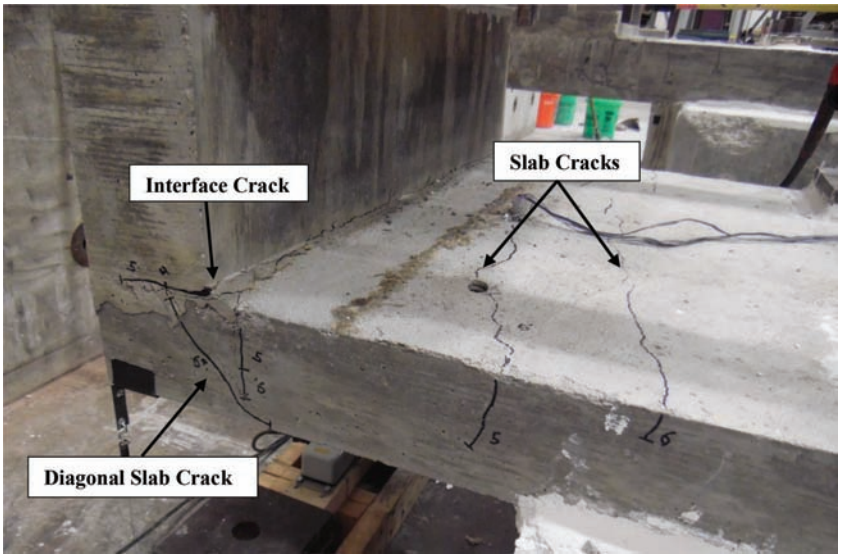

Figure 5.29 Strip Specimen 7 cracking at 6.4 kip.

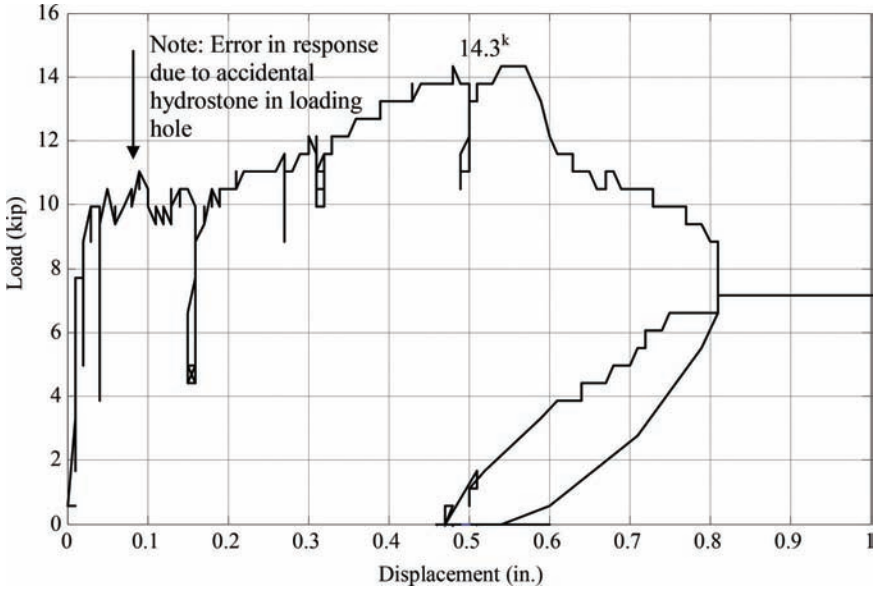

Figure 5.30 Load deflection (Strip Specimen 1).

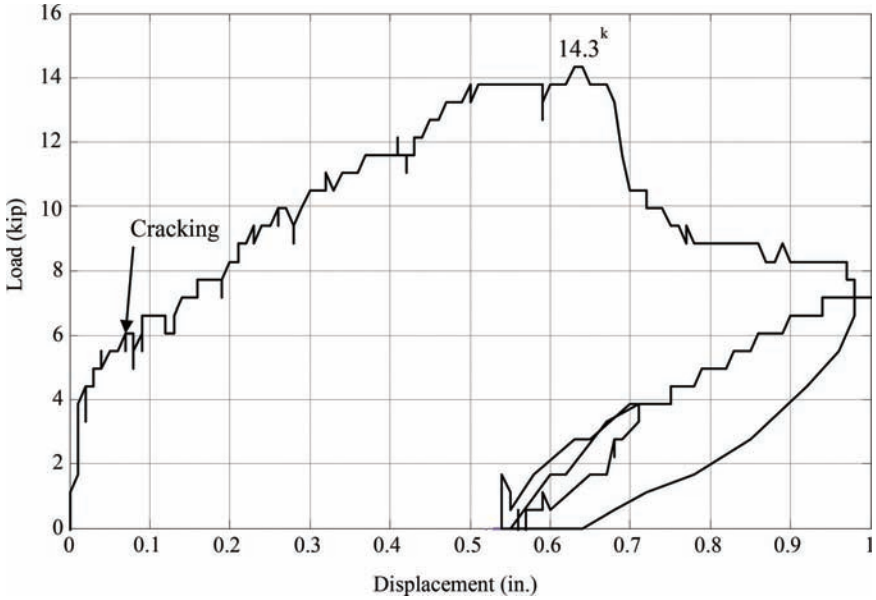

Figure 5.31 Load deflection (Strip Specimen 2).

vertical slab crack at a maximum sustainable load of 6.4 kips. Strip Specimen 7 experienced a diagonal tension failure in the slab.

5.7.2 Load-Deflection Response

5.7.2.1 Full-Scale Strip Specimens. The load versus midspan deflection for the five full-scale strip specimens is provided in Figure 5.30 through Figure 5.34. Overall, the strip specimens showed consistent cracking behavior (with the exception of strip Specimen 1 which experienced an initial problem of hydrostone in the loading hole) and cracking occurred between 6 and 7 kips. The shape of load deflection curves for the strip specimens were nearly identical, and a comparison of the load deflection curves is provided in Figure 5.35. The maximum sustainable load of the five strip specimens were essentially identical (within one kip of each another) despite the different top transverse slab reinforcement and anchorage conditions used in the specimens. This behavior supports the experimental observation that a diagonal tension slab failure occurred, and this mode of failure controlled the capacity of all specimens.

5.7.2.2 Half-Scale Strip Specimens. The load versus midspan deflection for the half-scale strip specimens is

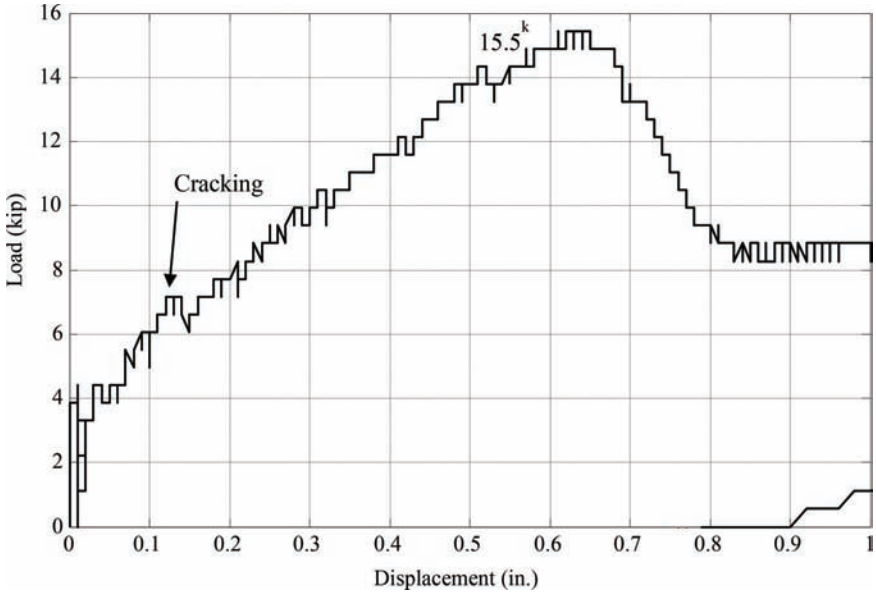

Figure 5.32 Load deflection (Strip Specimen 3).

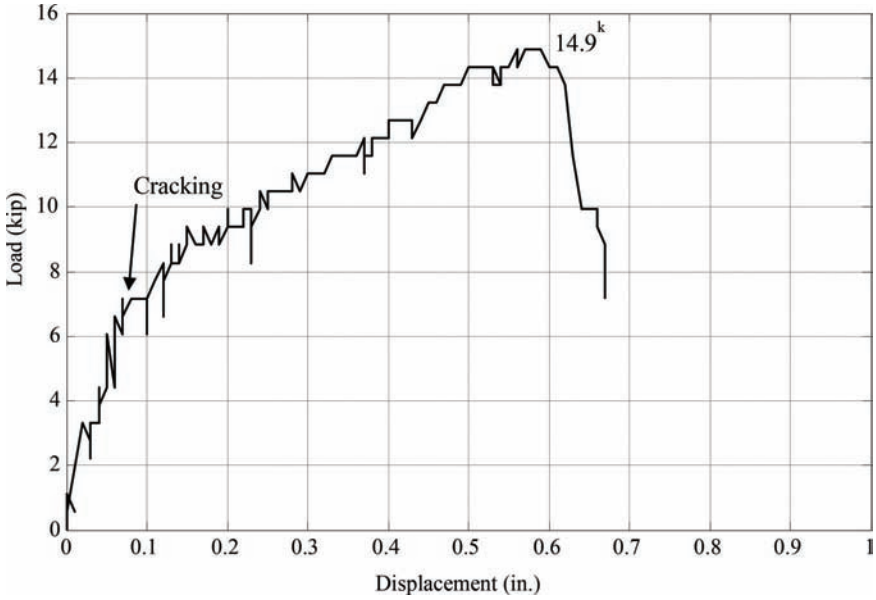

Figure 5.33 Load deflection (Strip Specimen 4).

provided in Figure 5.36 and Figure 5.37. A comparison of both load-deflection curves is shown in Figure 5.38. The load-deflection curves in both specimens show similar slopes in the linear region until cracking at approximately 4 kips. Each specimen experienced a similar reduction in stiffness after cracking, and the maximum sustainable loads for Strip Specimen 6 and 7 were 8.2 kips and 6.2 kips respectively. Due to the identical nature of failure, it was anticipated that the ultimate load capacity would be the same. However, the capacity of Specimen 6 was higher. This may be experimental scatter that is inherent with a diagonal tension failure. Smaller scale specimens typically exhibit larger scatter in tension strength which may explain this variation.

5.7.3 Global Deflection Response

5.7.3.1 Full-Scale Strip Specimens. The vertical and horizontal displacements were plotted across the 3 ft length of the five full-scale strip specimens. Figure 5.39 shows the vertical displacement behavior at each loading interval. The strip specimens experienced uniform deflection across the slab length indicating uniform

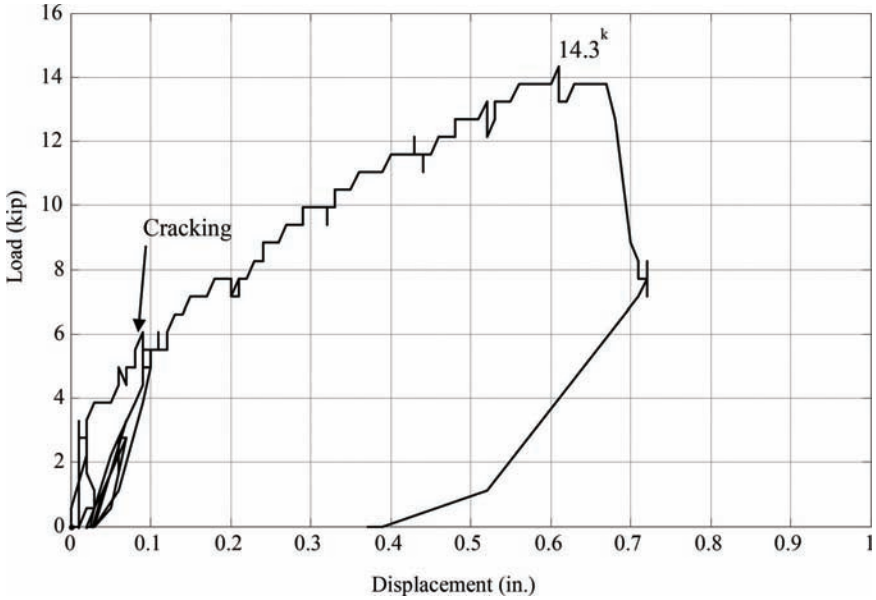

Figure 5.34 Load deflection (Strip Specimen 5).

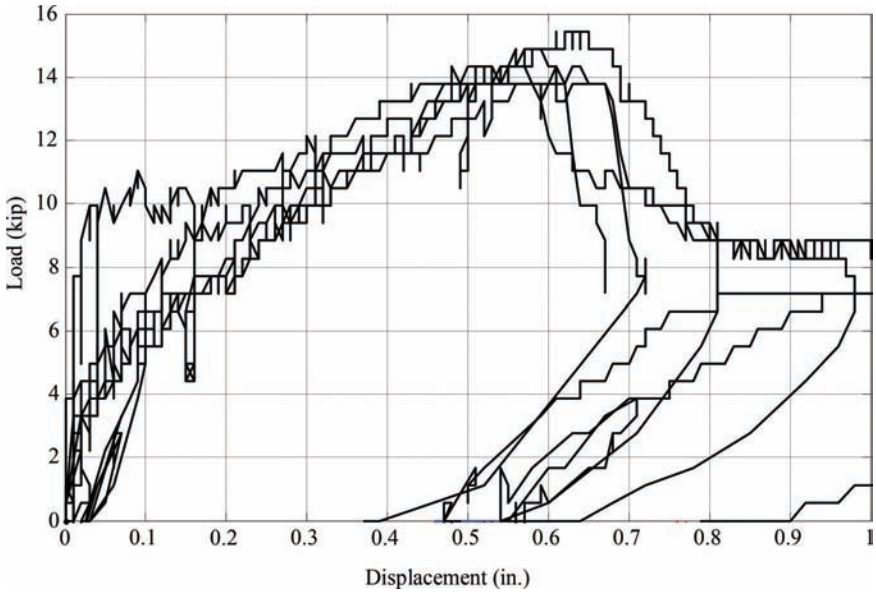

Figure 5.35 Full-scale strip specimen load-deflection comparison.

bending behavior in the slab as was expected. The maximum vertical displacement for the strip specimens ranged between 0.32 in. and 0.42 in. Horizontal displacement behavior was also plotted as shown in Figure 5.40 and indicate uniform horizontal displacement across the 3 ft length. The maximum horizontal displacement experienced in the five strip specimens varied between approximately 0.5 in. and 0.6 in.

5.7.3.2 Half-Scale Strip Specimens. The vertical and horizontal displacements were plotted across the 3 ft length of the two half-scale strip specimens. Figure 5.41 shows the vertical displacement behavior at each loading interval. Again, the strip specimens experienced uniform deflection across the slab length. The maximum vertical displacement for Strip Specimen 6 and 7 was approximately 0.15 in. and 0.17 in. respectively. Similarly, horizontal displacement is shown in Figure 5.42 and again show a uniform behavior across the slab length. The maximum horizontal displacement experienced for Strip Specimen 6 and 7 was approximately 0.35 in. and 0.25 in., respectively.

5.7.4 Global Strain Response

5.7.4.1 Full Scale Strip Specimens. The two top transverse bars closest to the midspan of the slab were instrumented with strain gages to measure the strain resulting

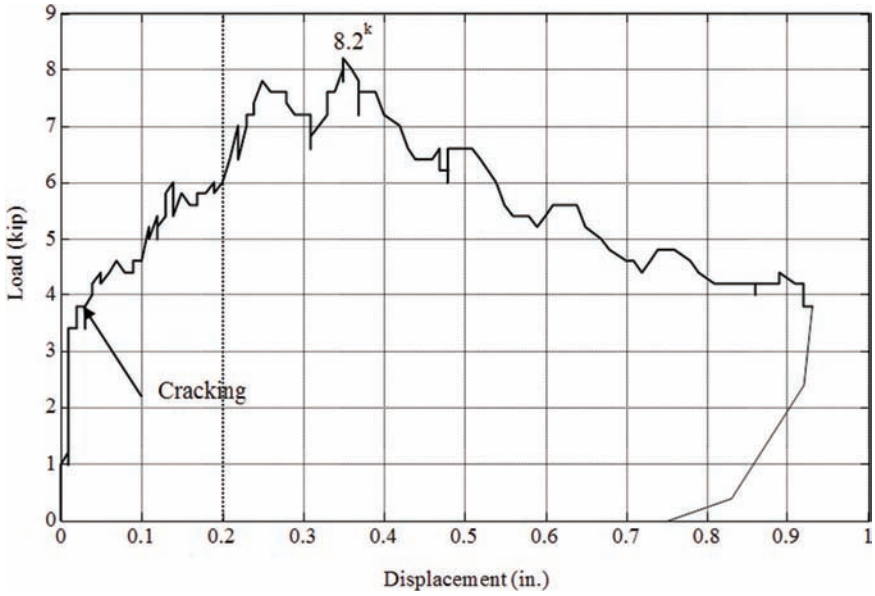

Figure 5.36 Load deflection (Strip Specimen 6).

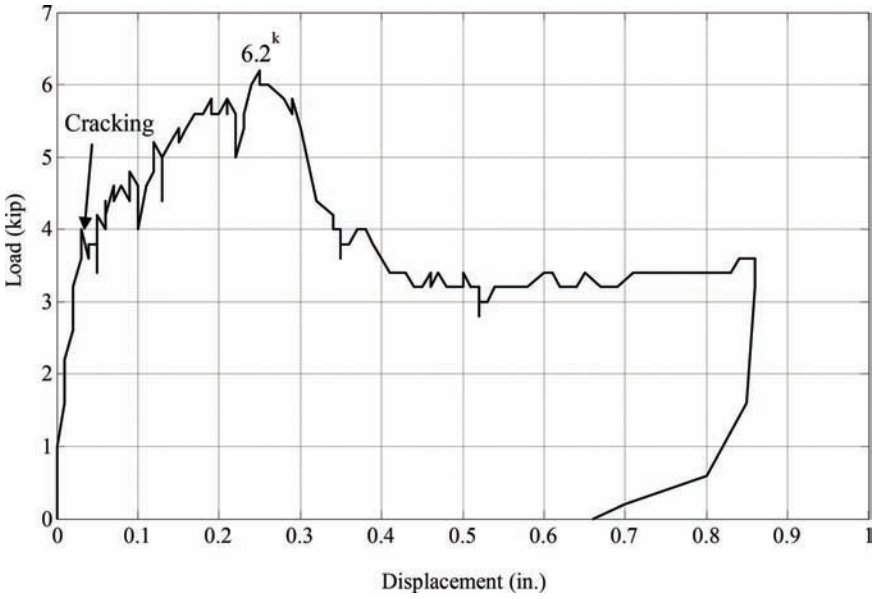

Figure 5.37 Load deflection (Strip Specimen 7).

from the lateral force applied on the barrier. Strain gages were placed at the barrier interface and over the edge of the support block (Figure 5.16) to measure strain at these locations and understand the development of the top transverse bars.

The strain at each location is plotted at each loading increment in Figure 5.43. At the barrier interface, (location B) the strain in the five strip specimens varied from approximately 1000 με to 1400 με at maximum load which indicates that the bars did not reach yield due to the premature diagonal tension failure mechanism. At the edge of the support block (location M1 and M2), the strains ranged from approximately 1200 με to 1400 με.

5.7.4.2 Half-Scale Strip Specimens. The two top transverse bars closest to the midspan of the slab were instrumented with strain gages to measure the strain resulting from the lateral force applied on the barrier. Strain gages were placed at the barrier interface and over the edge of the support block (Figure 5.17). The strain at each location is plotted at each loading increment in Figure 5.44. At the barrier interface (location B), the strain was approximately 1500 με at maximum load which indicates that the bars did not reach yield due to the premature diagonal tension failure mechanism. At the edge of the support block (location M1 and M2), the strains ranged from approximately 1000 με to 1300 με.

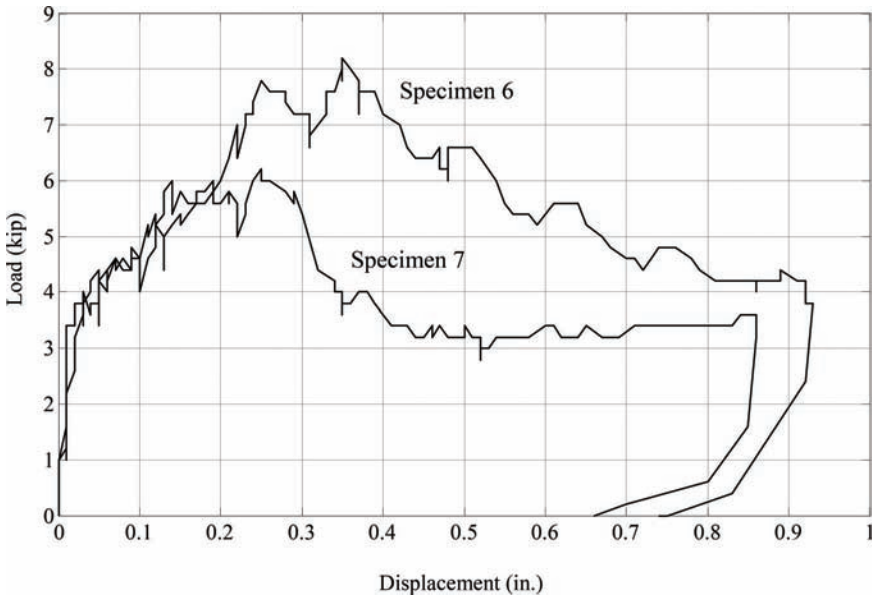

Figure 5.38 Half-scale strip specimen load-deflection comparison.

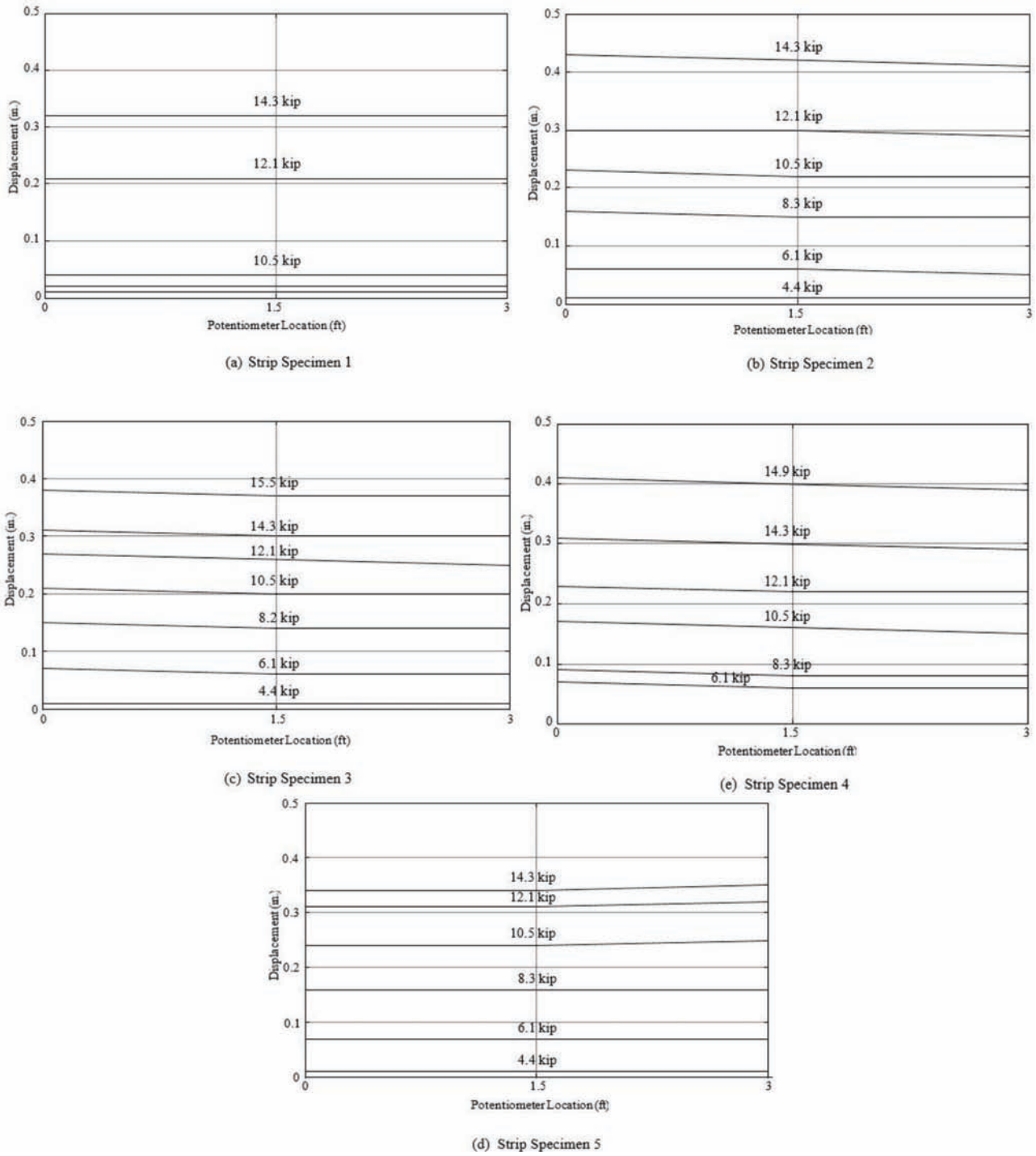

Figure 5.39 Vertical displacement distribution (full-scale strip specimens).

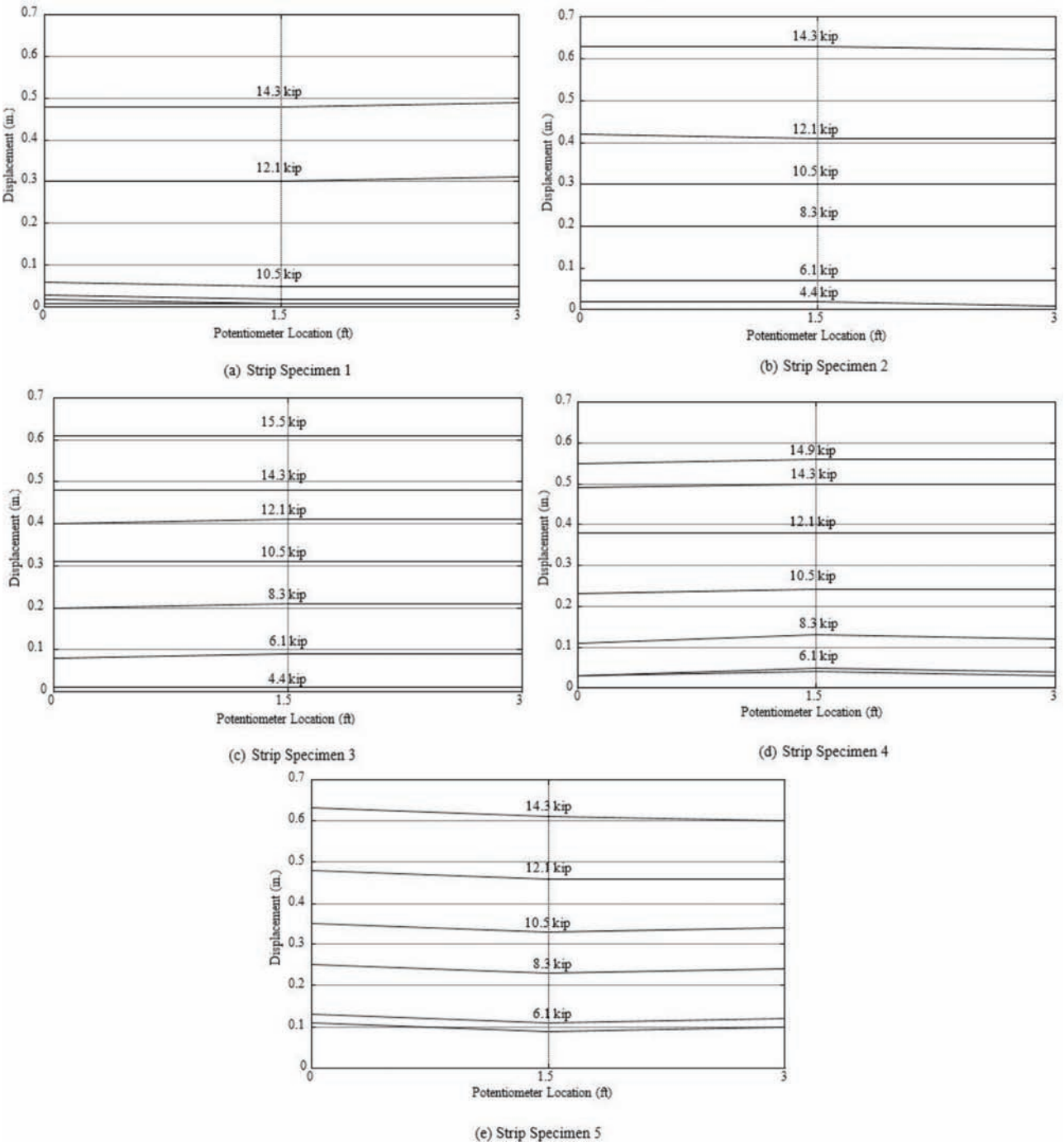

Figure 5.40 Horizontal displacement distribution (full-scale strip specimens).

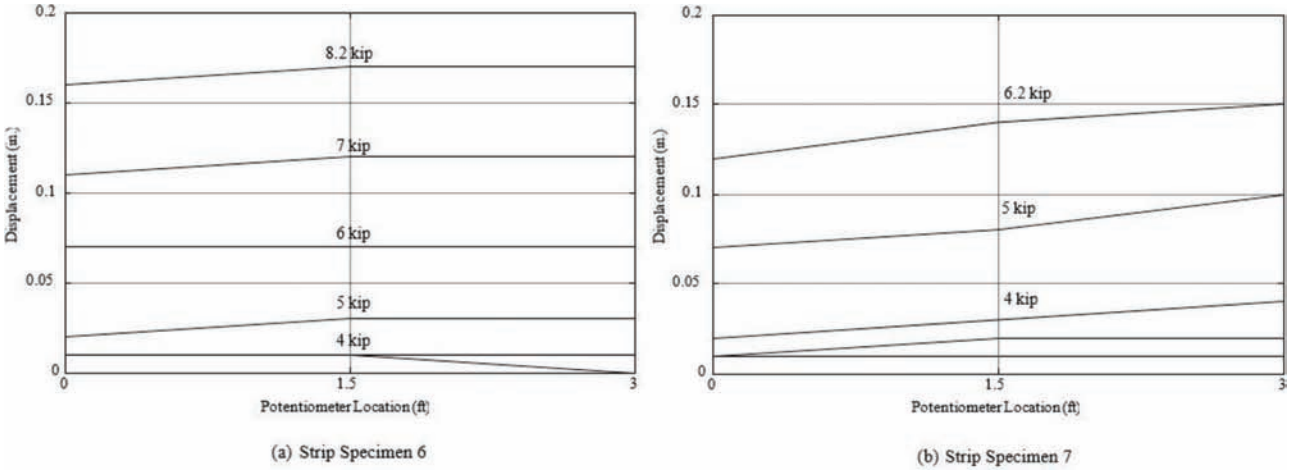

Figure 5.41 Vertical displacement distribution (half-scale strip specimens).

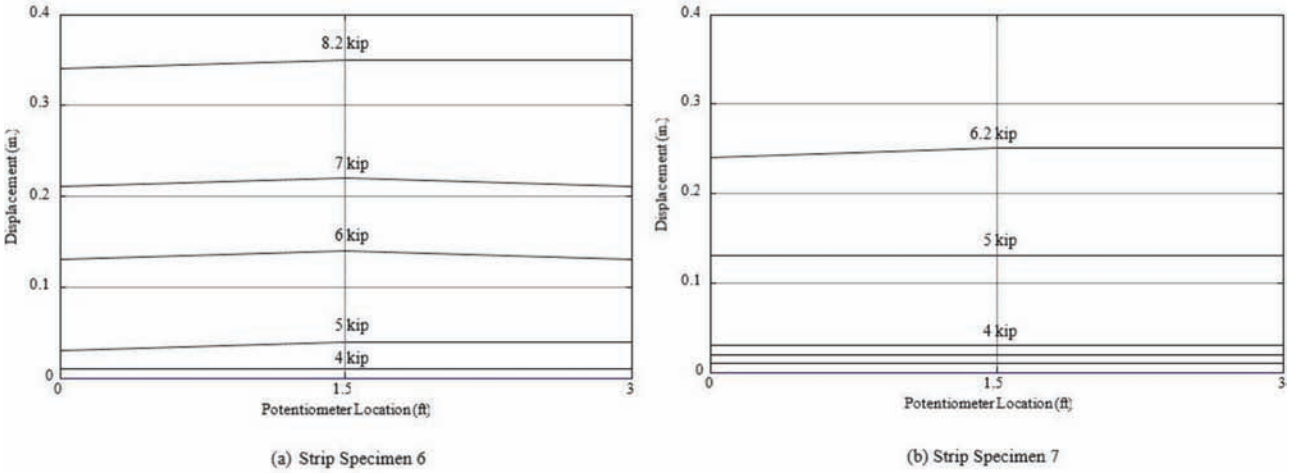

Figure 5.42 Horizontal displacement distribution (half-scale strip specimens).

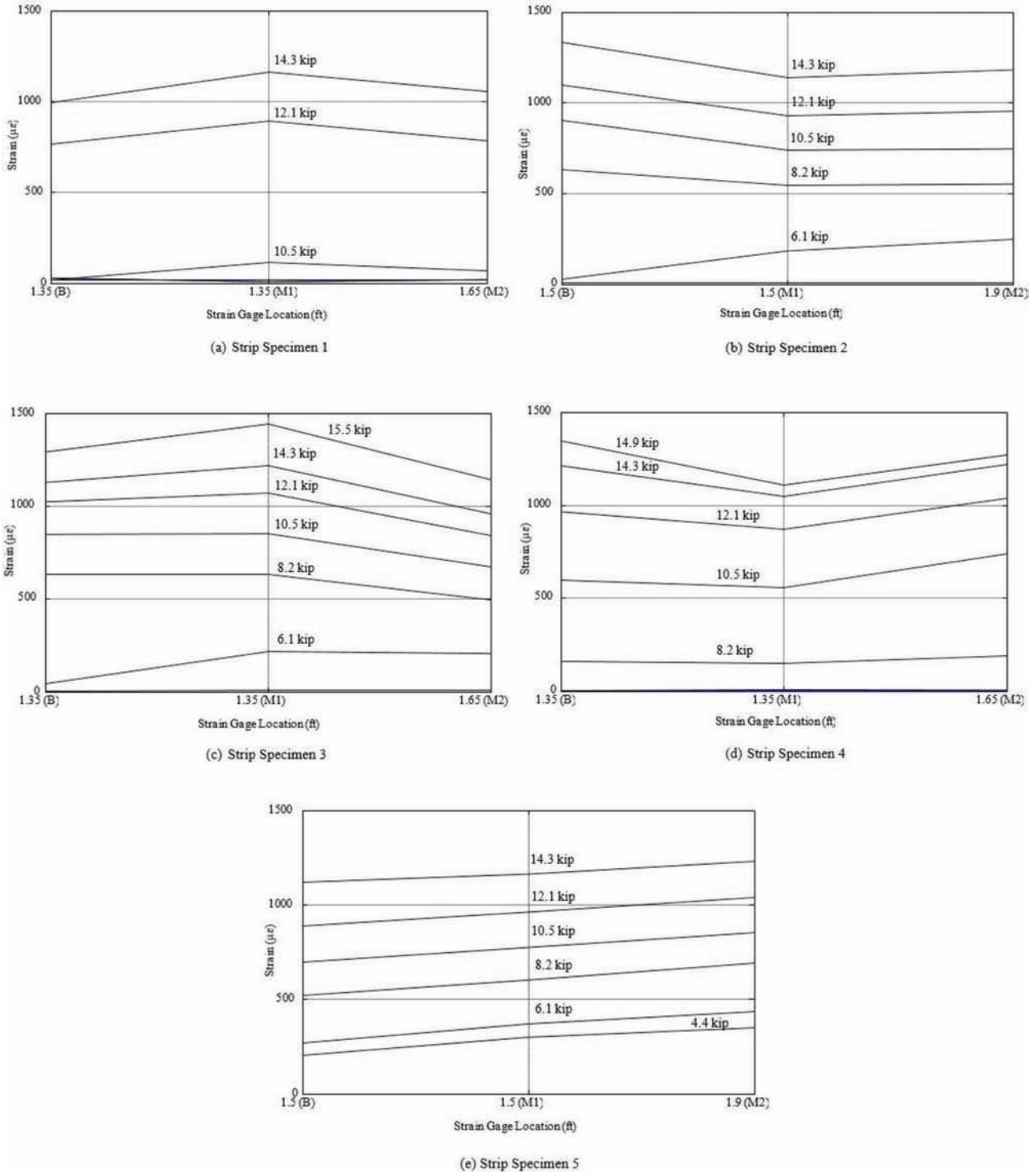

Figure 5.43 Jacking strain distribution (full-scale strip specimens).

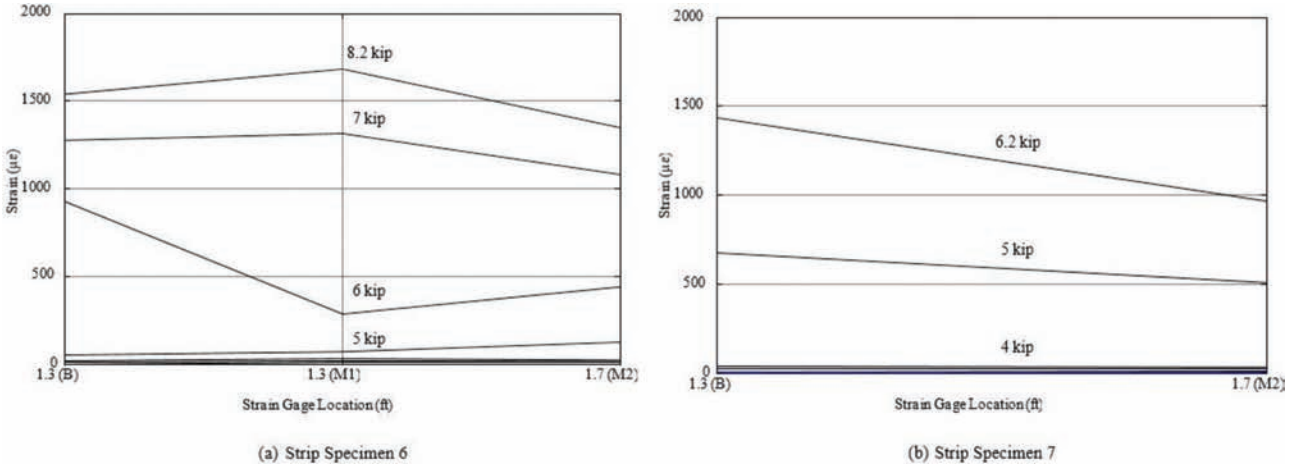

Figure 5.44 Jacking strain distribution (half-scale strip specimens).

6. ANALYSIS OF BEHAVIOR

6.1 Introduction

The results of the sectional and system tests were further analyzed to evaluate the strength and force distribution of the deck-barrier wall system.

6.2 Analysis of Sectional Test Results

All of the sectional test specimens failed through diagonal tension. As shown in Table 5.6, all of the full-scale specimens failed at approximately the same load with the minimum value being 14.3 kips which was observed in three of the specimens (1, 2, and 5). It was originally expected that there would be differences between the test results due to the variations in anchorage details as there are fairly short distances in which the top longitudinal bars in the slab can develop their full capacity. However, as noted by the failure mode and the similarity in capacities, failure occurred through shear in the deck occurring inside the region and propagating outside the joint towards the interior of the bridge deck as shown in Figure 6.1.

As a simplified analysis, the horizontal force from the loading results in shear forces that must be transferred through the join and ultimately results in a net tension in the bridge deck as shown in Figure 6.2. Based on a unit block, horizontal and vertical shear stresses must be in equilibrium. Therefore, the critical shear strength is based upon the vertical shear capacity of the deck due to its thinner dimension. Based on this simplified analysis, critical shear strengths were computed based on the test results as shown in Table 6.1. On average, a vertical shear strength of approximately $1.1\sqrt{f'_c}bd$ was achieved. It has been previously established (Tureyen and Frosch 2003) that shear strength is a function of the longitudinal reinforcement ratio; therefore, the neutral axis depth, c, provides a better relationship. Therefore, the shear strength in terms of c was also computed which provides an average strength of $3\sqrt{f'_c}bc$. Furthermore, the strengths computed using this approach indicate that both the half-scale (Specimen 6 and 7) had strengths comparable to the full-scale specimens. In fact, the lowest strengths achieved were identical at a coefficient of 2.83. While Specimen 6 indicates the highest value of all of the specimens tested, it should be noted that increased scatter in shear test results is expected in smaller scale specimens. What is significant is that the lower range strengths are consistent.

Using this analysis approach, the failure strengths of all of the specimens can be reasonably approximated (Table 6.2). As shown, the lower bound results are more consistent with the expression based on the neutral axis depth.

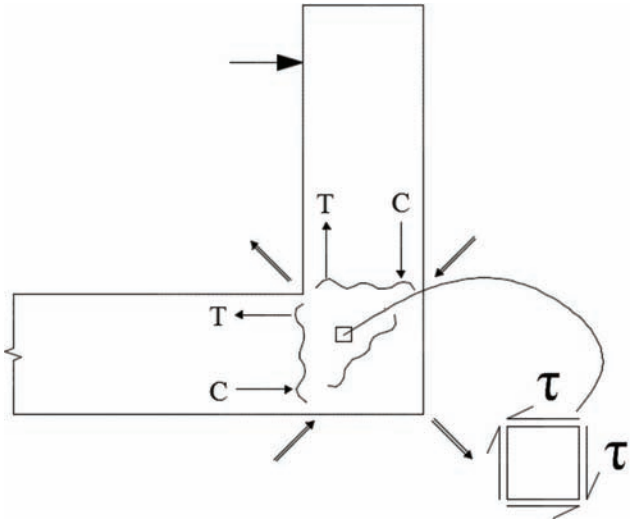

Figure 6.2 Joint shear schematic.

Figure 6.1 Joint shear failure.

TABLE 6.1
Joint Shear Strength (Sectional Specimens)

Specimen	V_{test} (kips)	d (in.)	$f'c$ (psi)	A_s (in.^{2} /ft)	ρ	c(in.)	$\frac{V_{test}}{\sqrt{f'_c}bd}$	$\frac{V_{test}}{\sqrt{f'_c}bc}$
1	14.3	5.19	4650	1.06	0.017	2.04	1.12	2.86
2	14.3	5.13	4650	1.11	0.018	2.05	1.14	2.83
3	15.5	5.19	4650	1.06	0.017	2.04	1.22	3.10
4	14.9	5.19	4650	1.06	0.017	2.04	1.17	2.98
5	14.3	5.13	4650	1.11	0.018	2.05	1.14	2.83
6	8.2	3.06	4650	0.29	0.008	0.89	1.09	3.75
7	6.2	3.06	4650	0.29	0.008	0.89	0.82	2.83

TABLE 6.2
Calculated Joint Shear Strength (Sectional Specimens)

Specimen	V_{test} (kips)	$V_{calc} = 1.1\sqrt{f'_c}bd$ (kips)	$V_{calc} = 2.8\sqrt{f'_c}b$ (kips)
1	14.3	14.0	14.0
2	14.3	13.8	14.1
3	15.5	14.0	14.0
4	14.9	14.0	14.0
5	14.3	13.8	14.1
6	8.2	8.3	6.1
7	6.2	8.3	6.1

6.3 Analysis of System Test Results

6.3.1 Short Specimens (15 ft)

Both of the 15 ft specimens (Specimens 1 and 2) experienced a diagonal tension failure over the entire 15 ft length of the deck. The failure mode was identical to that experienced in the 3 ft sectional tests (Figure 6.3). As discussed in Chapter 5, the entire deck was capable of distributing the lateral load resulting in essentially a simultaneous shear failure within the joint region.

Using an analysis similar that that for the sectional specimens, the average shear strengths were calculated and are presented in Table 6.3. It can be seen that the coefficient for shear strength based on the effective depth d decreases significantly as the reinforcement ratio is halved. However, as discussed previously, the neutral axis depth, c, captures the response of the varying reinforcement resulting in essentially the same coefficient for the shear strength. These ratios are similar to that calculated from the sectional specimens, but are slightly lower with an average shear strength of 2.6. In all, this analysis approach reasonably estimates of the strength of the specimens. Even if the estimated strength of 2.8 as obtained from the sectional specimens is used, the test strengths are reasonably approximated (Table 6.4). However, it is recommended to use a slightly lower value of $2.5\sqrt{f'_c}bc$ to approximate the strength of this failure mode for the bridge deck-barrier rail system as also presented in Table 6.4. This value is interesting in that it is half the sectional shear strength recommended to calculate beam shear, $5\sqrt{f'_c}bc$. This reduction in shear strength seems appropriate due to the geometry of this cross section where the joint is not confined.

As previously discussed, the entire 15 ft length of deck overhang was effective in resisting the lateral load. As shown in Figure 4.54, vertical displacements across the entire specimen were essentially identical indicating that all of the reinforcement was strained identically. While variations in strains measured from the overhang reinforcing bars are noted (Figure 4.58), it is observed that high strains were developed across the entire specimen with the highest actually being noted at the edges. As previously discussed, the variations in strains are likely the result of the location of the gage relative to the location of cracking. Overall, it was found that the entire 15 ft length of the overhang was effective is resisting the lateral concentrated load. This distribution length is significantly greater than assumed the typically assumed value of (L_c +2H) which is 8.2 ft for these specimens. Considering the horizontal distribution of the applied loading (18 in.), the load was distributed for 180 in. or 10 times the horizontal loading dimension.

6.3.2 Long Specimens (27 ft)

Both of the 27 ft specimens (1L and 2L) experienced a punching shear failure. As shown in Figure 6.4, the punching shear failure of Specimen 1L occurred adjacent and around the loading plate. For Specimen 2L, the loading plate was changed to provide a larger punching shear area and resulted in a different punched region. As shown in Figure 6.5, the punch extended away from the loading plate and aligned with the first diagonal yield line cracks which is more consistent with a one-way shear failure.

As a simplified analysis, the perimeter of punching for Specimen 1L was considered as shown in Figure 6.6(a), and the average punching shear strength was computed as $4.4\sqrt{f'_c}b_o d$ (Table 6.5). The perimeter of punching for Specimen 2L was considered as shown in Figure 6.6(b) which results in an average punching shear strength of $2.1\sqrt{f'_c}b_o d$. This significantly lower punching shear strength produces a strength more consistent with one-way shear which in also consistent with the different failure mode. From this analysis, it appears that as the loading is distributed across more of the face of the barrier, the failure model can change from one of a

Figure 6.3 Joint shear failure (Specimen 1).

TABLE 6.3
Joint Shear Strength (System Specimens)

Specimen	V_{test} (kips)	d (in.)	f_c' (psi)	A_s (in.^{2} /ft)	ρ	c (in.)	$\frac{V_{test}}{\sqrt{f_c'}bd}$	$\frac{V_{test}}{\sqrt{f_c'}bc}$
1	26.8	3.06	4500	0.293	0.008	0.90	0.72	2.47
2	21.5	3.06	4500	0.147	0.004	0.67	0.58	2.67

TABLE 6.4
Calculated Joint Shear Strength (System Specimens)

Specimen	V_{test} (kips)	$V_{calc} = 2.8\sqrt{f_c'}bc$ (kips)	$V_{calc} = 2.5\sqrt{f_c'}bc$ (kips)
1	26.8	30.3	27.1
2	21.5	22.6	20.1

localized punch adjacent to the loading to a more global punch across a larger region of the barrier.

A majority of the length of the overhang was effective in resisting the lateral load. As shown in Figure 4.56, the overhang deflected vertically over the entire length of the deck and were fairly uniform in both specimens. For Specimen 1L, uniform displacements were recorded up to a load of approximately 23 kips. Beyond this value, the displacement pattern became more unsymmetrical with lower values on the right side of the specimen. Overall, the majority of the overhang participated in resistance. For Specimen 2L, the displacements were more uniform throughout the loading. Slightly less deflection was observed at the edges of the slab (2.5 ft from the edge). Resistance across the entire deck width is evident from the measured reinforcing strains (Figure 4.59). This specimen supports that at least 10 times the horizontal loading dimension can be considered as the distribution length for design of the overhang.

6.3.3 Comparison of Short and Long Specimens

As observed, the failure mode changed as the overall length of the test specimen increased. The punching shear strength for the original HSS loading system was measured as 29.2 kips in Specimen 1L while the joint shear strength in Specimen 1 (identical reinforcement) was measured as 26.8 kips. Based on the analysis conducted above, a specimen length of approximately 16'-4" is required for the failure mode to transfer from joint shear to punching shear. For yield line development (Figure 6.7), the capacity using the actual yield strength of the reinforcement (73 ksi) was computed as 35 kips (Appendix D). Based on these tests and analyses, it is observed that the yield line mechanism cannot occur and failure will be controlled by punching shear if there is sufficient length of bridge deck overhang provided to eliminate a joint shear failure. For these specimens, a length of approximately 16.5 ft will preclude joint shear failure.

6.4 Full-Scale Barriers

Based on the results, it is possible to consider the failure strength of full-scale barriers. There are three primary failure modes to consider, and these consist of (1) joint shear, (2) punching shear, and (3) a yield line mechanism.

Figure 6.4 Punching shear failure (Specimen 1L).

Figure 6.5 Punching shear failure (Specimen 2L).

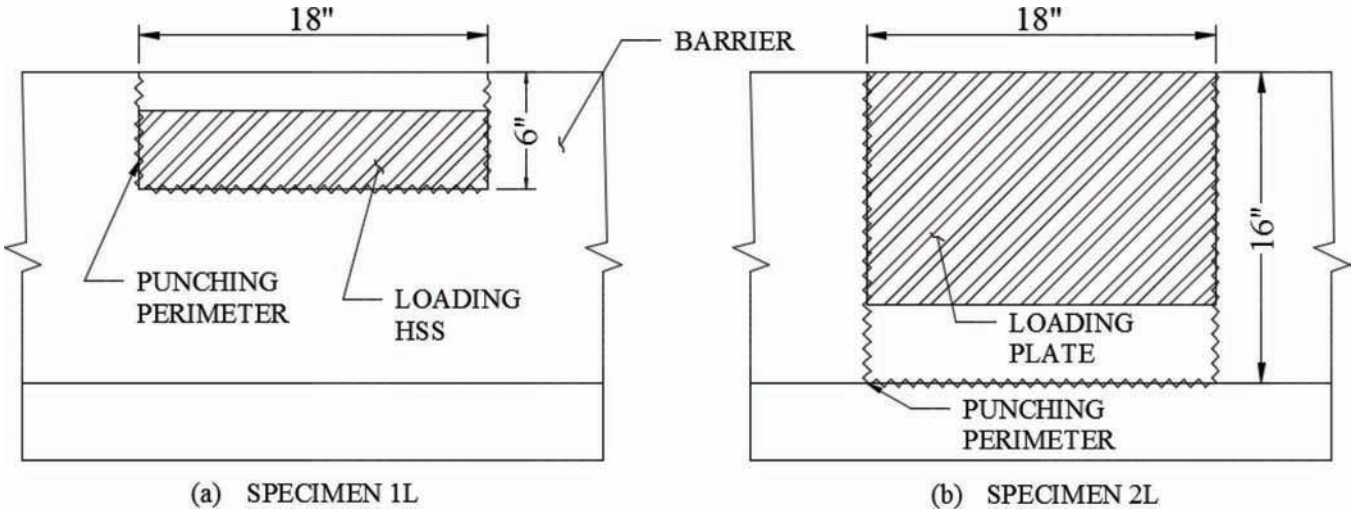

Figure 6.6 Punching shear perimeter.

6.4.1 Joint Shear Strength

Joint shear strength can simply be computed as presented above where $V_c = 2.5\sqrt{f'_c}bc$. As presented in Table 6.6, the strength of an 8 in. deck typically reinforced with No. 5 bars using 4000 psi concrete is calculated as approximately 4 kips/ft of rail. For comparison purposes, the tests on the full-scale rails conducted here which had 4650 psi concrete resulted in a strength of 4.8 kips/ft.

6.4.2 Punching Shear Strength

Punching shear strength can similarly be computed. Due to the diagonal layout of the vertical reinforcing bars, an average effective depth of the reinforcement must be considered. Based on the design dimensions, an estimate of the average effective depth of the reinforcement (horizontal and vertical) on the interior face of the barrier is approximately 8 in. Two potential punching shear failures are considered: loading towards the top of the wall (Figure 6.8(a) consistent with that tested in this research program for the full-scale specimens and loading spread out over the entire depth of the wall (Figure 6.8(b)) similar to the loading used for Specimen 2L. The strength of both failure modes are presented in Table 6.7. An average shear strength of $V_c = 4\sqrt{f'_c}b_o d$ is used for the top loading consistent with two-way behavior while a shear strength of $V_c = 2\sqrt{f'_c}b_o d$ is used for the vertically distributed loading consistent with one-way behavior. Loads are considered spread horizontally a dimension L_t as given in AASHTO (2014).

As indicated in Table 6.7, the failure loads for both loading conditions are essentially identical at approximately 110 kips. It is anticipated that as load is spread vertically down, there is a transition in the shear coefficient (K) from 4 to 2 such that the failure load for this failure mode remains at approximately 110 kips.

TABLE 6.5
Punching Shear Strength

Specimen	V_{test} (kips)	d_{avg} (in.)	f'_c (psi)	b_o (in.)	$\frac{V_{test}}{\sqrt{f'_c}b_o d}$
1L	29.2	3.625	3770	30	4.37
2L	23.7	3.625	3770	50	2.13

6.4.3 Yield Line Mechanism

The strength of the yield line mechanism was previously determined as 150 kips as discussed in Section 2.5. Complete calculations are available in Appendix B.

6.4.4 Rail Capacity

Based on the analyses conducted above, a punching shear failure is the most likely failure mode for the TL-4 rail as this strength is below that of the yield line mechanism. To eliminate a joint shear failure, sufficient length of the deck must be provided. Considering that the system provides 4 kips/ft, a longitudinal length of approximately 27.5 ft is needed. This short length is typically always provided in actual bridges, and failure of this mode should not be considered to control. The rail/overhang system has been shown based on the system tests conducted here to be capable of spreading the loading out sufficiently that the 8 in. thick overhang does not limit the strength of the system. Rather, the strength of the system is controlled by punching shear.

6.5 Field Behavior

The testing program is very insightful into the behavior of the overhang/rail system. While the laboratory tests simulate rail loadings and are consistent with load distributions indicated by AASHTO, it is instructive to consider actual failures of the barrier rail system. It is important to consider that the AASHTO load distributions are simply models are not necessarily representative of impacts of actual vehicles.

Figure 6.9 shows the impact of a semi-truck on the barrier wall of the I65 NB bridge over I70 WB & CD lanes at the North Split (Str. #I65-113-5747 BNBL) which occurred on November 5, 2015. As shown, a punching shear failure occurred producing a V-notch failure similar to the failure profile experienced by Specimen 2L. It appears that the barrier was loaded over most of its height resulting in this vertically spread type failure pattern. The deck overhang was not damaged.

TABLE 6.6
INDOT Overhang/Barrier Strength

d (in.)	f'_c (psi)	A_s (in.^{2}/ft)	ρ	c (in.)	$V_c = 2.5\sqrt{f'_c}bc$
5.19	4000	1.06	0.017	2.10	4.0 k/ft

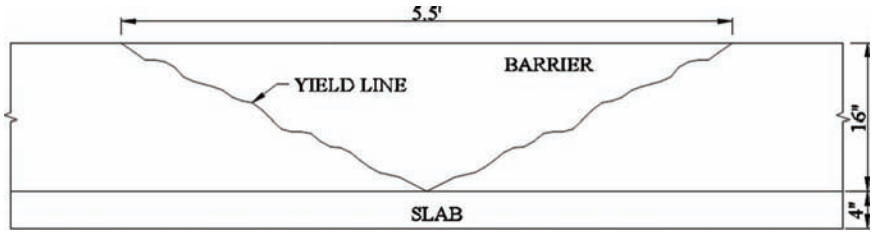

Figure 6.7 Yield line mechanism.

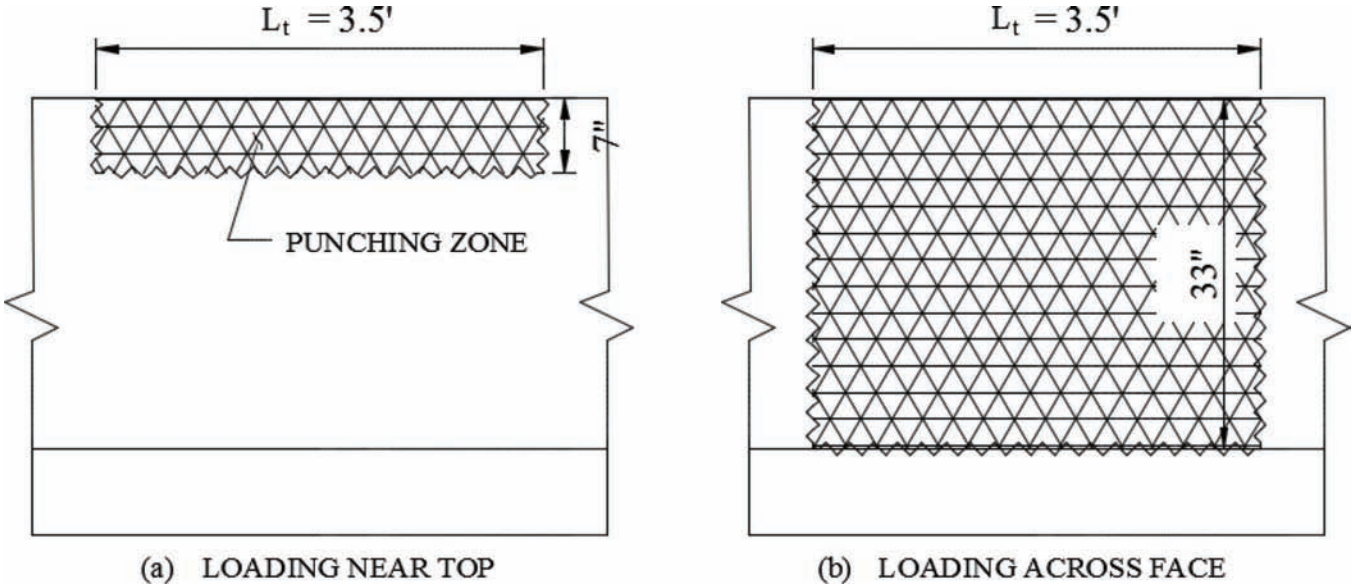

Figure 6.8 Punching shear failure (TL-4).

TABLE 6.7
INDOT TL-4 Barrier Punching shear Strength

Loading	d_{avg} (in.)	f_c'	b_o (in.)	K	$V_c = K\sqrt{f_c'}bd$ (kips)
Top	8	4000	56	4	113
Over Face	8	4000	108	2	109

Figure 6.9 V-notch barrier failure (INDOT, n.d.).

Another example of a railing failure is observed on Bridge 30-75-04215C EBL which was struck on January 12, 2016. As shown in Figure 6.10(a), a slightly different failure mode was exhibited. The failure of this rail is more consistent with a higher impact that caused a punching shear failure around the impact zone. This failure

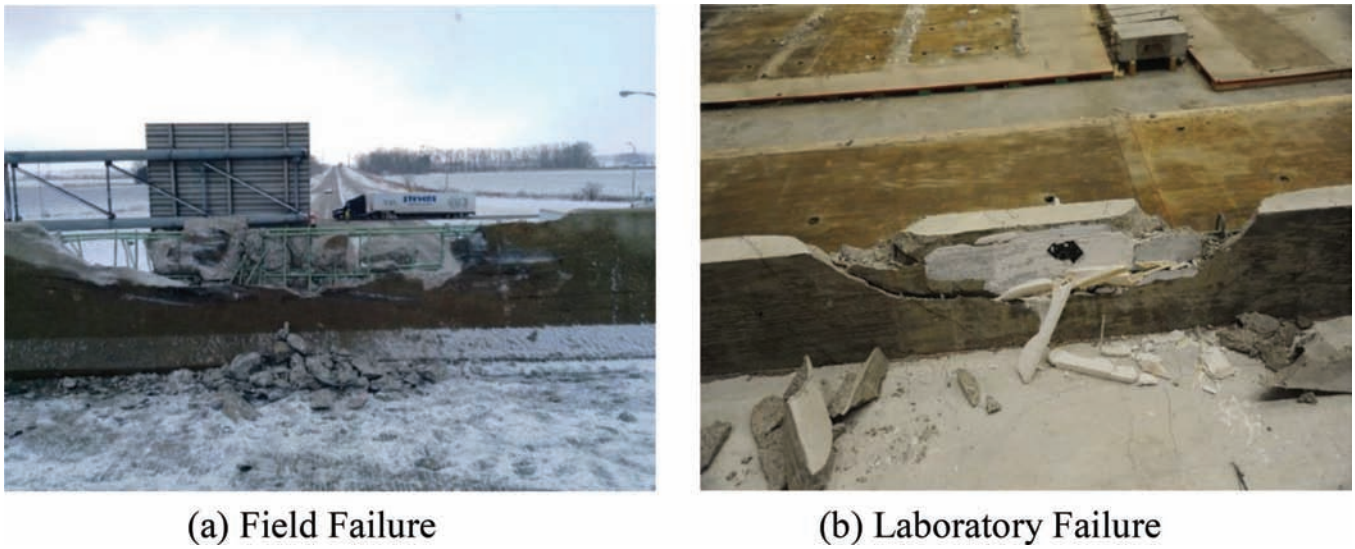

Figure 6.10 Higher impact failure (INDOT, n.d.).

Figure 6.11 Nonsymmetrical impact failure (INDOT, n.d.).

mode is consistent with that exhibited by Specimen 1L (Figure 6.10(b)) and visually identical.

Depending on the location of the impact, nonsymmetrical punches can occur. A semi-truck struck the I65 NB bridge over I70 WB & CD lanes at the North Split (Str. #I65-113-5747 BNBL) on September 10, 2014. Due to a vertical joint in the barrier, the punch was limited as the vertical joint served as the edge of the punching shear geometry (Figure 6.11). The load required to achieve this punch is estimated to be less than the full punch geometry as the punching perimeter (b_o) is reduced. Providing a similar calculation as presented in 6.4.2 with a perimeter of 49 in. results in a strength of approximately 100 kips which still provides strength greater than design (54 kips) but further limits the forces required to be resisted by the deck overhang.

A similar nonsymmetrical punch occurred on I65 NB bridge at the 112+03 RP (Str. # I65-113-5747 BNBL) which was struck on January 3, 2015. This is the same structure as just discussed, but at a different location. Again, the vertical joint isolated the punch to form only half of the failure surface (Figure 6.12). Again, this type of failure reduced the load resisted, but also reduced the load that must be resisted by the overhang.

Figure 6.12 Nonsymmetrical impact failure (INDOT, n.d.).

As illustrated in the various document cases, the failure modes are consistent with that observed in the laboratory testing supporting the validity of the test results and the failure modes. In addition, in all of the field cases, no damage was observed in the overhang.

6.6 Conclusions

Based on laboratory and field results, the strength of the overhang/railing system is limited by the punching shear strength of the barrier rather than the yield line mechanism. The punching shear strength, in fact, is significantly lower than that calculated for the yield line mechanism assumed by AASHTO (approximately 75% of the yield line capacity for an INDOT TL-4 barrier). Barrier impact loads are transferred to the bridge system through the deck overhang over a large distribution length which is capable of resisting the full punching strength of the barrier. The distribution length is significantly greater than assumed by AASHTO. Considering the testing conducted here, it was found that the load can be considered distributed to the overhang at least 10 times the horizontal loading dimension (L_t). For a TL-4 loading, this results in an effective distribution length (Figure 6.13) of approximately 35 ft. Because of the wide distribution length along with the lower maximum forces that need to be developed, there are low demands on the overhang reinforcement from the barrier impact force. Based on the results of this study, there is no need to consider the transverse impact force in the design of the bridge deck overhang. The bridge deck overhang should be designed considering only vertical forces. If there is desire to evaluate the overhang for the impact force, it is recommended that the distribution length (L_{eff}) be computed as $10L_t$.

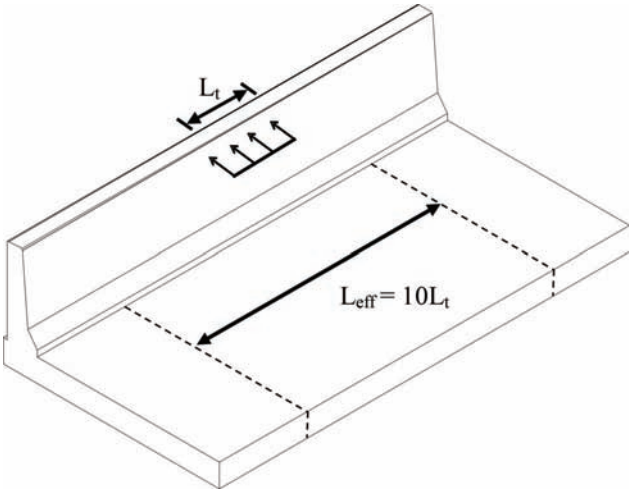

Figure 6.13 Overhang distribution length.

7. SUMMARY AND CONCLUSIONS

7.1 Introduction

Bridge deck overhangs currently require increased amounts of top transverse reinforcement relative to past practice due to changes in design requirements set by the AASHTO bridge design specification. The objective of this research was to investigate the design of the deck overhang and determine if reduced amounts of reinforcement in the deck overhang are possible while maintaining safety.

7.2 Experimental Program

7.2.1 System Behavior of Bridge Deck-Barrier Wall

Four approximately half-scale overhang specimens were tested with different amounts of top transverse reinforcement to understand the effect of this reinforcement on overhang behavior. Two specimens were 15 ft in length while two specimens were 27 ft in length. For one specimen of each length, the transverse reinforcement was provided in accordance with AASHTO (2014) requirements while the transverse reinforcement was halved in the companion specimen to evaluate its influence. A lateral force was applied to the barrier at mid-length along the specimen. Overall load-displacement behavior of the system was monitored along with strain in the top transverse bars.

Both 15 ft long specimens experienced a diagonal tension failure at the deck/barrier joint along the entire length of the specimen. Overall, the behavior of the two specimens was similar with the specimen containing half the reinforcement failing at a slightly lower load (21.5 kips vs 26.8 kips). This difference in load capacity agrees well with the failure mode which is dependent upon the reinforcement ratio provided in the deck. The displacement response indicates that the entire 15 ft overhang was effective in resisting forces developed from the applied lateral load.

The 27 ft specimens experienced a different failure mode. Failure for these specimens was controlled by punching shear. Two different failure surfaces were produced due to the different bearing areas used for the two specimens. When the loading plate was applied towards the top of the specimen, punching was more localized around the bearing area. When the loading place was spread the load out over much of the vertical face of the barrier, a broader punching occurred with the lower perimeter of the failure surface moving towards the deck/barrier interface. Displacement response indicate that the entire overhang resisted the forces developed from the applied lateral load. It does appear, however, from the displacement profile that the central 15 ft region was more effective in providing that resistance.

7.2.2 Sectional Behavior of Bridge Deck Barrier Wall

Five full-scale and two half-scale specimens were tested to evaluate the sectional behavior of the bridge deck-barrier wall connection. Of particular interest was anchorage of the top transverse bars in the overhang due to the relatively short anchorage length at this location. Furthermore, there was concern from the failure of the 15 ft long system specimens that an anchorage failure of the top transverse reinforcement may have contributed to the joint shear failure. The top transverse reinforcement was varied with respect to bar size, bar coating, and anchorage detail. A lateral force was applied to the barrier, and overall load-displacement behavior of the system was monitored along with strain in the top transverse bars.

It was observed that all specimens experienced a diagonal tension failure at the deck/barrier joint. Anchorage failure was not observed any of the specimens. The ultimate capacity of a given size specimen was approximately the same due to the type of failure mode which is primarily controlled by the thickness of the deck and the concrete strength.

7.3 Conclusions

The following conclusions were made based on this research program:

1. A diagonal tension failure in the deck overhang/barrier joint is a potential failure mode. However, this failure mode is only possible for very short bridge lengths (< 30 ft) and will not control the capacity of the overhang/barrier system of a typical bridge deck.
2. The strength of the overhang/barrier wall system is controlled by punching shear rather than the yield-line mechanism. This finding is significant in that design of the overhang according to AASHTO (2014) requirements is based on the yield line strength. Review of in-service barrier impacts support the finding that punching shear controls the capacity of the system with field failures producing the same failure surfaces as observed in the laboratory.
3. Barrier impact loads are transferred to the bridge system through the deck overhang over a large distribution length. Load was found to be distributed to the overhang at least 10 times the horizontal loading dimension (L_t), significantly larger than considered by current design provisions. Because of this very effective distribution, there are significantly lower demands on the overhang reinforcement from the barrier impact force than considered using current design provisions. Consequently, a significant reduction in transverse reinforcement relative to that currently required by the AASHTO design specification can be achieved.

7.4 Design Recommendations

It is recommended that the bridge deck overhang be designed considering vertical forces as outlined as Design Case 2 and 3 in the AASHTO (2014) specifications. Considering the very effective lateral force transfer to the overhang and the maximum applied lateral force as limited through the punching shear capacity of the barrier, design of the overhang to resist the lateral impact force is not required. If there is desire to consider the lateral impact force in design, two modifications from current design requirements as specified by AASHTO are recommended for design of the bridge deck overhang:

1. Applied lateral force should be based on the lesser of the punching shear strength of the barrier and the yield line strength. Punching shear strength can be computed as recommended in Section 6.4.2. For the INDOT TL-4 barrier considered here, the punching shear strength controls.
2. The deck overhang distribution length should be considered as $10L_t$ where L_t is the longitudinal length of distribution of impact force.

REFERENCES

AASHTO. (1994). *LRFD bridge design specifications*. Washington, DC: American Association of State Highway and Transportation Officials.

AASHTO. (2014). *LRFD bridge design specifications* (7th ed.). Washington, DC: American Association of State Highway and Transportation Officials.

ASTM A370. (2014). *Standard test methods and definitions for mechanical testing of steel products*. West Conshohocken, PA: ASTM International.

ASTM C39. (2015). *Standard test method for compressive strength of cylindrical concrete specimens*. West Conshohocken, PA: ASTM International.

Beal, D. B. (1981). *Strength of concrete bridge decks* (Publication No. FHWA/NY/RR-81-89). Albany, NY: New York State Department of Transportation.

Bligh, R. P., Briaud, J., Kim, K. M., & Abu-Odeh, A. (2010). *Design of roadside barrier systems placed on MSE retaining walls* (NCHRP Report 663). Washington, DC: Transportation Research Board.

Calloway, B. R. (1993). *Yield line analysis of an AASHTO New Jersey concrete parapet wall* (Master's thesis). Blacksburg, VA: Virginia Polytechnic Institute and State University. Retrieved from https://vtechworks.lib.vt.edu/handle/10919/34936

Darwin, D., Nilson, A. & Dolan, C. (2010). *Design of concrete structures* (14th ed.). New York, NY: McGraw Hill Education.

Hirsch, T. J. (1978). *Analytical evaluation of Texas bridge rails to contain buses and trucks* (Publication No. FHWATX78-230-2). College Station, TX: Texas Transportation Institute. Retrieved from http://static.tti.tamu.edu/tti.tamu.edu/documents/230-2.pdf

Hognestad, E. (1953). Yield-line theory for the ultimate flexural strength of reinforced concrete slabs. *ACI Journal Proceedings*, *49*(3), 637–656. https://doi.org/10.14359/11842

Holt, J. M., & Smith, A. (2014, Sept./Oct.). Reducing steel in bridge decks. *Concrete bridge views*, *78*. Retrieved from http://www.concretebridgeviews.com/i78/Article3.php

INDOT. (n.d.). *Standard drawings—English section 700*. Indianapolis, IN: Indiana Department of Transportation. Retrieved September 18, 2014, from http://www.in.gov/dot/div/contracts/standards/drawings/sep12/e/sep700.htm

INDOT. (2008). Bridge decks. Chapter 61 in *Indiana design manual*. Indianapolis, IN: Indiana Department of Transportation. Retrieved February 24, 2015, from http://www.in.gov/dot/div/contracts/standards/dm-Archived/08%20English/Part6/ECh61/ch61.htm

PCI. (2011). *PCI bridge design manual* (3rd ed.). Chicago, IL. Precast/Prestressed Concrete Institute.

Ross, H. E., Jr., Sicking, D. L., Zimmer, R. A., & Michie, J. D. (1993). *Recommended procedures for the safety performance evaluation of highway features* (NCHRP Report 350). Washington, DC: Transportation Research Board. Retrieved from http://onlinepubs.trb.org/onlinepubs/nchrp/nchrp_rpt_350-a.pdf

Tureyen, A. K., & Frosch, R. J. (2003). Concrete shear strength: Another perspective. *ACI Structural Journal*, *100*(5), 609–615. https://doi.org/10.14359/12802

Wassef, W., Smith, C., Clancy, C., & Smith, M. (2003). *Comprehensive design example for prestressed concrete girder superstructure with commentary* (Task Order DTFH61-02-T-63032). Arlington, VA: Federal Highway Administration. Retrieved from https://www.fhwa.dot.gov/bridge/lrfd/fhwanhi04043.pdf

APPENDICES

APPENDIX A: DERIVATION OF HIRSCH EQUATIONS

The derivation presented here is similar to the derivation procedure of many academic papers found in the literature. Specifically, Calloway (1993) from the Virginia Polytechnic Institute performed extensive research on yield line analysis of Jersey Barriers and formerly derived the Hirsch equations.

The deformed area (A_d) under the transversely applied load is calculated to determine the external work done on the railing system. Through similar triangles, the height (h_d) is determined and the total area is calculated (Figure A.1).

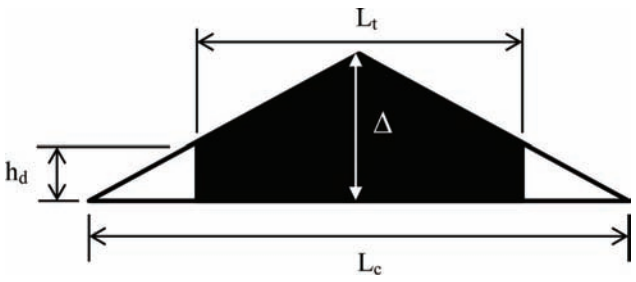

Figure A.1 Deformed area under transverse load.

Derivation of External Work

1. $$h_d = \frac{\Delta\left(\frac{L_c - L_t}{2}\right)}{(L_c/2)} = \frac{\Delta(L_c - L_t)}{L_c}$$

2. $$A_d = \left(\frac{2.A_d = \left(\frac{\Delta(L_c - L_t)}{L_c}\right) L_t + \frac{L_t}{2}\left[\Delta - \left(\frac{\Delta(L_c - L_t)}{L_c}\right)\right] = \frac{\Delta L_t\left(L_c - \frac{L_t}{2}\right)}{L_c}(L_c - L_t)}{L_c} \right)$$

The expression for external work is calculated as the product of the transverse line load and the deformed area.

$$W_{EXT} = \frac{F_t \Delta L_t \left(L_c - \frac{L_t}{2}\right)}{L_c}$$

To find the internal work for the system, the negative and positive resisting moments are multiplied by their respective angles of rotation. Three flexural resistances of the railing are considered for internal work calculations. The cantilevered wall provides resistance about the longitudinal axis (M_c) due to transverse (vertical) reinforcement. The wall also provides flexural resistance about the vertical axis with presence of longitudinal (horizontal) reinforcement (M_w) and beam action in the top of the rail (M_b). The positive and negative yield lines for the parapet barrier are depicted in Figure A.2.

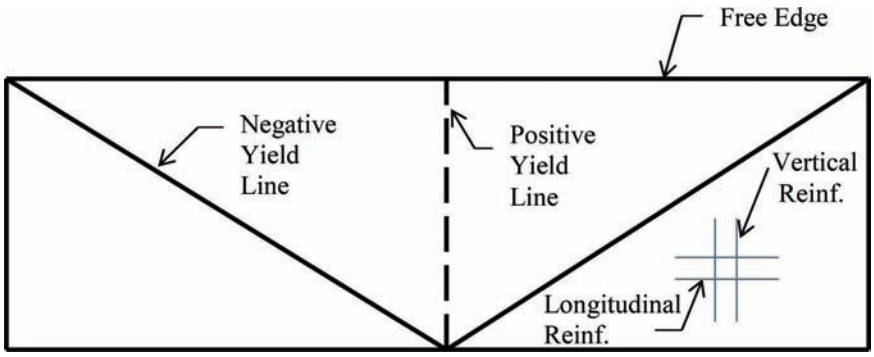

Figure A.2 Concrete parapet yield line pattern.

Derivation of Internal Work

1. $W_{int} = M_b\theta + M_w\theta + M_c\theta$

The internal work is computed as the sum of the work done by the beam, wall (Figure A.3), and cantilevered components (Figure A.4).

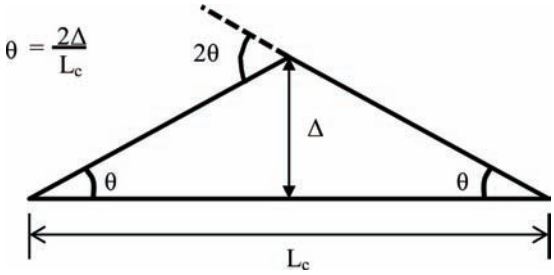

Figure A.3 Plan view of deformed concrete parapet barrier.

Work Done by Beam Component

2. $(M_b\theta + M_b\theta + M_b 2\theta) = M_b 4\theta$
3. $W_{IMB} = \dfrac{8M_b\Delta}{L_c}$

Work Done by Wall about Vertical Axis

4. $(M_w\theta + M_w\theta + M_w 2\theta) = M_w 4\theta$
5. $W_{IMW} = \dfrac{8M_w\Delta}{L_c}$

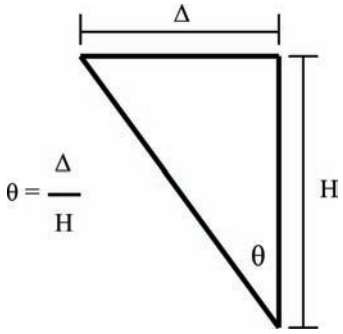

Figure A.4 Side view of cantilevered wall for M_c.

Work Done by Wall about Longitudinal Axis

6. $W_{IMC} = L_c m_c \theta = \dfrac{L_c m_c \Delta}{H}$

For the computation of internal work, the direction of reinforcement impacts moment resistance about each axis. In the case of bending about the vertical axis, reinforcement is only considered running in the longitudinal direction as shown in Figure A.5. The number of bars crossing the negative and positive moment yield lines with respective rotations is used to compute internal work for the wall and cantilevered components. Half of the wall is shown in Figure A.5 and Figure A.6.

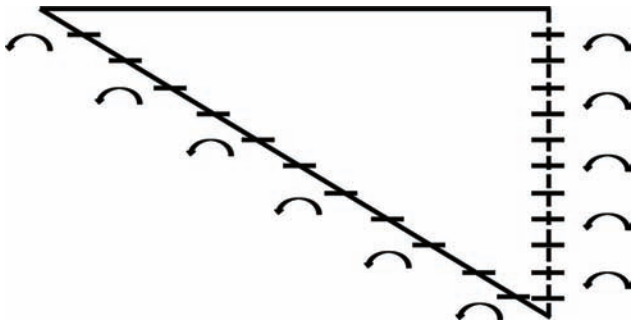

Figure A.5 M_w resistance of parapet.

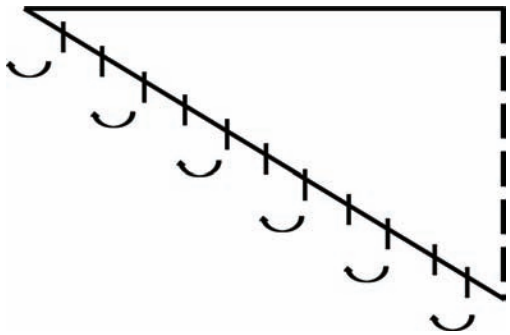

Figure A.6 M_c resistance of parapet wall.

After calculating the internal work of the system, it is equated to the external work resulting in the derivation of AASHTO Equation A13.3.1-1 for R_w (Equation A.1). Note that the railing resistance, R_w, is the product of the transverse load and the length for which the load is applied.

Equating Internal and External Work

$$W_{INT} = W_{EXT}$$

$$\frac{8M_b\Delta}{L_c} + \frac{8M_w\Delta}{L_c} + \frac{L_cM_c\Delta}{H} = \frac{F_t\Delta L_t\left(L_c - \frac{L_t}{2}\right)}{L_c}$$

$$R_w = \frac{2}{2L_c - L_t}\left[8M_wH + 8M_b + \frac{M_cL_c^2}{H}\right] \tag{A.1}$$

To derive the "critical wall length" through which the yield line acts, Equation A13.3.1-1 must be minimized with respect to L_c. AAHSTO Equation A13.3.1-2 is derived for L_c by differentiating Equation A13.3.1-1 and setting it equal to zero (Equation A.2).

Derivation of Critical Wall Length (L_c)

$$\frac{dR_w}{dL_c} = \frac{4L_cM_c}{H(2L_c - L_t)} - 4\left[\frac{M_cL_c^2/H}{(2L_c - L_t)^2} + \frac{8M_b}{(2L_c - L_t)^2} + \frac{8M_b}{(2L_c - L_t)^2}\right]$$

$$L_c = \frac{L_c}{2} + \sqrt{\left(\frac{L_t}{2}\right)^2 + \frac{8HM_b}{M_c} + \frac{8HM_w}{M_c}} + \frac{L_t}{2} \tag{A.2}$$

APPENDIX B: BRIDGE RAILING CALCULATIONS

Example 1: Analysis of T221 (TxDOT): TL-4 Railing Test Level

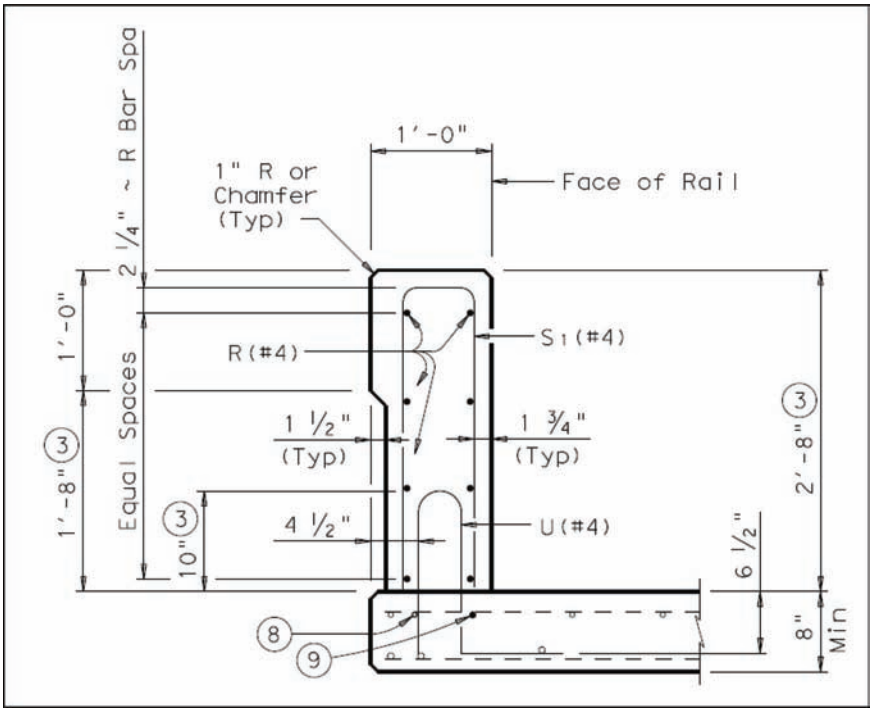

Figure B.1 T221 bridge railing detail (TxDOT 2015).

Given Properties

$c_c = 1.75\ in.$ $d_4 = 0.5\ in.$ $f_y = 60\ ksi$

$H_r = 32\ in.$ $f_c = 4000\ psi$ $L_t = 3.5\ ft$

$h_{avg} = 11.8\ in.$ *Average weighted height of railing

$A_{sc} = 0.2\ in.^2 x \frac{12}{6} = 0.4\ in.^2$ *Vertical steel area per foot of railing in the longitudinal direction

$d_c = h_{avg} - c_c - \frac{d_4}{2} = 9.8\ in.$ *Effective depth of vertical steel

Moment Capacity (M_c)

$a = \frac{A_{sc} f_y}{0.85 f'_c b} = 0.59 in.$ *Width of compression block; unit width b = 12 in.

$M_c = A_{sc} f_y (d_c - a/2) = \frac{19 kip.ft}{ft}$ *Moment capacity per foot longitudinally

$A_{sw} = 0.2\ in.^2 x 4 = 0.8\ in.^2$ *Longitudinal tension steel area

$d_w = h_{avg} - c_c - d_4 - \frac{d_4}{2} = 9.3\ in.$ *Effective depth of longitudinal steel

Moment Capacity (M_w)

$a = \frac{A_{sw} f_y}{0.85 f'_c b} = 0.44\ in.$ *Width of compression block; b = 32 in. height of the railing

$M_w = A_{sw} f_y (d_w - a/2) = 36.3\ kip{\cdot}ft$ *No beam action, $M_b = 0$

Nominal Railing Resistance

$L_c = \frac{L_c}{2} + \sqrt{\left(\frac{L_t}{2}\right)^2 + \frac{8HM_b}{M_c} + \frac{8HM_w}{M_c}} + \frac{L_t}{2} = 8.4\text{ft}$ *Yield Line Clear Length

$R_w = \frac{2}{2L_c - L_t}\left[8M_w H + 8M_b + \frac{M_c {L_c}^2}{H}\right] = 119 kip$ *Nominal Railing Resistance

Example 2: Analysis of BR221 (ODOT): TL-4 Railing Test Level

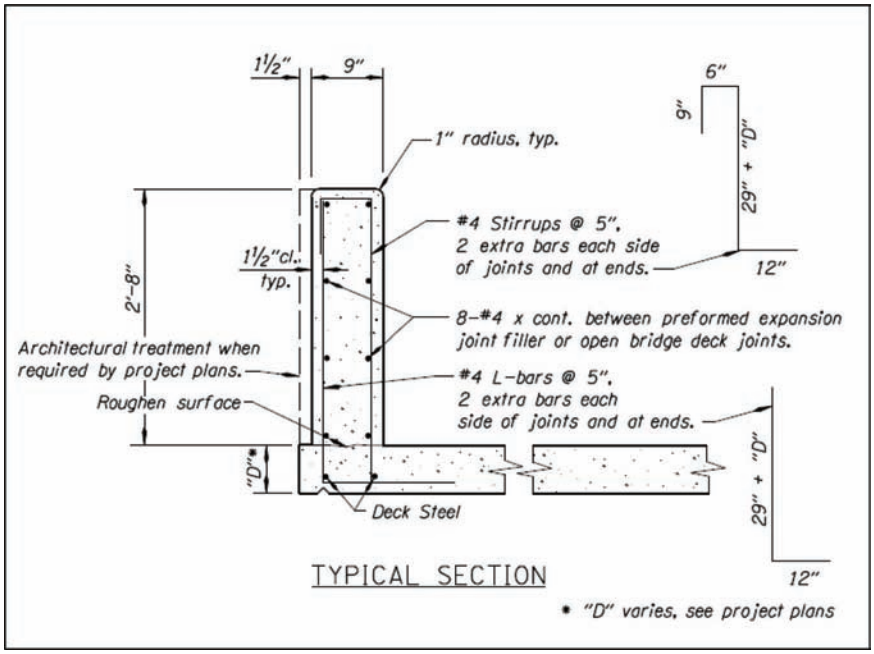

Figure B.2 BR221 bridge railing detail.

Given Properties

$c_c = 1.5\ in.$ $d_4 = 0.5\ in.$ $f_y = 60\ ksi$

$H_r = 32\ in.$ $f_c = 4000\ psi$ $L_t = 3.5\ ft$

$h_{avg} = 9\ in.$ *Average weighted height of railing

$A_{sc} = 0.2\ in.^2 x \frac{12}{5} = 0.48\ in.^2$ *Vertical steel area per foot of railing in the longitudinal direction

$d_c = h_{avg} - c_c - \frac{d_4}{2} = 7.25\ in.$ *Effective depth of vertical steel

Moment Capacity (M_c)

$a = \frac{A_{sc} f_y}{0.85 f'_c b} = 0.71\ in.$ *Width of compression block; unit width b = 12 in.

$M_c = A_{sc} f_y (d_c - a/2) = \frac{16.6\ kip{\cdot}ft}{ft}$ *Moment capacity per foot longitudinally

$A_{sw} = 0.2\ in.^2 x4 = 0.8\ in.^2$ *Longitudinal tension steel area

$d_w = h_{avg} - c_c - d_4 - \frac{d_4}{2} = 6.75\ in.$ *Effective depth of longitudinal steel

Moment Capacity (M_w)

$a = \frac{A_{sw} f_y}{0.85 f'_c b} = 0.44\ in.$ *Width of compression block; b = 32 in. height of the railing

$M_w = A_{sw} f_y (d_w - a/2) = 26.1\ kip{\cdot}ft$ *No beam action, $M_b = 0$

Nominal Railing Resistance

$L_c = \frac{L_c}{2} + \sqrt{\left(\frac{L_t}{2}\right)^2 + \frac{8HM_b}{M_c} + \frac{8HM_w}{M_c}} + \frac{L_t}{2} = 7.8\ \text{ft}$ *Yield Line Clear Length

$R_w = \frac{2}{2L_c - L_t}\left[8M_w H + 8M_b + \frac{M_c L_c^2}{H}\right] = 97\ kip$ *Nominal Railing Resistance

Example 3: Analysis of 706-BRSF Railing Type FC (INDOT): TL-4 Test Level

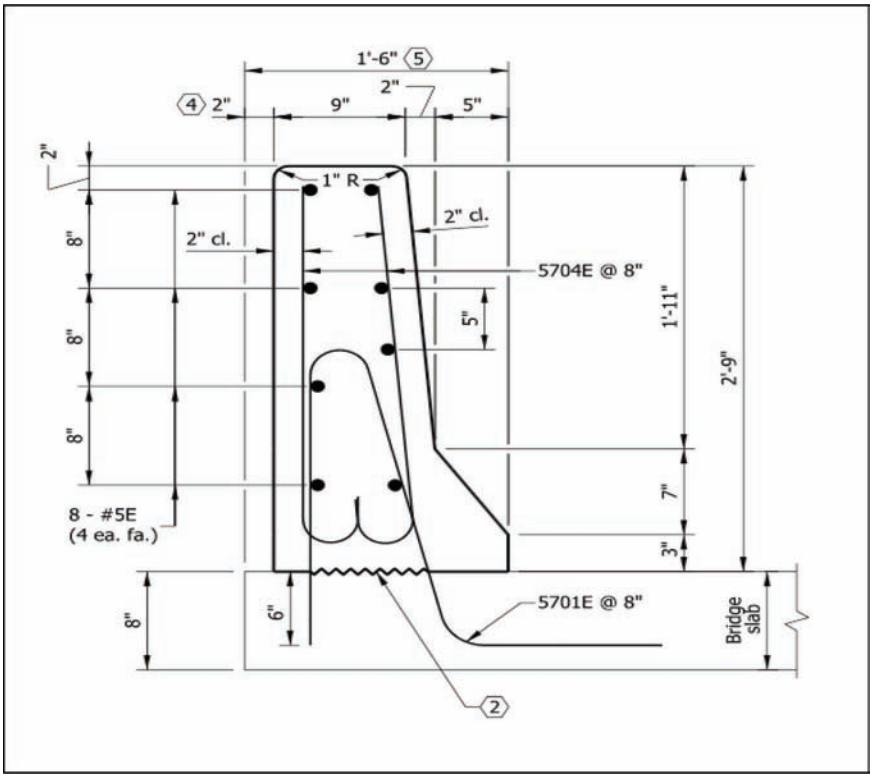

Figure B.3 Type FC bridge railing detail (INDOT, 2015).

Given Properties

$c_c = 2\ in.$ $d_5 = 0.625\ in.$ $f_y = 60\ ksi$

$H_r = 33\ in.$ $f_c = 4000\ psi$ $L_t = 3.5\ ft$

$h_{avg} = 12.1\ in.$ *Average weighted height of railing

$A_{sc} = 0.31\ in.^2\ x\frac{12}{8} = 0.47\ in.^2$ *Vertical steel area per foot of railing in the longitudinal direction

$d_c = h_{avg} - c_c - \frac{d_5}{2} = 9.79\ in.$ *Effective depth of vertical steel

Moment Capacity (M_c)

$a = \frac{A_{sc} f_y}{0.85 f'_c b} = 0.68\ in.$ *Width of compression block; unit width b = 12 in.

$M_c = A_{sc} f_y (d_c - a/2) = \frac{22\ kip{\cdot}ft}{ft}$ *Moment capacity per foot longitudinally

$A_{sw} = 0.31\ in.^2\ x4 = 1.24\ in.^2$ *Longitudinal tension steel area

$d_w = h_{avg} - c_c - d_5 - \frac{d_5}{2} = 9.16\ in.$ *Effective depth of longitudinal steel

Moment Capacity (M_w)

$a = \frac{A_{sw} f_y}{0.85 f'_c b} = 0.66\ in.$ *Width of compression block; b = 33 in. height of the railing

$M_w = A_{sw} f_y (d_w - a/2) = 54.8\ kip{\cdot}ft$ *No beam action, $M_b = 0$

Nominal Railing Resistance

$L_c = \frac{L_c}{2} + \sqrt{\left(\frac{L_t}{2}\right)^2 + \frac{8HM_b}{M_c} + \frac{8HM_w}{M_c}} + \frac{L_t}{2} = 9.4\ \text{ft}$ *Yield Line Clear Strength

$R_w = \frac{2}{2L_c - L_t}\left[8M_w H + 8M_b + \frac{M_c {L_c}^2}{H}\right] = 150\ kip$ *Normal Railing Resistance

APPENDIX C: OVERHANG DESIGN CALCULATIONS

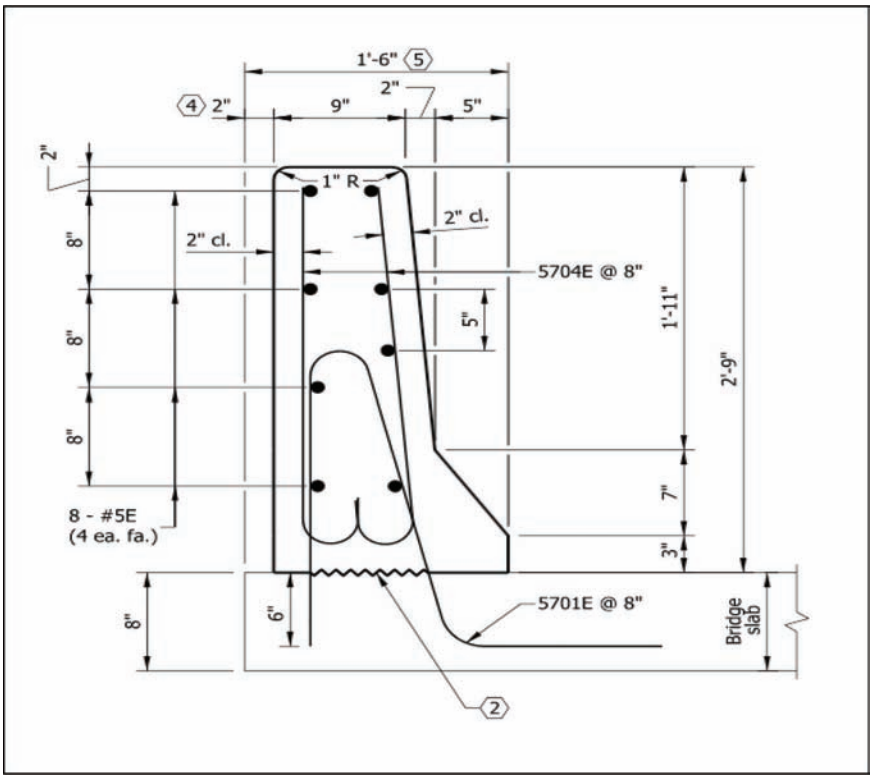

Figure C.1 Type FC bridge railing detail (INDOT, 2015).

Two overhang specimens were scaled from the INDOT Type FC Railing. Bridge railing calculations for this railing are provided in Appendix B.

Scaled Overhang Specimens

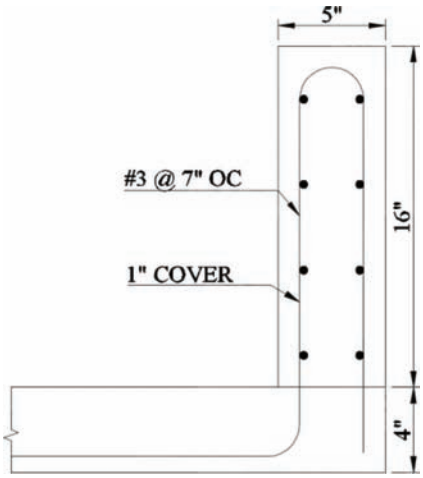

Figure C.2 Scaled specimen barrier.

Given Properties

$c_c = 1\ in.$ $f_y = 60\ ksi$ $f_c = 4000\ psi$

$H_r = 16\ in.$ *Height of railing

$t_s = 4\ in.$ *Thickness of scaled slab

$h = 5\ in.$ *Width of scaled railing

$A_{sc} = 0.11\ in.^2\ x \frac{12}{7} = 0.19\ in.^2$ *Vertical steel area per foot of railing in the longitudinal direction

$d_c = h - c_c - \frac{d_3}{2} = 3.81\ in.$ *Effective depth of vertical steel

Moment Capacity (M_c)

$a = \frac{A_{sc} f_y}{0.85 f'_c b} = 0.27\ in.$ *Width of compression block; unit width b = 12 in.

$M_c = A_{sc} f_y (d_c - a/2) = \frac{3.4\ kip{\cdot}ft}{ft}$ *Moment capacity per foot longitudinally

$A_{sw} = 0.11 in.^2\ x4 = 0.44\ in.^2$ *Longitudinal tension steel area

$d_w = h - c_c - d_3 - \frac{d_3}{2} = 3.44\ in.$ *Effective depth of longitudinal steel

Moment Capacity (M_w)

$a = \frac{A_{sw} f_y}{0.85 f'_c b} = 0.49\ in$ *Width of compression block; b = 16 in. height of the railing

$M_w = A_{sw} f_y (d_w - a/2) = 7\ kip{\cdot}ft$ *No beam action, $M_b = 0$

Nominal Railing Resistance $L_t = 1.5$ ft

$L_c = \frac{L_c}{2} + \sqrt{\left(\frac{L_t}{2}\right)^2 + \frac{8HM_b}{M_c} + \frac{8HM_w}{M_c}} + \frac{L_t}{2} = 5.5$ ft *Yield Line Clear Length

$R_w = \frac{2}{2L_c - L_t}\left[8M_w H + 8M_b + \frac{M_c L_c^2}{H}\right] = 28\ kip$ *Nominal Railing Resistance

Design of Overhang Based on Scaled Parapet (AASHTO Method):

Top Transverse Reinforcement

Design Section 1-1.

$T = \frac{R_w}{L_c + 2H} = 3.45 \frac{kip}{ft}$ *Axial tension force in slab

$M_s = 0.005 \frac{kip{\cdot}ft}{ft}$ *Self-weight slab moment

$M_s = 0.02 \frac{kip{\cdot}ft}{ft}$ *Self-weight barrier moment

$M_u = M_c + 1.25(M_s + M_b) = 3.44 \frac{kip \cdot ft}{ft}$ *Ultimate moment per design section 1-1

*Use #3 bars spaced at 4.5 in. O.C.

$A_s = 0.11\ in.^2\ x \frac{12}{4.5} = 0.29\ in.^2$ *Primary reinforcement per foot

$d_e = h_s - c_c - \frac{d_3}{2} = 3.06\ in.$ *Effective depth of top transverse steel

$C = A_s f_y - T = 14.15 \frac{kip}{ft}$ *Compression force minus axial tension in the slab

$a = \frac{C}{0.85 f'_c b} = 0.35\ in.$ *Width of compression block; b = 12 in. unit width

$M_n = A_s f_y (d_e - a/2) - T\left(d_e/2 - a/2\right) = 3.85 \frac{kip \cdot ft}{ft}$

Design Section 2-2.

$D_s = 2\ ft$ *Distance from critical section to the edge of the concrete barrier

$M_{cred} = \frac{M_c L_c}{L_c + 2D_s\left(tan\left(\frac{30}{180}\right)\right)} = 2.41 \frac{kip \cdot ft}{ft}$ *Distribution of moment to critical section 2-2

$T = \frac{R_w}{L_c + 2D_s + 2D_s\left(tan\left(\frac{30}{180}\right)\right)} = 2.39 \frac{kip}{ft}$ *Distribution of tensile forces to critical section 2-2

$C = A_s f_y - T = 15.21 \frac{kip}{ft}$ *Compression force minus axial tension in the slab

$a = \frac{C}{0.85 f'_c b} = 0.37\ in.$ *Width of compression block; b = 12 in. unit width

$M_s = 0.1 \frac{kip \cdot ft}{ft}$ *Self-weight slab moment

$M_b = 0.14 \frac{kip \cdot ft}{ft}$ *Self-weight barrier moment

$M_u = M_{cred} + 1.25(M_s + M_b) = 2.71 \frac{kip \cdot ft}{ft}$ *Ultimate moment per design section 2-2

$M_n = A_s f_y (d_e - a/2) - T\left(d_e/2 - a/2\right) = 3.95 \frac{kip \cdot ft}{ft}$

Due to the fact that $M_n > M_u$ for each design section, O.K.

Development Length (maximum of three cases)

$l_d = \frac{1.25 d_b f_y}{\sqrt{f'_c}} = 4.1\ in.$

$l_d = 0.4 d_b f_y = 9\ in.$

$l_d = 12\ in.$

Due to the fact that 23.25 in. of available length (from edge of parapet to edge of support) exceeds 12 in., O.K.

Specimen #1 Deck Reinforcement Proportioning

Top Transverse: 4.5 in. O.C

Top Longitudinal: 12 in. O.C.

Bottom Transverse: 12 in. O.C.

Bottom Longitudinal: 12 in. O.C.

Specimen #2 Deck Reinforcement Proportioning

Top Transverse: 9 in. O.C

Top Longitudinal: 12 in. O.C.

Bottom Transverse: 12 in. O.C.

Bottom Longitudinal: 12 in. O.C.

About the Joint Transportation Research Program (JTRP)

On March 11, 1937, the Indiana Legislature passed an act which authorized the Indiana State Highway Commission to cooperate with and assist Purdue University in developing the best methods of improving and maintaining the highways of the state and the respective counties thereof. That collaborative effort was called the Joint Highway Research Project (JHRP). In 1997 the collaborative venture was renamed as the Joint Transportation Research Program (JTRP) to reflect the state and national efforts to integrate the management and operation of various transportation modes.

The first studies of JHRP were concerned with Test Road No. 1—evaluation of the weathering characteristics of stabilized materials. After World War II, the JHRP program grew substantially and was regularly producing technical reports. Over 1,500 technical reports are now available, published as part of the JHRP and subsequently JTRP collaborative venture between Purdue University and what is now the Indiana Department of Transportation.

Free online access to all reports is provided through a unique collaboration between JTRP and Purdue Libraries. These are available at: http://docs.lib.purdue.edu/jtrp

Further information about JTRP and its current research program is available at: http://www.purdue.edu/jtrp

About This Report

An open access version of this publication is available online. This can be most easily located using the Digital Object Identifier (doi) listed below. Pre-2011 publications that include color illustrations are available online in color but are printed only in grayscale.

The recommended citation for this publication is:

Frosch, R. J., & Morel, A. J. (2016). *Guardrails for use on historic bridges: Volume 2—Bridge deck overhang design* (Joint Transportation Research Program Publication No. FHWA/IN/JTRP-2016/34). West Lafayette, IN: Purdue University. https://doi.org/10.5703/1288284316361